الخلاصة

تم تطوير نموذج مجسم يصف عملية االتكثيف خلال عملية الحرق الزجاجي (التزجيج) لمادة تحتوي على محتويات صلبة. هذا النموذج تم تطويرة من نموذج سابق للباحث Scherer والذي وضع نموذج يصف عملية التكثيف خلال عملية الحرق لمادة لا تحتوي على محتويات صلبة.النموذج المطور أستخدم لمحاكاة معدل التكثيف خلال عملية الحرق لمواد سيراميكية غير متجانسة تتكون من خليط من بعض الاطيان العراقية و التي تم تحضيرها من بحث سابق. النموذج المطور تم أستخدامة لدراسة تأثير عدة عوامل على عملية التكثيف خلال عملية الحرق وهي درجة حرارة الحرق، زمن الحرق والنسبة بين حجم المواد الصلبة الى حجم السائل الزجاجي، كما أستخدم النموذج المطور في تقدير قيم اللزوجة الفعالة للسائل الزجاجي المتكون خلال عملية الحرق. كذلك تم تطبيق نموذجان اخران للمواد غير المتجانسة هما نموذج الكرة المركبة و نموذج المكون الذاتي و جرى أستخدامهما لدراسة تأثير درجة حرارة الحرق و زمن الحرق على عملية االتكثيف لغرض مقارنة النتائج من هذين النموذجين مع نتائج النموذج المطور.

كذلك تم أستخدام النموذج المطور لدراسة تأثيرتوزيع حجوم المسامات على عملية التكثيف و ذلك بفرض توزيع كاوس لحجوم المسامات وأعادة صياغة المعادلات للموديل المطور لجعلها تعتمد على الانحراف المعياري لتوزيع حجوم المسامات.

العوامل الفيزيائية مثل اللزوجة تم حسابها من خلال عملية المطابقة (fitting) للنتائج العملية لعملية الحرق للنماذج.

تم تصميم برامج حاسوبية بلغة (FORTRAN 90) لدراسة تأثير درجة حرارة الحرق على عملية االتكثيف باستخدام النموذج المطور، نموذج الكرة المركبة و نموذج المكون الذاتي. هذة البرامج تم تحويرها فيما بعد لمحاكاة عملية االتكثيف كدالة لزمن الحرق.

كذلك برنامج اخر تم تصميمة لدراسة تأثيرتوزيع حجوم المسامات على عملية التكثيف خلال عملية الحرق باستخدام النموذج المطور.

النتائج من برنامج الموديل المطور تحقق أفضل مقاربة للنتائج العملية تليها النتائج من برنامج موديل الكرة المركبة.

النتائج من برنامج تأثيردرجة حرارة الحرق تشير عموما" الى زيادة معدل االتكثيف مع زيادة درجة حرارة الحرق، رغم ذلك، عندما تكون نسبة المواد الصلبة عالية نسبيا" فإن اللزوجة

تزداد عند الدرجات الحرارية العالية (حوالي ١٤٠٠س^{o}) يعزى ذلك الى عملية نمو بلوري محتملة، و علية يؤدي ذلك الى نقصان معدل االتكثيف.

النتائج من برنامج تأثير زمن الحرق تشيرالى ان النموذج المطوريتنبأ بزيادة شبة لوغارتمية للكثافة النسبية مع الزمن، بينما يتنبأ النموذجان الآخران (نموذج الكرة المركبة و نموذج المكون الذاتي) بزيادة أسية للكثافة النسبية مع الزمن. النتائج من البحوث السابقة تتفق مع توقع النموذج المطور. النتائج من برنامج تأثيرتوزيع حجوم المسامات على عملية التكثيف تدل على أن هذا العامل لة تاثير قوي عندما يكون التوزيع عريضا" فقط على المراحل النهائية لعملية التكثيف لأن المسامات الكبيرة غلقها بطىء نسبيا".

ABSTRACT

A mathematical model describing the densification process during viscous sintering process of a material contains solid inclusions is developed (modified) from a Scherer model which describes the rate of densification during sintering for a free solid inclusions material. The modified model is used to simulate the rate of densification during sintering process for ceramic heterogeneous materials consist from mixtures of some Iraqi clays that had been prepared in a previous work. In addition the modified model is used to study the effect of several factors on densification during sintering process and used in predicting the effective viscosity of the viscous phase that formed during sintering. The factors are the sintering temperature, sintering time, and the ratio of solid inclusions volume to viscous phase volume.

Another two heterogeneous models which are the composite sphere and the self consistent models are also applied and used to study the effect of sintering temperature and sintering time on densification during sintering for comparison with the present developed model.

The modified model is also used to study the effect of pore size distribution on densification process by assuming a Gaussian distribution for the pore sizes and reformulating the equations of the modified model to make them depend on the standard deviation of pore size distribution.

The physical parameters like viscosity are computed from the fitting process of the practical data of the samples.

Computer programs in FORTRAN 90 language are designed to study the effect of sintering temperature on densification process using the developed model, the composite sphere and the self consistent models.

These programs are modified to simulate the densification process versus time duration of the sintering process. Another program is designed to study the effect of pore size distribution on sintering process using the developed model.

The results from the developed (modified) Scherer model are better fit the practical data, then the composite sphere model.

The results from the program of the effect of sintering temperature indicates in general that the rate of densification is increased with increasing sintering temperature, this is due to the decrease in the viscosity with temperature increasing. However, when the ratio of the solid inclusions is high the viscosity is increased at relatively high sintering temperatures (about $1400^{o}C$) this increase in viscosity may be due to induced crystallization processes, accordingly the rate of densification is decreased at these circumstances.

The results from the program of the effect of sintering time indicate that the modified model predicts that the increase in density is semi logarithmic with time, while the other two models predict an exponential increase with time.

The results from the program of the effect of pore size distribution indicate that this parameter has a strong effect if the distribution is broad only in the last stages of densification because the largest pores are relatively slow to close.

Acknowledgments

It has been a long journey completing this M.Sc. and it would have been much harder without the assistance of many excellent people. I would like to thank my supervisors Dr. Fadhil A. Rasen and Dr. Ahmad K. Ahmad for suggestion this project and helping me in accomplishing it. They have been excellent – always available when I needed a help, and always providing good advice.

I would also like to thank the Dean of the College of Science Dr. Laith A. Al-Ani and all the staff of the College of Science in Al-Nahrain University and specially the staff of the physics department.

I would also like to thank my best supporters Father and Mother; Father gave me some important scientific ideas that helped me in the project. Mother gave me the motive to accomplish the work with full rest.

I would also like to thank my advisors, my best friend brother Ali Abbas and Mr. Wael F. Wahayb and Mr. Abdul Wahaab F. Wahayb and Miss Layla Fadhil and Mr. Belal Abdul Satar and Mr. Ammar Abdul Satar and Mr. Mohammad Abdul Wahaab and Mr. Ameer Faisal and Mr. Kadim Ali and Mr. Zaid Ganim for useful advice about more general aspects of doing my M.Sc., And lastly, a heart felt thanks to my relatives, and my friends.

بِسْمِ اللَّهِ الرَّحْمَنِ الرَّحِيم

لا يُكَلِّفُ اللَّهُ نَفْساً إِلَّا وُسْعَهَا لَهَا مَا كَسَبَتْ وَعَلَيْهَا مَا اكْتَسَبَتْ رَبَّنَا لا تُؤَاخِذْنَا إِنْ نَسِينَا أَوْ أَخْطَأْنَا رَبَّنَا وَلا تَحْمِلْ عَلَيْنَا إِصْراً كَمَا حَمَلْتَهُ عَلَى الَّذِينَ مِنْ قَبْلِنَا رَبَّنَا وَلا تُحَمِّلْنَا مَا لا طَاقَةَ لَنَا بِهِ وَاعْفُ عَنَّا وَاغْفِرْ لَنَا وَارْحَمْنَا أَنْتَ مَوْلانَا فَانْصُرْنَا عَلَى الْقَوْمِ الْكَافِرِينَ

صَدَقَ اللَّهُ الْعَظِيم

سورة البقرة-الآية ٢٨٦

Appendix-A

The integration of Eq. (2.22):

From Eq. (2.24) we have

$$y_x{}^3 = \frac{3\pi}{(1+\lambda)x} - 8\sqrt{2} \tag{A-1}$$

by rearranging we get

$$x = \frac{3\pi}{(1+\lambda)\left(y^3 + 8\sqrt{2}\right)} \tag{A-2}$$

Differentiating the above equation gives

$$dx = -\frac{9\pi y^2 dy}{(1+\lambda)\left(y^3 + 8\sqrt{2}\right)^2} \tag{A-3}$$

substituting in Eq. (2.22) gives

$$K(t-t_o) = \frac{-6}{(1+\lambda)} \int_{x_o}^{x} \frac{ydy}{\left(y^3 + 8\sqrt{2}\right)} \tag{A-4}$$

from reference [6] we have

$$-6\int_{x_o}^{x} \frac{ydy}{\left(y^3 + 8\sqrt{2}\right)} = -6\left(\frac{1}{6\alpha}\ln\left(\frac{\alpha^2 - \alpha y + y^2}{(\alpha+y)^2}\right) + \frac{1}{\sqrt{3}\alpha}\tan^{-1}\left(\frac{2y-\alpha}{\alpha\sqrt{3}}\right)\right)_{x_o}^{x} \tag{A-5}$$

so Eq. (A-4) becomes after the substitution of the last Equation in it

$$K(t-t_o) = -\frac{2}{\alpha(1+\lambda)}\left[\frac{1}{2}\ln\left(\frac{\alpha^2 - \alpha y + y^2}{(\alpha+y)^2}\right) + \sqrt{3}\tan^{-1}\left(\frac{2y-\alpha}{\alpha\sqrt{3}}\right)\right]_{x_o}^{x} \tag{A-6}$$

Which is the same as Eq. (2.26a).

SYMBOLS DEFINITION

Symbol	Definition
a	The particle size, which equals the cylinder radius.
a_{co}	The core radius for non sintering inclusion.
b	The cladding radius for sintering powder.
c	A constant equal ($8\sqrt{2}/3\pi$)
d	The pore diameter.
$\bar{d}$	The mean pore diameter
d0a	The mean pore diameter.
dN (l)	The number of cells with side length between (l) and (l +dl).
dp	The grain (or particle size).
f(t)	A function that represent the relation between K and the sintering temperature
E	Young's modulus
E_m	the viscous response of the porous material to a uniaxial stress.
E_f'	The rate of energy dissipation in the viscous flow.
E_s'	The reduction in surface area.
$f(y_i)$	Is a mathematical function of a variable y_i.
G	The effective shear modulus.
G_c	The shear viscosity of the continuum.
G_m	The shear modulus of the matrix or the apparent shear modulus.
G_m^E	The elastic shear modulus of the matrix.
h	The height of the compact unit cell cylinder.
K	The proportionality constant between the measured time and the reduced time.
K_o	is a constant that corresponds to the value of (Kt) at t=t_o
K_{cs}^E	The elastic bulk modulus of the matrix.
K_{s-c}	The bulk modulus of the composite in the self consistent model.
k0t	the initial value of Kt in the flow chart.
l	The side length of the composite unit cell.
l^*	The effective side length of the unit cell.
l_o	The initial length of the compacted unit cell.
$\bar{l}^*$	The average value of l^*.

Symbol	Definition
$\bar{l}$	The average value of *l*.
l_{in}	The side length of the solid inclusions in the compact.
l_{vis}	The side length of the viscous phase in the compact.
m	The value of the diameter that corresponds to maximum intruded volume.
n	The number of closed pores per volume of solid phase.
$\bar{n}$	The number of cells with side length $\bar{l}$ or diameter $\overline{d}$.
$\overline{n'}$	The number of pores with diameter $\bar{d}$.
$n'(d)$	The number of pores with diameter d .
$N(l)$	The number of cells with side length *l*.
p_r	The integral of the probability function.
pi	The constant ratio ≈3.14
r	The radius of the compact unit cell cylinder.
r_p	The radius of the particle.
$r\rho\rho s$	The final relative density of the compact in the flow chart.
S_c	The surface area of a single full cylinder in a compact cell.
t	The time of sintering.
ttm	A matrix contains the value of the sintering temperatures.
t_p	The practical time of sintering.
u	The radial displacement.
V_o	The initial volume of the compact.
V_C	The effective volume of one cylinder.
$V_{compact}$	The volume of the compact after sintering measured by Hg porosimetry.
V_i	The current value of the volume fraction of solid inclusions.
V_i^f	The final volume fraction in the fully sintered body.
V_i*	The critical volume fraction.
V_{in}	The theoretical volume of solid inclusions.
V_{ir}	The volume fraction of the rigid inclusions.
V_{iv}	The volume fraction of the voids.
V_{pore}	The volume of pores from Hg porosimetry.
$V_p(d)$	The volume of pores with diameter *d*.
V_S	The volume of the solid phase.

Symbol	Definition
V_{silica}	The true volume of viscous phase which is mostly formed from silica from Hg porosimetry.
V_{vis}	The theoretical volume of the viscous phase in the compact.
x	The ratio of the particle size (a) to the compacted length of the unit cell (l).
x_o	Is the initial value of x.
x_{max}	The highest value of x in Scherer model.
x_r	The neck radius.
y	Is a symbol related to l^* and σ_d assumed to make Eq. (2.40) a function to the standard deviation.
y_x	Is a variable inversely proportional with x assumed to make the integration of Eq. (2.22) easier.
y_o, y_{xo}	Are the initial values of y and y_x, respectively.
z	Is a variable related to the relative density assumed to make the integration of Eq. (2.30a) easier.
z_o	The initial value of z.
γ	The surface energy.
γ_b	The interface (or boundary) energy.
γ_{gh}	The grain boundary energy
γ_{sv}	The solid/vapor surface energy
ε_x	The strain in the x direction.
ε_f	The free strain.
ε_{fm}	The free strain of the matrix.
ε_c'	The strain rate of the composite.
η	The viscosity coefficient.
λ	The third root ratio of the theoretical volume of inclusion in the compact to the theoretical volume of viscous phase in the compact.
ν_m	Is Poisson's ratio.
ρ	The density of the cell.
ρ_o	The initial density of the unit cell or the initial value of ρ.
ρ_c	The relative density of the composite.
ρ_c'	The rate of the relative density of the composite.

Symbol	Definition
ρ_{co}	The initial value of the relative density of the composite.
$\overline{\rho}(\overline{Kt})$	The average relative density.
ρ_m	The relative density of the matrix.
ρ'_m	The rate of the relative density of the matrix.
ρ_{mo}	The initial value of the relative density of the matrix.
ρ_r	The radius of curvature at the surface.
ρ_{rd}	The relative density.
ρ_s	The theoretical density of the solid phase.
σ_m	The hydrostatic stress in the matrix.
σ_r	The radial component of the stress.
σ_{rm}	The radial component of the stress of the matrix.
σ_x, σ_y, and σ_z	The stresses in the x, y, and z directions, respectively.
σ_θ	The circumferential component of the stress.
$\sigma_{\theta m}$	The circumferential component of the stress of the matrix.
φ	The load-bearing function of the cross-sectional area.
φ_d	The equilibrium dihedral angle.

Chapter Five
Conclusions and Future Work

5.1 Introduction

This chapter is demonstrating the main conclusions obtained from the results which can be extracted from the model and from the fitting process. The development steps to this model are considered as a future work and are summarized and listed below.

5.2 Main Conclusions

The main concluded points can be summarized as follows:

1. The most limiting factor in the sintering of ceramic compacts that corresponded with the formation of viscous liquid is the magnitude of the effective viscosity of this liquid.
2. The solid inclusions have a strong effect in retarding the densification process, by increasing the value of the effective viscosity of the viscous liquid that is formed during sintering, which as a result decreases the rate of densification process.
3. The materials that can be regarded (or manipulated) as solid inclusions are the materials that didn't participate (or melted) in the viscous phase, and this is affected not only by the type of additive but also by the quantity of these additives, while a relatively little quantity of the materials (like alumina) reduces the viscosity of the viscous phase, a high quantity increases the viscosity and retards densification and act as solid inclusions as we saw in sample of group M21.

4. The particle size affects the densification process, because the higher particle size increases the viscosity of the viscous phase, as predicted by Coble [49], and retards densification.
5. The modified Scherer model predicts that; increasing the viscous phase may increase the densification rate slightly if the viscosity of this viscous phase is kept constant, because the more viscous phase will dissolve more solids in it; however the stronger effect is for the value of the effective shear viscosity.
6. The modified Scherer model predicts that increasing the sintering time increases the final density and the densification rate is retarded at final stages of sintering, this is due to full densification when the relative density approaches unity.
7. Increasing the firing temperature increases the densification rate because, this reduces the value of the effective viscosity of the viscous phase, but in condition that the increase in temperature doesn't induce much the crystallization processes, which may lead to increase the viscosity and as a result decreases the densification rate.
8. The modified Scherer model predicts well the results of densification process in ceramic materials, while the composite sphere and the self consistent models predicted a different shape of the densification curve; they predicted that the densification curve is exponential, but the present model and the experimental data of clay materials predict a semi logarithmic curve.
9. The present modified model predicts that the pore size distribution have a strong effect only in the last stages of densification if the distribution is wide, because the largest pores are relatively slow to close.

5.3 Future Work

The suggestions for future work are

1. The volume ratio of the solid inclusions to the viscous phase is better to be calculated directly from the phase diagrams, instead of supposing all the materials that may dissolve and compose the viscous phase participate in the viscous phase during sintering process as done in the present case.
2. Using the present geometrical model in building a numerical model which uses the finite element method or Monte Carlo method to see its applicability to the sintering process in ceramic materials.
3. The major factor that may test the applicability of the modified Scherer model and explains its modification advantages over the previous Scherer model is the viscosity of the viscous phase formed during sintering process; we suggest that this factor is measured practically to compare the practical results with the predicted viscosity values from this model and from Scherer model.

Chapter Four

Results and discussion

4.1 Introduction:

In this chapter we display the results from the fitting process that used to describe the manner of the effective viscosity of the used materials versus sintering temperature in addition to some densification related parameters. Then we display the results from the manipulation of the developed model in addition to the composite sphere model and the self consistent model which describes the effect of sintering temperature and the sintering time and the effect of pore size distribution on the densification process. Then we discus these results and curves and compare them with the practical data if they are available and compare them with the results of other publishing.

4.2 Models Related Parameters:

4.2.1 Viscosity:

The behavior of viscosity (η) as a function of sintering temperature as predicted by the modified Scherer model is as shown in the figure (4.1) and the figure (4.2) for samples of groups M21and M22 respectively.

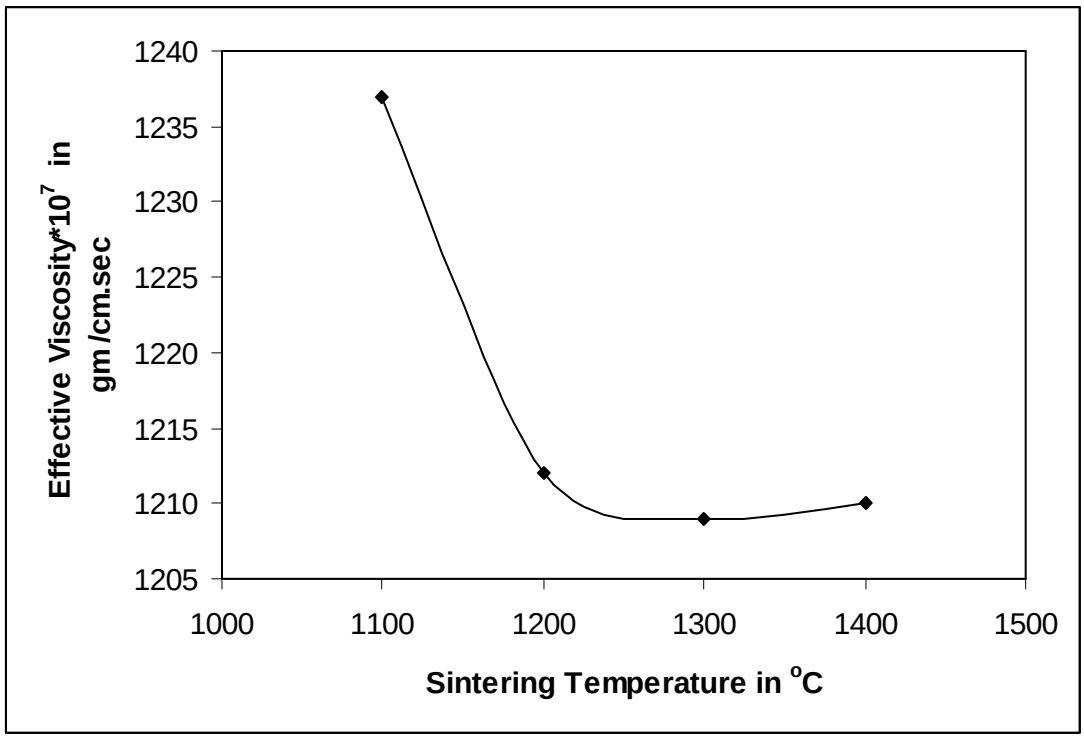

Figure (4.1) Viscosity versus sintering temperature of samples of group M21 (λ=0.723) as predicted by the Modified Scherer Model.

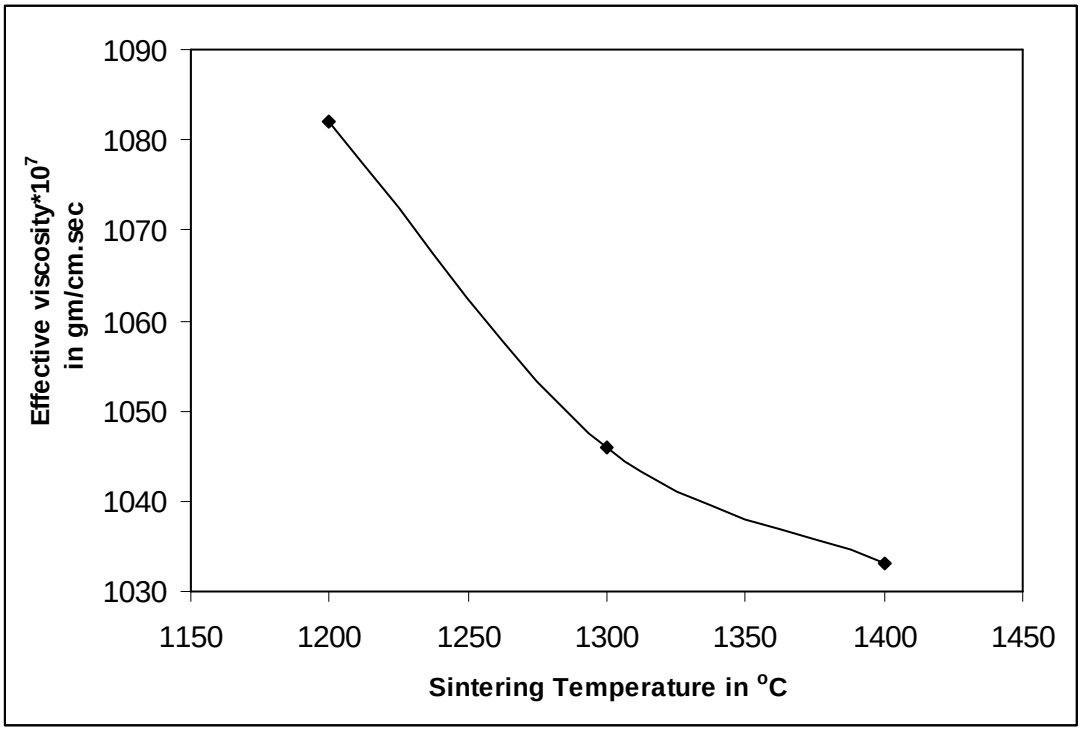

Figure (4.2) Viscosity versus sintering temperature of samples of group M22 (λ=0.669) as predicted by the Modified Scherer Model.

For comparison, figurers (4.3) and (4.4) show the values of effective viscosities versus sintering temperature for samples of groups M21 and M22 respectively as predicted by the Scherer model.

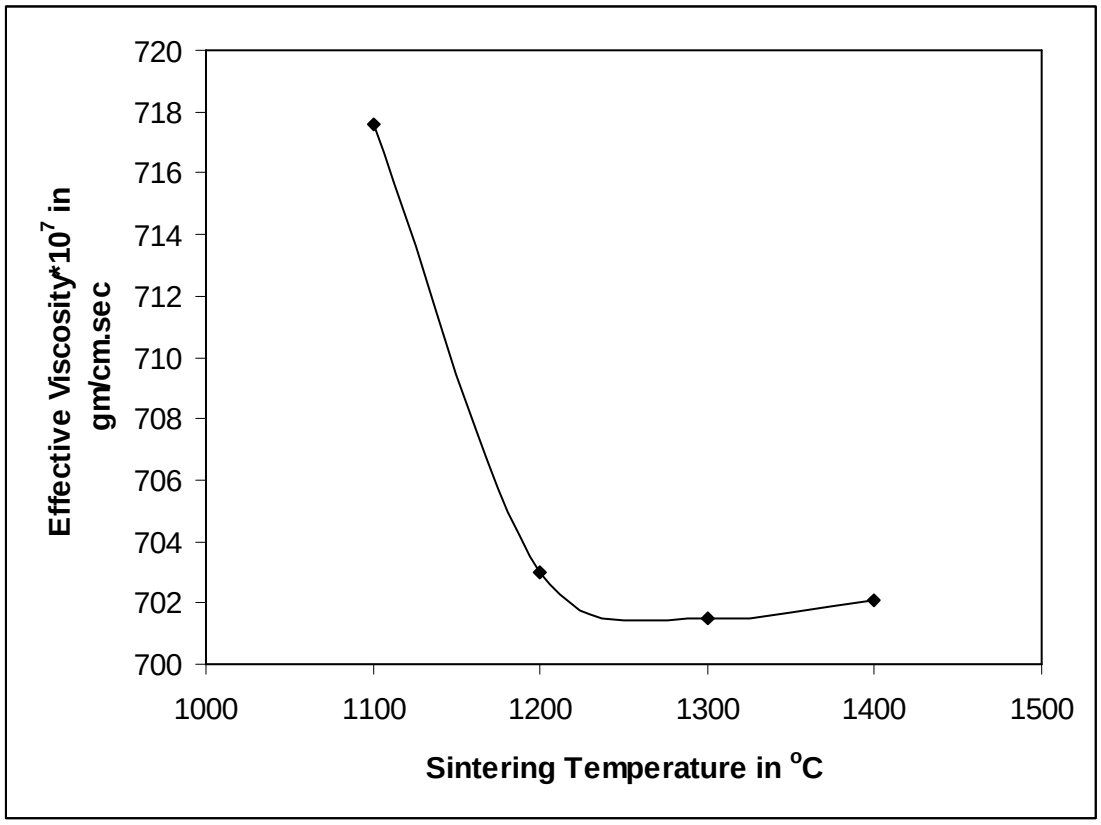

Figure (4.3) Viscosity versus sintering temperature of samples of group M21as predicted by the Scherer Model.

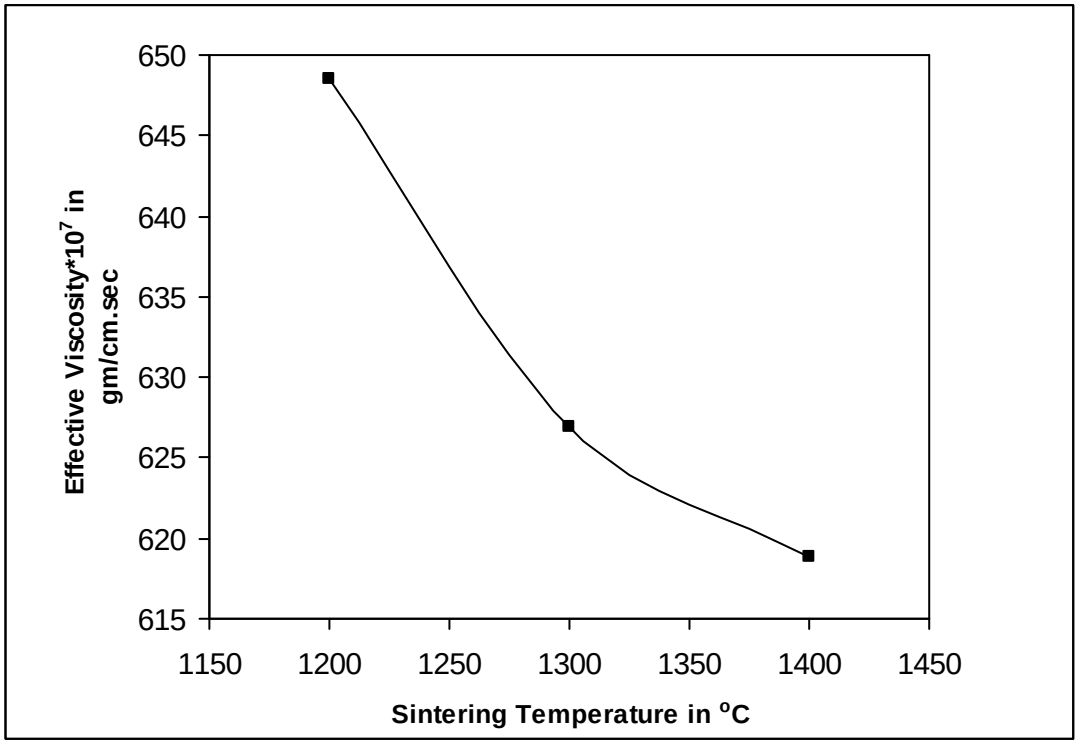

Figure (4.4) Viscosity versus sintering temperature of samples of group M22 as predicted by the Scherer Model.

4.2.2. Ratio of the Side Length of the Inclusions in the Cell per Unit Side Length of the Viscous Phase (λ):

Figure (4.5) shows the effect of the ratio (λ), which is the ratio of the side length of solid inclusions in the cell per unit side length of viscous phase on the relation between the relative density and the ratio (x), which is the ratio of the particle size per unit side length of the composite unit cell.

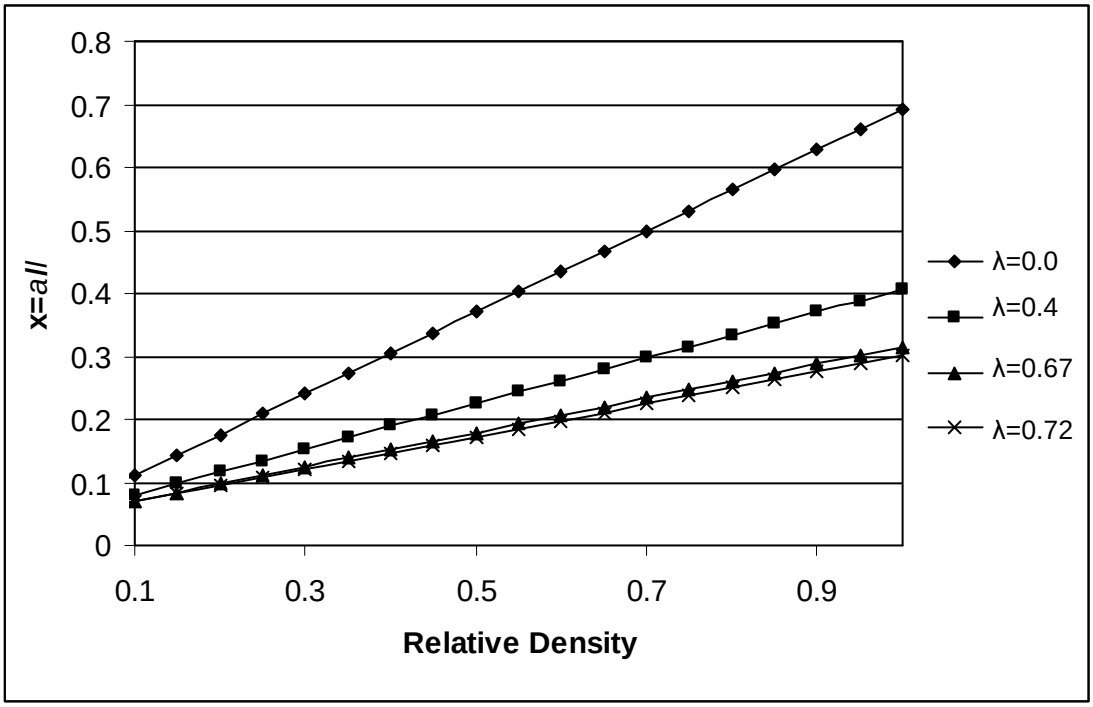

Figure (4.5) x versus relative density, λ=0, 0.4, 0.67 & 0.72.

4.3. Models Results:

Generally the results fall on three categories, which they are as follows:

1. Results that describe the effect of sintering temperature on the density after firing. These results come from the simulation by the modified Scherer model, the composite sphere model and the self consistent model.
2. Results that describe the variation of the relative density with sintering time.
3. Results that describe the effect of the standard deviation of pore size distribution on the densification process during sintering.

4.3.1 Results of the Effect of Sintering Temperature on Density after Firing:

The results are shown in figure (4.6). from figure (4.6) it is obvious that the results from the modified Scherer model are so close from the practical

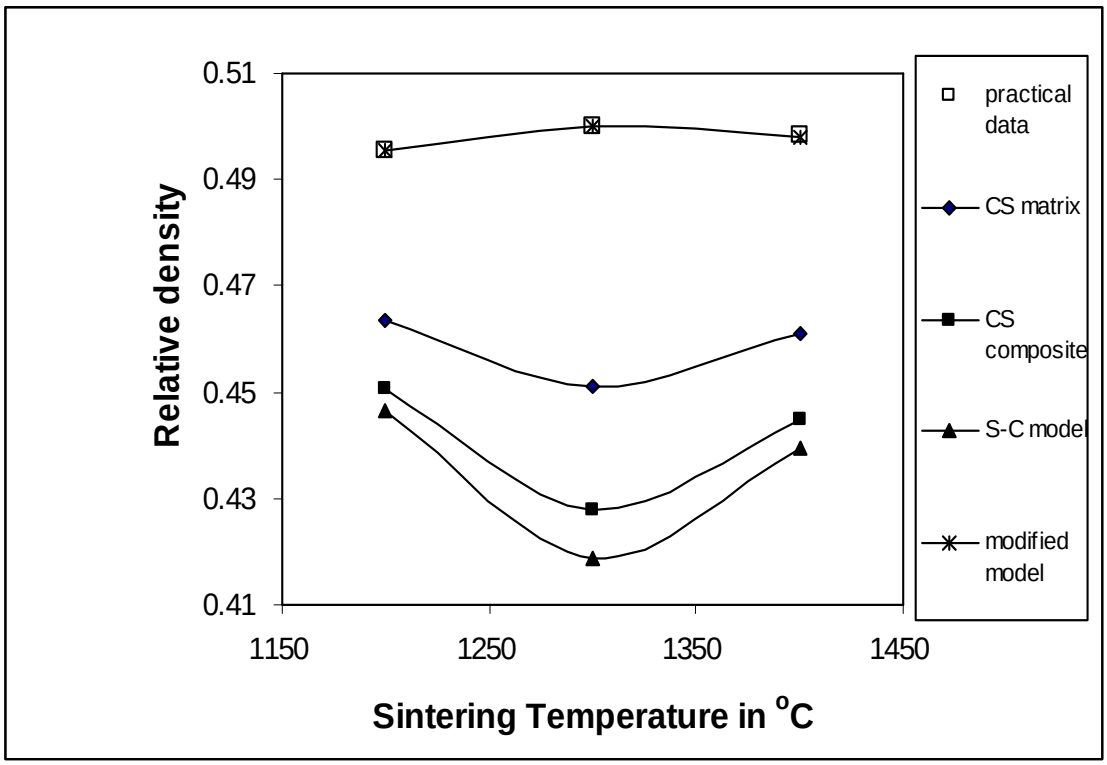

Figure (4.6) Relative density from various heterogeneous models versus sintering temperature for samples of group M21 fired for two hours.

results. Other models also offer good approximation to the practical results, but the best approximation from them is offered by the composite sphere model, which describes the densification process of the matrix of the composite. These results will be discussed later.

4.3.2 Results of the Variation of the Relative Density with Sintering Time:

The results are shown in figure (4.7). These results are computed using the modified Scherer model for the values of x less than x_{max} and for the

values greater than x_{max} the modified Mackenzie-Shuttleworth model is used by applying Eq. (2.32). From the figure it's obvious that the solid inclusions have a strong effect on densification process as the present model predicts.

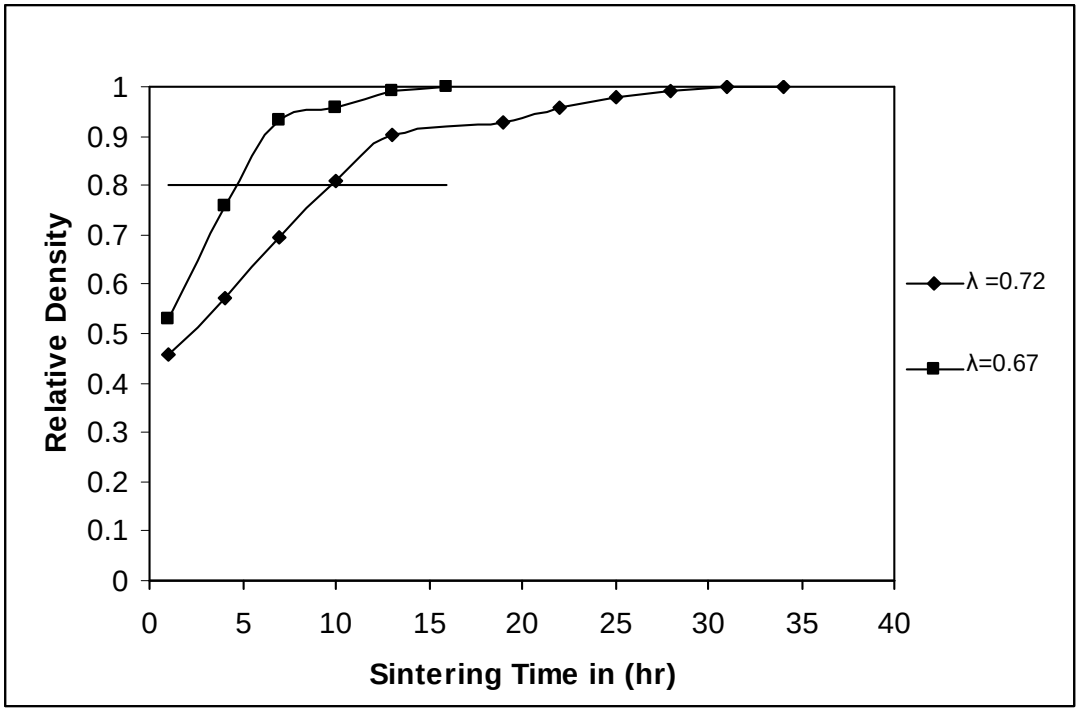

For comparison between models a sample from group M21 which was sintered at 1200 ^{o}C had been taken and the following models had been applied to it: the composite sphere model which describes the composite densification (CS composite) using Eq. (2.79) and Eq. (2.76a), the composite sphere model which describes the matrix densification (CS matrix) using Eq. (2.83), and the self consistent model (S-C model) using Eq. (2.93) and (2.79). These models had been applied, in addition to the modified Scherer model and the results are shown in figure (4.8).

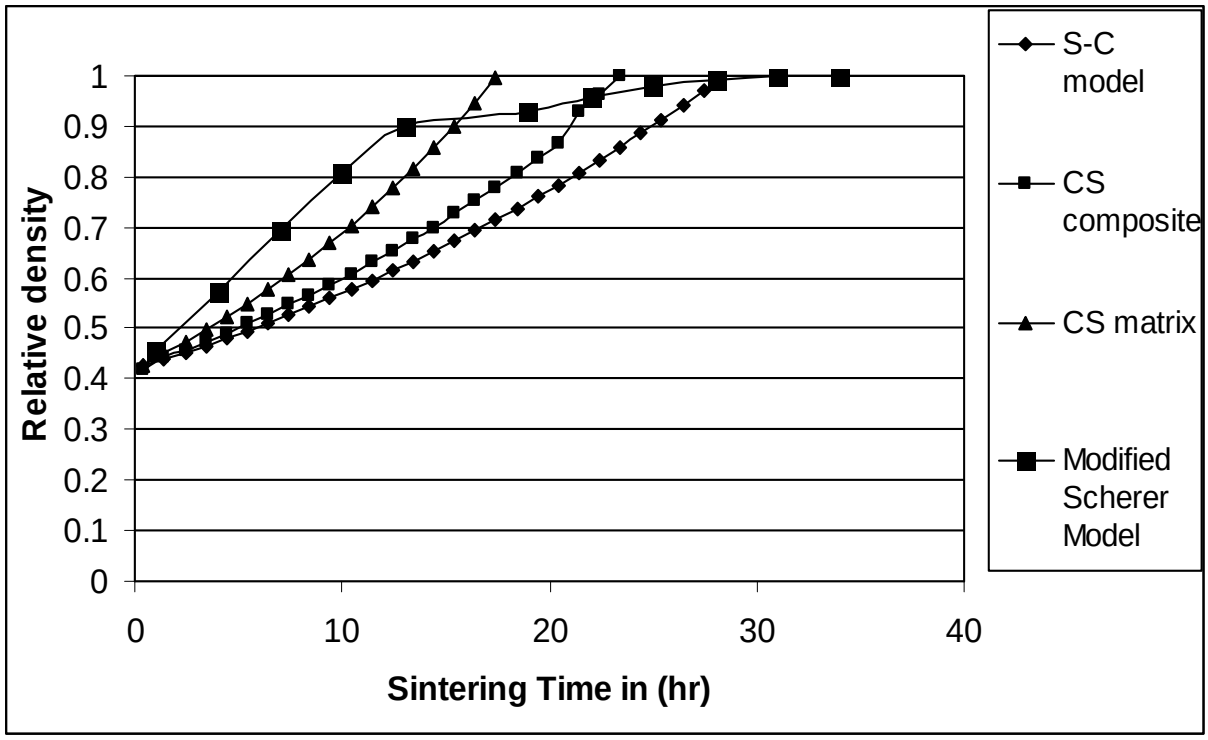

Figure (4.8) Relative density versus sintering time for sample from group M21 (λ=0.723) sintered at temperature equal 1200^{o}C found using various heterogeneous models as indicated in the list.

4.3.3 Results of the Effect of the Standard Deviation of Pore Size Distribution on the Densification Process during Sintering:

The results are shown in the figures (4.9) and (4.10) for samples of group M21 sintered at temperature 1200 ^{o}C and 1300 ^{o}C, respectively. From figures it is clear that the pore size distribution has a little effect on the densification process. However, generally it retards the densification process specially at the final stage of sintering process as the figures indicate.

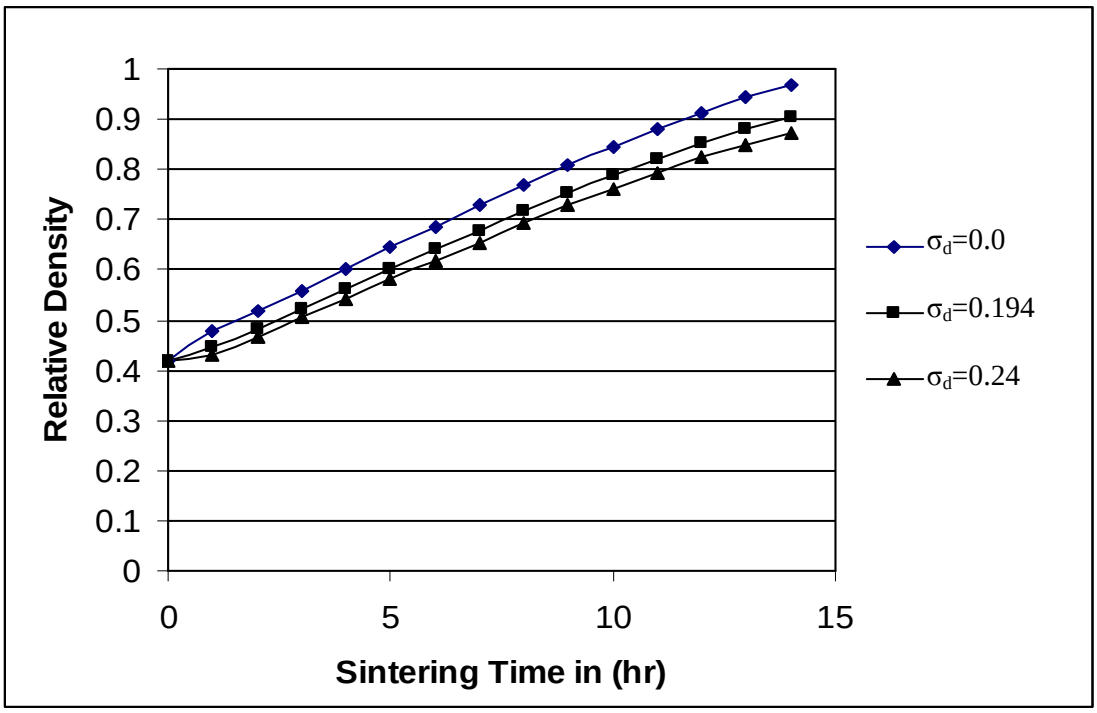

Figure (4.9) Effect of standard deviation of pore size distribution of sample from M21 group sintered at 1200°C.

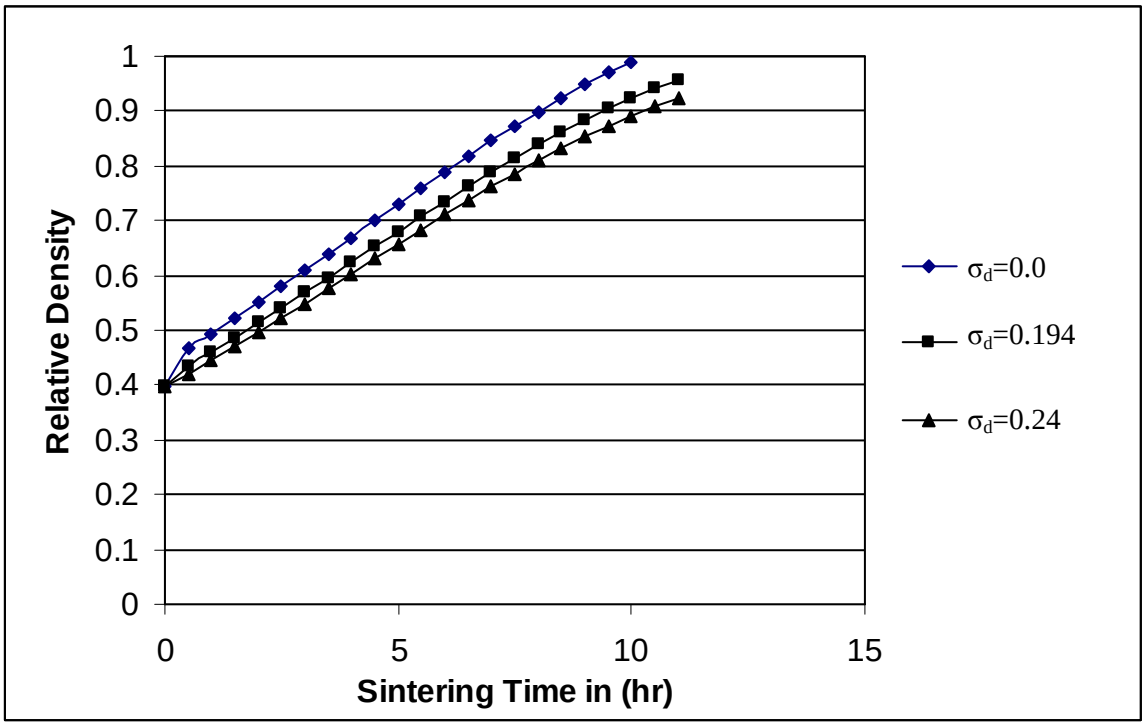

Figure (4.10) Effect of standard deviation of pore size distribution of sample from M21 group sintered at 1300°C.

4.4 Discussion:

In this work the Scherer model for viscous sintering of open pore systems for materials such as glass or silica gel, which did not contain solid inclusions in a considerable amount is modified and applied to some heterogeneous multiphase systems that known to be sintered by viscous sintering and contains a considerable (non negligible) amount of solid inclusions such as some of the silicate systems (ex: porcelain or kaolin). These systems form a viscous phase during sintering (basically consisted from silica) [12, 52]. The silicate melt formed at high temperatures has a very high viscosity about (10^{13}) poise. In this case, the formation of the dense, strong product is due to the continuity of the very viscous silicate melt over the whole system; the melt serves, then, as a bond for the solid grains dispersed in it [13]. On this base and according to Scherer model [6] it has been supposed that the body of the compact consists from a cubic array formed by intersecting cylinders, which represent the strings of silicate particles. These cylinders work as a bond for the solid grains (inclusions) dispersed in the viscous phase. A unit cell is assumed as Scherer did, the cylinders penetrate the cell as in figure (2.1b), and the solid inclusions are supposed to be placed at the center of the cylinders. The effect of solid inclusions is taken into account by considering the effect of solid inclusions on the side length of the unit cell that the viscous phase can propagate through it. These solid inclusions will decrease the length side that the viscous phase can propagate through it and achieve densification. Each unit cell will contain a volume ratio from inclusions equal to the volume ratio in the compact. According to these assumptions the formulas derived by Scherer [6, 36] are modified and used to study the densification process during sintering for some of the Iraqi clays and to simulate the effect of several parameters on it. The first studied parameter is the effect of sintering temperature on the densification process. Here, also two models of heterogeneous systems (that also modified by Scherer) have

been applied to compare their results with the results from the modified model, and to study the applicability of each model. The models are the composite sphere model (which used to study the matrix densification (CS matrix) and the composite densification (CS composite)), and the self consistent (S-C) model.

From figure (4.1) it is obvious that for samples of group M21 the effective viscosity drops fast initially until a value of sintering temperature slightly above 1200^{o}C where the curve stop decreasing and become a semi plateau curve. The semi plateau end is as a result of crystallization process. This indicates that the crystallization process largely affect the viscosity of the viscous phase in the compact as the predictions of reference [53].

From figure (4.2) for samples of group M22 it has been noted that the curve of the effective viscosity continues decreasing with temperature increasing, and no semi plateau end is found. This indicates that the crystallization process in samples of group M22 is less than that for M21. Also it has been noted that the magnitudes of the viscosity coefficient of samples of group M21 is higher than that for M22.This may be due to the higher ratio of solid inclusions (λ) in M21 especially from alumina, because high amounts reduce the mobility of liquid glassy phase, because of induced structural forms in the liquid phase [12]. This could induce crystallization in M21 and makes the values of viscosity for M21 higher than that for M22.

From figures (4.1) and (4.3) and figures (4.2) and (4.4) it is clear that the viscosity values predicted by the modified Scherer model equal about $(1+\lambda)$ the viscosity values predicted by Scherer model. So the modified Scherer model predicts a higher effect for the solid inclusions in increasing the values of the effective viscosity of the viscous phase formed during the sintering process, unfortunately, there are no practical measurements of the effective viscosity for the simulated samples, so which value is correct this will be a proposal for the future work to prove it practically.

Figure (4.5) also shows another difference between the values of the ratio x as predicted by Scherer model versus the relative density, and that as predicted by the modified Scherer model, the last one predicts a lower values of x versus the relative density with increasing the solid inclusions, because the geometry of the cell in the modified Scherer model describes the geometry of the matrix cell, so when the solid inclusions is increased the volume of the matrix cell will be decreased by a factor $(1+\lambda)^3$ and the relative density of the matrix will be higher than that predicted by Scherer model for the same value of x, but this does not mean the increasing in the rate of densification with increasing the solid inclusions because, the rate of increasing x in the modified Scherer model is slower than that in Scherer model as appeared from the comparison between Eq. (2.26a) for the modified Scherer model and Eq. (2.26b) for Scherer model, if these two equations are solved numerically for y and then the value of x is determined, it will be found that the value of x which is given from Eq. (2.26a) is lower than that given by Eq. (2.26b). This is due to the factor $(1+\lambda)$ which makes the solving of Eq. (2.26a) for (y) gives a higher value for (y) and as a result gives a lower value for (x). The conclusion from applying the model is with increasing the ratio of the solid inclusions to the viscous phase; the effective side length l^* of the matrix unit cell, which represent the cell that the viscous phase can propagate through it, will be shorter, then any increase in the value of x will have more effect in densifying the matrix that represented by the viscous phase, but this does not mean the increasing in the rate of densification because the rate of increasing x becomes slower with increasing the solid inclusions, and this retards densification with increasing the solid inclusions ratio. The decreasing in the side length of the unit cell that the viscous phase propagates through it leads to the decrease in the range of x, which can the modified Scherer model be applied in it on the densification process, as discussed in the explanation of Eq. (2.29b).

From figure (4.6) it is obvious that the results from the present modified model offer best applicability to the practical results. This may be due to the approximation for the value of interface energy, which is assumed to have the same value as that for silica, on the base that the silica represents the major material in the composite. The interface energy is applied in the case of the composite sphere and the self consistent models, while in applying the modified Scherer model there is no need to interface energy because the constant of proportionality between the reduced time and the practical time (K) is used directly to find the relative density, and this is an advantage point from the present model. The results also show that the composite sphere model considering the matrix densification (Eq. (2.83)) gives results better than the composite sphere considering the densification of the composite (Eq. (2.79)). This may be because the equation of free strain rate Eq. (2.94), is determining the free strain rate for the matrix not for the composite, but in the present work, Scherer [20] suggestion had been followed to use this equation to describe the free strain rate of the composite and to substitute it as ε_c' in Eq. (2.77). Generally the composite sphere model is better applied to the densification than the self consistent model; this is due to the enormous liberties with the geometry of the material combination of the self consistent model [21].

Figure (4.7) shows the densification process for samples of groups M22 and M21; for the values of x larger than x_{max} the modified Mackenzie-Shuttleworth model is used. The figure shows obviously the effect of solid inclusions on the values of the relative density versus sintering time. While M22 reaches a relative density equal 0.8 at firing time equal about five hours, sample M21 reaches the same relative density at firing time more than ten hours as the modified Scherer model predicts. So the solid inclusions strongly affect the densification process in viscous sintering, but the type of their effect is limited by the type of the inclusions and their quantity and the temperature

of sintering [12]. However, their effect on sample M21 was increasing the value of viscosity, and as a result retards densification.

Figure (4.8) shows the predicted densification process for sample of group M21 with the modified Scherer model, the composite sphere model considering matrix and composite densification and the self consistent model. All the last three models predict an exponential relation between the relative density and time, just the modified Scherer model predicted a semi logarithmic relation, unfortunately no detailed data is available for the densification process to limit which model is better applied, but the data from figure (1.9) for porcelain agrees well with shape of the curve predicted by the modified Scherer model but this does not mean that the simulated samples in this investigation will have the same densification curve because the used materials are different. However the investigation results of Rahaman and DeJonghe [54] on the solid inclusions in glass and as figure (4.11) clarifies agrees well with the composite sphere and the self consistent models predictions of the effect of solid inclusions on the densification process, the numbers at the end of the curves represent the volume fractions (V_i^f) of each sample. As it is obvious from figure (4.8) the modified Scherer model predicts that the densification is relatively fast at the initial stages of the sintering process, but at the last stages the densification rate becomes relatively slow. This happened because the densification rate is retarded due to full densification when the relative density approaches unity [53]. This part is predicted by the Mackenzie-Shuttleworth model, when the pores become closed pores and the rate of densification decreases.

The figures (4.9) and (4.10) show the effect of the pore size distribution represented by the standard deviation of pore size distribution on the densification process, the result agrees with the Scherer result [31], which was the standard deviation of pore size distribution has a little effect on densification process, even when the distribution is quite broad, it has a strong

effect only in the last stages of densification because the largest pores are relatively slow to close.

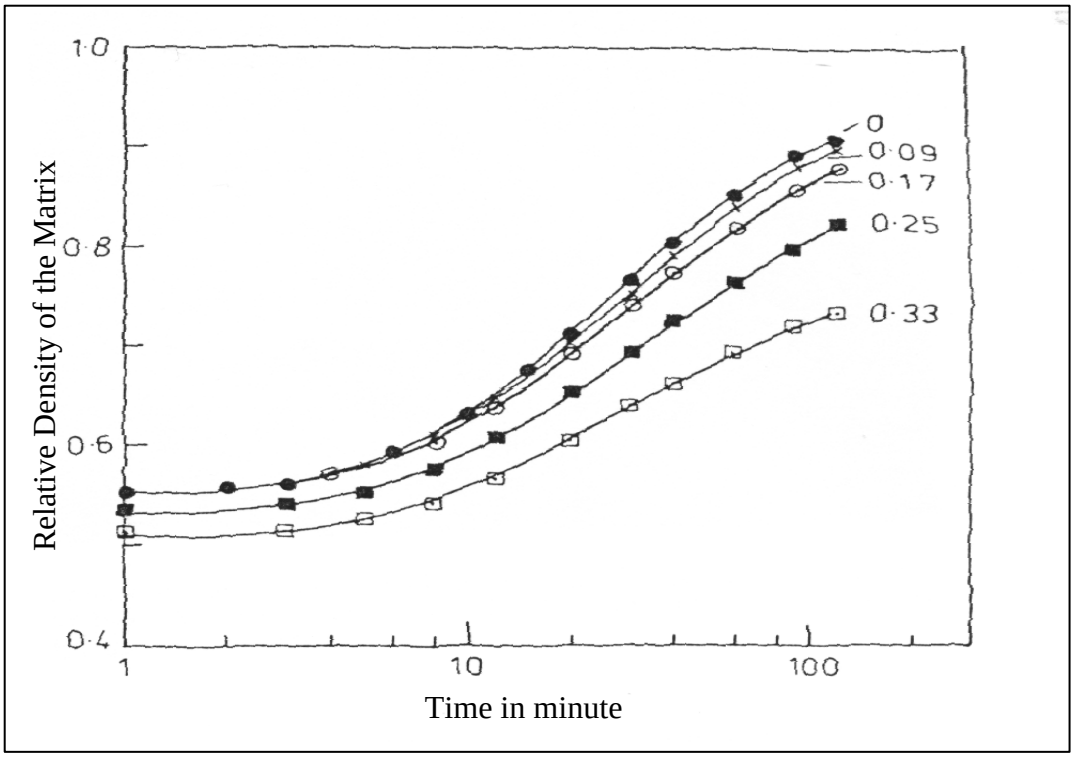

Figure (4.11) Relative density of the matrix versus Time in minute [54].

The effect of sintering temperature on the densification process is also observed from the figures, which is the predicted time is decreased by about five hours when the temperature of sintering is 1300^{o}C rather than 1200^{o}C. This is due to the decrease in the effective viscosity as the figure (4.1) indicates for sample M21 with the increasing of the sintering temperature from 1200^{o}C to 1300 ^{o}C.

Finally, it is difficult to put a collective model that describes the sintering process in ceramic, with any type of additive and at any quantity, because each type or each quantity may give a different action to the composite material, even the conditions of experiment may change the action of additives and the densification manner of the microstructure itself.

بسم الله الرحمن الرحيم

Chapter One
General Introduction

1.1 Introduction

The sintering process has been used throughout history. The ancient Egyptians sintered metal and ceramics as far back as 3000 B.C. [1]. Today, sintering process is used to manufacture a wide range of products, including rocket nozzles, nuclear fuel elements, golf clubs and porcelain plumbing fixtures [2]. Sintering process is a complex phenomenon in which several processes are occurring simultaneously [1]. By Herring, sintering is '…understood to mean any changes in shape which a small particle or a cluster of particles of uniform composition undergoes when held at high temperature' [3]. It is an inexpensive way of making parts, provided the finished part can be used as it is, and does not require additional machining. The difficulty is that, when a part is sintered, its size and shape change non-linearly, which needs to be taken into account by the designer of the unfired piece [2].

During the usual processing of ceramics, crystalline or non-crystalline powders are compacted and then fired at a sufficient temperature to develop useful properties. During the firing process, changes may occur initially because of the decomposition or phase transformation in some of the phases present. On further heating of the fine-grained, porous compact, three major changes commonly occur:

1. There is an increase in grain size
2. There is a change in pore shape
3. There is a change in size and number of pores, usually to give a decreased porosity [4].

Various models have been developed for the sintering process describing the densification and the change in porosity during this process. Mackenzie and Shuttleworth [5] calculated the rate of densification of a viscous body containing closed spherical pores.

Another model developed by Scherer [6], which describes the rate at which a cubic array of cylinders densifies by viscous flow driven by surface energy reduction, this model will be described in details in the next chapter. Kellett and Lange [7] put a model describes the densification process in solid state sintering.

The investigation is concerned with the modifications of assumed previous model for sintering process using different concepts to simulate the densification process, and study the effect of various parameters on the densification during the sintering of ceramic heterogeneous systems. The results were compared with the experimental data for the compacted sintered ceramic samples. The raw materials of the samples are from Iraqi kaolin and other materials.

1.2 Types of Sintering Processes

Sintering can occur in the presence or absence of a liquid phase. In the former case, it is called liquid-phase sintering, where the compositions and firing temperatures are chosen such that some liquid is formed during processing, as shown schematically in figure (1.1a). In the absence of a liquid phase, the process is referred to as solid-state sintering (figure 1.1b) [1]. In general, there are three types of sintering processes, which are:

1. Solid state sintering: All constituents of the compact remain solid during the entire process; all densification is achieved by change in grain shape. Sintering aids that will not form a liquid may be added in amounts ranging from a few hundred parts per million to over 20 %. This method is preferred for the production of technical ceramics with good

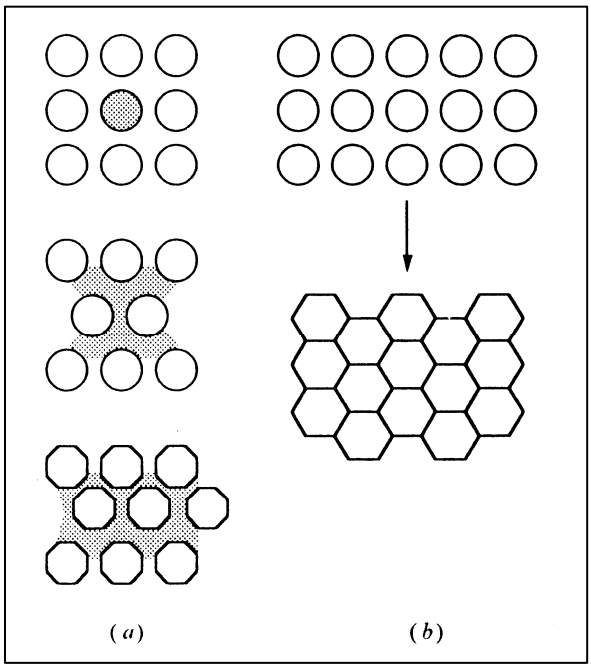

Figure (1.1) (a) Liquid-phase sintering (b) solid-state sintering [1]

mechanical, electronic or optical properties, particularly where optimum high temperature properties are required [8]. The macroscopic driving force operative during sintering is the reduction of the excess energy associated with surfaces. This can happen by: (1) The elimination of solid/vapor interfaces and the creation of grain boundary area, followed by grain growth, which leads to densification (figure 1.2a), and/or (2) Reduction of the total surface area by an increase in the average size of the particles, which leads to coarsening (figure 1.2b). These two mechanisms are usually in competition. If the atomic processes that lead to densification dominate, the pores get smaller and disappear with time and the compact shrinks. But if the atomic processes that lead to coarsening are faster, both the pores and grains coarsen and get larger with time [1]. The difference in free energy or chemical potential between the neck area and the surface of the particle provides a driving force which causes the transfer of material by the fastest means available.

If the vapor pressure is low, material transfer may occur more readily by solid-state processes, several of which can be imagined. As shown in

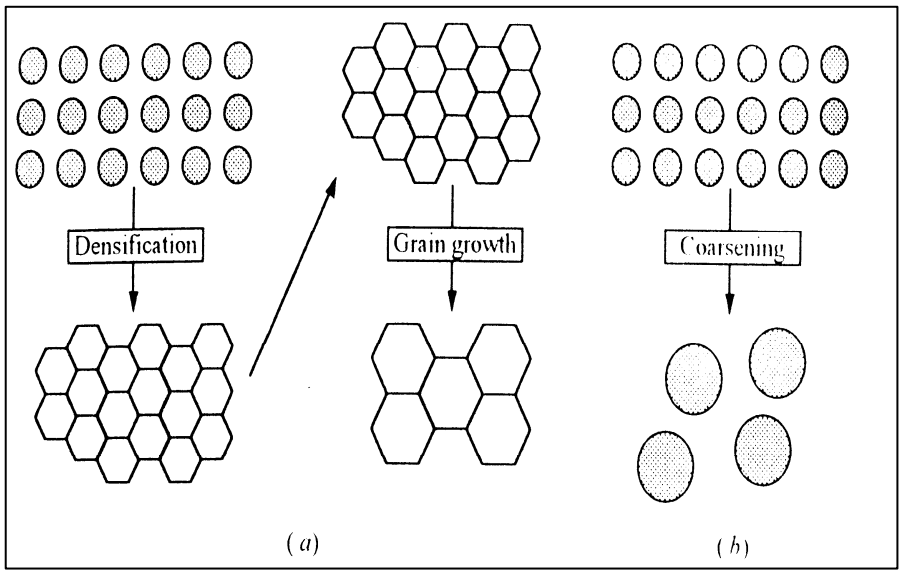

Figure (1.2), Schematic of two possible paths by which a collection of particles can lower its energy :(a) Densification followed by grain growth. In this case, shrinkage of the compact has to occur. (b) Coarsening where the large grains grow at the expense of the smaller ones [1].

figure (1.3) and table (1.1), in addition to vapor transport (process 3), matter can move from the particle surface, from the particle bulk, or from the grain boundary between particles by surface, lattice, or grain-boundary diffusion. Which one or more of these processes actually contributes significantly to the sintering process in a particular system depends on their relative rates, since each is a parallel method of lowering the free energy of the system. There is a most significant difference between these paths for matter transport: the transfer of material from the surface to the neck by surface or lattice diffusion, like vapor transport, does not lead to any decrease in the distance between particle centers. That is, these processes do not result in shrinkage of the compact and a decrease in porosity. Only transfer of matter from the

particle volume or from the grain boundary between particles causes shrinkage and pore elimination [4].

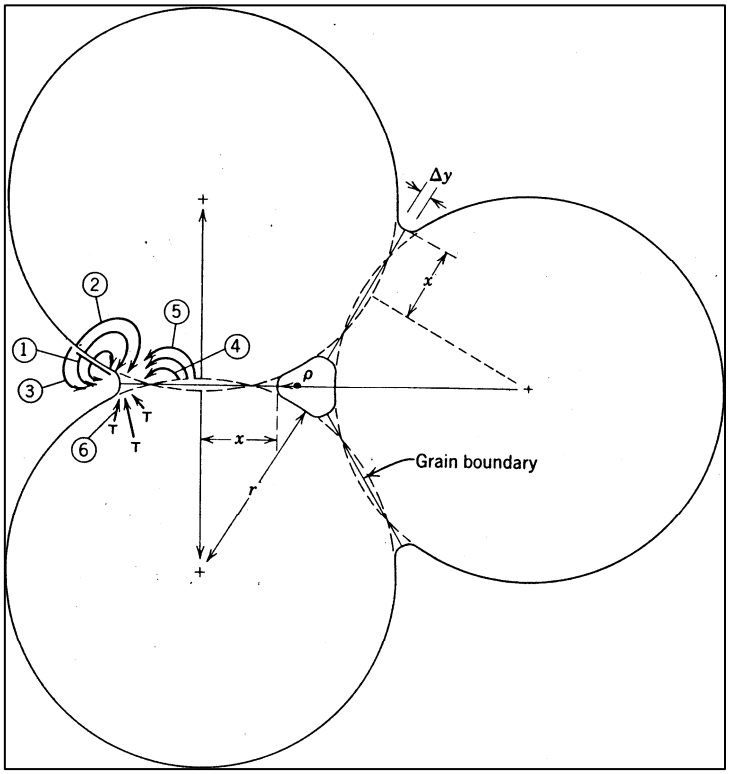

Figure (1.3): Alternate paths for matter transport during the initial stages of sintering [4].

A necessary condition for sintering to occur is that the grain boundary energy γ_{gb} be less than twice the solid/vapor surface energy γ_{sv}, which implies that the equilibrium dihedral angle φ_d which defined by the following equation has to be less than 180° for densification to occur [1]:

$$\gamma_{gb}=2\gamma_{sv}\cos(\varphi_d/2) \qquad (1.1)$$

Table 1.1 Alternate Paths for Matter Transport During the Initial Stages of Sintering [4].

Mechanism Number	Transport Path	Source of Matter	Sink of Matter
1	Surface diffusion	Surface	Neck
2	Lattice diffusion	Surface	Neck
3	Vapor transport	Surface	Neck
4	Boundary diffusion	Grain boundary	Neck
5	Lattice diffusion	Grain boundary	Neck
6	Lattice diffusion	Dislocations	Neck

2. Liquid phase sintering: The composition is such that enough liquid forms at the firing temperature to allow easy rearrangement of the particles, but not enough to fill the initial porosity; subsequent solution and reprecipitation of the solid in the liquid phase then allows re-shaping of the particles and formation of a dense body. This method is often effective and reasonably inexpensive, but the resulting grain boundary phase may be detrimental to the high temperature mechanical properties (e.g., creep resistance) [8].

   Liquid-phase sintering offers two significant advantages over solid-state sintering first, it is much more rapid; second, it results in uniform densification. The presence of a liquid reduces the friction between particles and introduces capillary forces that result in the dissolution of sharp edges and the rapid rearrangement of the solid particles. During liquid-phase sintering, the composition of the starting solids is such as to result in the formation of a liquid phase upon heating. The liquid

fanned has to have an appreciable solubility of the solid phase and wet the solid [1].

3. Vitrification: Heat treatment, which produces enough viscous liquid at the firing temperature, which implies to fill completely the porous spaces in the original powder compact, this process is called vitrification [8]. The factors determining the vitrification rate are the pore size, viscosity of the overall composition (which depends on amount of liquid phase present and its viscosity), and the surface tension. Equivalent densification results from longer periods of time at the same temperature. In controlling the process, the temperature dependence is great because of the increase in liquid content and lowered viscosity at higher temperatures. Changes in processing and changes in composition affect the vitrification process as they affect these parameters [4]. This process is relatively inexpensive and is of particular importance in the production of porcelain and clay-based ceramics [8]. For satisfactory firing the amount and viscosity of the liquid phase must be such that densification occurs in a reasonable time without the ware slumping or warping under the force of gravity. The relative and absolute rates of these two processes (shrinkage and deformation) determine to a large extent the temperature and compositions suitable for satisfactory firing [4]. For the materials of the present work vitrification process is the major kinetics of sintering process, so we will take it in more details.

1.3 Viscous Sintering Kinetics

If we consider two particles initially in contact as in figure (1.4), there is a negative pressure at the small negative radius of curvature ρ_r compared with the surface of the particles. This causes a viscous flow of material into the

pore region. On this concept Frenkel [9] derived an expression of the rate of initial neck growth which is given as:

$$\frac{x_r}{r_p} = \left(\frac{3\gamma_b t}{2\rho_r \eta} \right)^{1/2} \tag{1.2}$$

where x_r: is the neck radius, ρ_r: is the radius of curvature at the surface, r_p: is the radius of the particle, η: is the viscosity coefficient, γ_b: is the interface (or boundary) energy, and t: is sintering time.

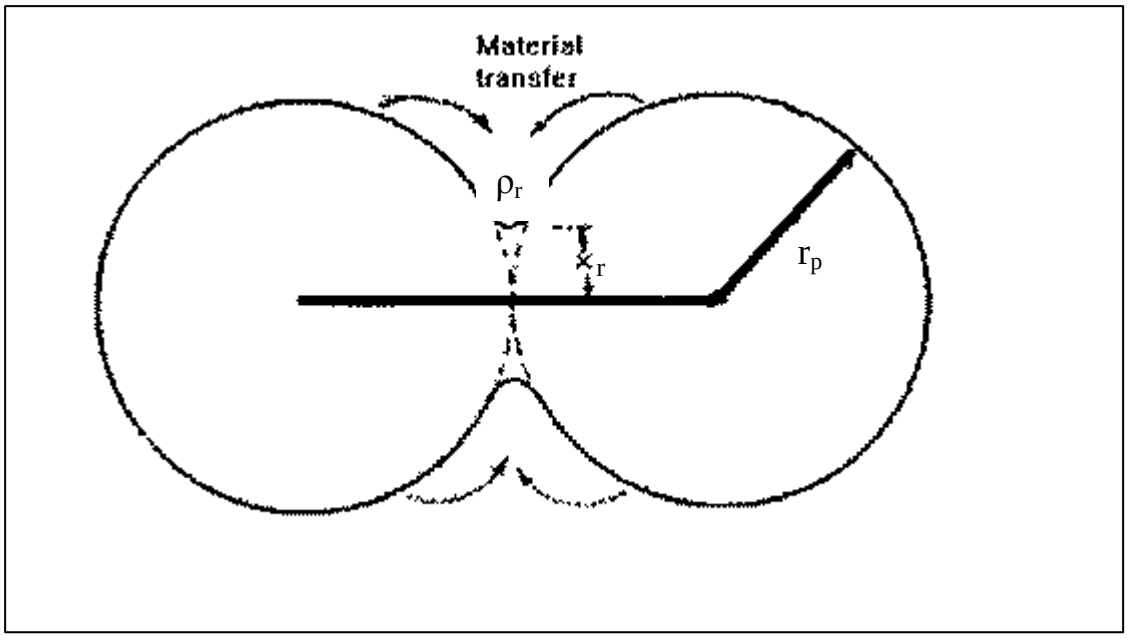

Figure (1.4) Initial stages of sintering by evaporation-condensation [4].

The increase in contact diameter is proportional to $t^{1/2}$; the increase in area between particles is directly proportional to time. Factors of most importance in determining the rate of this process are the surface tension, viscosity, and particle size. The shrinkage which takes place is determined by the approach between particle centers and is also given by Frenkel [9] as:

$$\frac{\Delta V}{V_0} = \frac{3\Delta L}{L_0} = \frac{9\gamma_b}{4\eta r_p} t \tag{1.3}$$

where ΔV, ΔL are the changes in compact volume and length respectively, and V_o, L_o are the initial volume and length of the compact. From the last relation, initial rate of shrinkage is directly proportional to the surface tension, inversely proportional to the viscosity, and inversely proportional to the particle size. The situation after long periods of time can best be represented as small spherical pores in a large body (Figure 1.5).

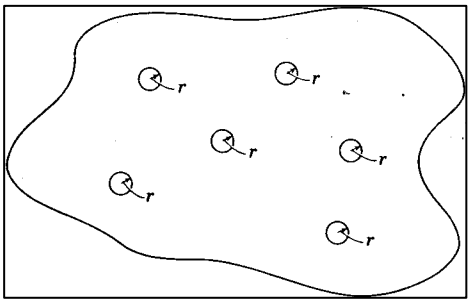

Figure1.5 Compact with isolated spherical pore near the end of the sintering process [4].

The time for complete densification is given by Kingery et al. [4] as:

$$t \approx \frac{1.5\, r_{po}\, \eta}{\gamma_b} \tag{1.4}$$

where (r_{po}) is the initial radius of the particles.

Different mechanisms dominate at different points in the sintering process, and different materials exhibit different mechanisms. For instance, viscous flow is the dominant mechanism when sintering amorphous materials, while grain boundary diffusion (obviously) plays no part. The opposite is generally true for crystalline materials. In liquid-phase sintering, viscous flow and related mechanisms play a significant role [2]. The importance of vitrification lies in the fact that most silicate systems form a viscous glass at the firing temperature and that a major part of densification results from viscous flow under the pressure caused by fine pores, and because the materials under study is from silicate systems we will take them in more details [4].

1.4 Silicate systems:

Silicates are materials composed primarily of silicon and oxygen, the two nominated abundant elements in the earth's crust; consequently, the bulk of soils, rocks, and sand come under the silicate classification [10].

Bragg [11] postulated that all silicates are built around a unit tetrahedron, composed of a silicon ion at the centre of four symmetrically placed oxygen ions. This unit is shown in figure (1.6) and may be chemically represented as $(SiO_4)^{4-}$.

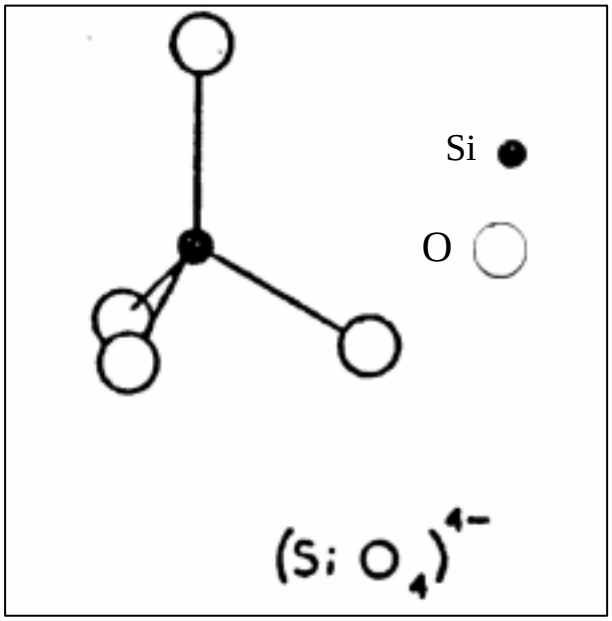

Figure (1.6) The Silicate tetrahedron [12].

There is a significant covalent character to the interatomic Si-O bonds; these bonds are directional and relatively strong. Regardless of the character of the Si-O bond, there is a (-4) charge associated with every SiO_4^{4-} tetrahedron, since each of the four oxygen atoms requires an extra electron to achieve a stable electronic structure. Various silicate structures arise from the different ways in which the SiO_4^{4-} units can be combined into one-, two-, and three-dimensional arrangements. We are concerned here with the layered silicates because their basic structure is characteristic of the clays and other minerals. The layered silicates are a two-dimensional sheet or layered

structure that produced by the sharing of three oxygen ions in each of the tetrahedral [10]. The system K_2O-Al_2O_3-SiO_2 will be taken because the eutectic in the subsystem potash-feldspar-silica-mullite determines the firing behavior in many compositions. Let us consider figure (1.7) , which shows an isothermal cut at 1200°C in the K_2O-Al_2O_3-SiO_2 system; this is the lower range of firing temperatures used for semivitreous porcelain bodies composed of about 50% kaolin (45%Al_2O_3, 55% SiO_2), 25% potash-feldspar, and 25% silica. In actual practice only a small part of the silica present as flint enters into the liquid phase, and the composition of the liquid depends on the fineness of the grinding as well as on the overall chemical composition. However, the amount of silica which dissolves does not have a large effect on the amount and composition of the liquid phase present. The liquid is siliceous and has a high viscosity; the major effect of compositional changes is to alter the relative amounts of mullite and liquid phases present. Since mullite is very fine-grained, the fluid flow properties of the body correspond to those of a liquid having a viscosity greater than the pure liquid phase [4]. The introduction of Na_2O or K_2O to silicate melts leads to the breaking of a certain number of oxygen bridges binding the silicon-oxygen tetrahedra with one another. As a consequence of breaking some of the oxygen bridges, the silicon-oxygen anions in the melt become smaller and the viscosity of the melt decreases. The melt becomes relatively homogeneous [13]. Fine grinding and intimate mixing also reduce the vitrification temperature. This change is caused in part by increased tendencies toward fusion equilibrium and uniform mixing of constituents and in part by the smaller initial particle and pore size.

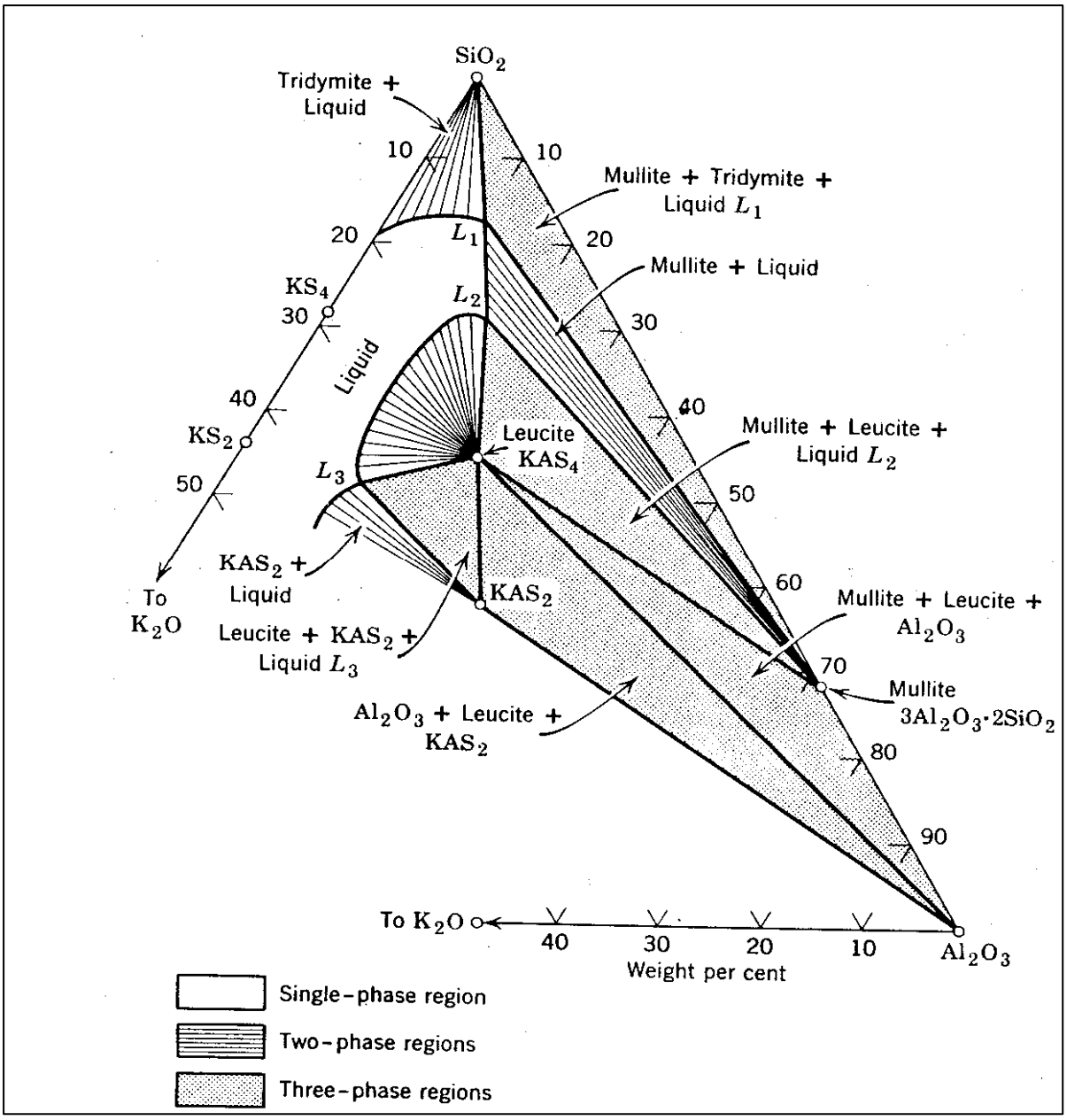

Figure (1.7) Isothermal cut in the K_2O-Al_2O_3-SiO_2 diagram at 1200°C [4].

The time-temperature relationship and the great dependence, of vitrification processes on temperature can perhaps be seen best in the experimental measurements illustrated in figures (1.8) and (1.9). As shown in these two figures, the time required for a porcelain body to reach an equivalent maturity changes by almost an order of magnitude with a 50°C temperature change. There are changes in both the amount and viscosity of the glassy phase during firing, so that it is difficult to elucidate a specific activation energy for the

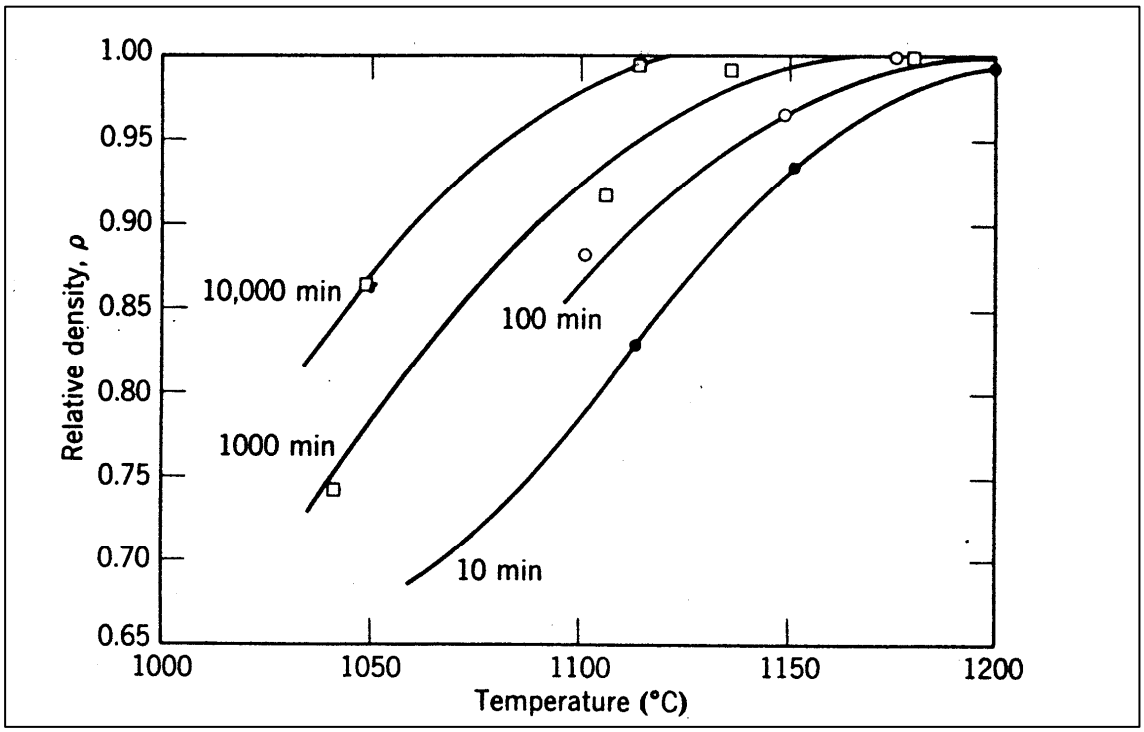

Figure (1.8) Effect of sintering temperature on the vitrification in porcelain [4].

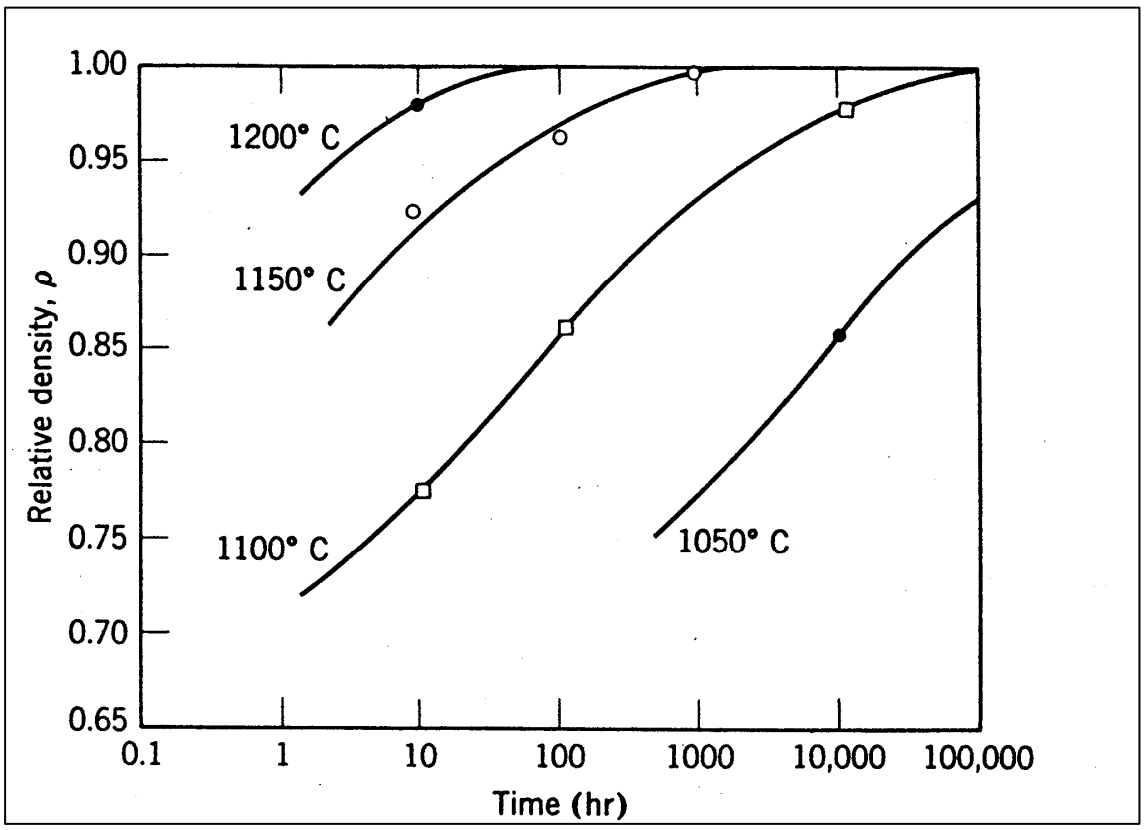

Figure (1.9) Effect of sintering time on the vitrification in porcelain [4].

process with which to compare the activation energy for viscous flow. However, the temperature dependence of the vitrification rate of a composition such as this (a mixture of clay, feldspar, and flint) is greater than the temperature dependence of viscosity alone. This is to be expected from the increased liquid content at the higher firing temperatures [4]. The last type of the sintering processes will be taken in more details in the next chapter, due to the complicated operations in the sintering process in kaolin.

1.5 Sintering Stages

Coble [14] described a sintering stage as an “Interval of geometric change in which pore shape is totally defined (such as rounding of necks during the initial stage sintering) or an interval of time during which the pore remains constant in shape while decreasing in size". Basing on that definition, three stages have been identified, and they are as follow:

1. Initial Stage: During this stage the interparticle contact area increases by neck growth and the relative density increases from about 60 to 65 percent. Neck formation is driven by the energy gradient resulting from the different curvatures of the particles and the neck [2]. For this stage the analysis is based on assumed geometric changes that occur between pairs of contacting spheres. When the grain boundary is the material source, shrinkage will occur, while when the particle surface is the material source only neck growth will take place. The processes of evaporation-condensation and surface diffusion can only supply material from the particle surface and hence only causes neck growth [15]. Surface diffusion is usually the dominant mass-transport mechanism during the early stages of neck growth, as the compact is heated to the sintering temperature [2].

2. Intermediate Stage: Intermediate phase sintering begins when adjacent necks begin to impinge upon each other [2], which is characterized by continuous pore channels that are coincident with three grain edges. During this stage, the relative density increases from 65 to about 90 percent by having matter diffuse toward, and vacancies away from the long cylindrical channels [1]. The packing density and coordination number of the green packing are important during this stage. A high green packing density produces rapid sintering with relatively few pores in the final object. Very low green packing densities, which are also associated with low coordination numbers, can lead to coarsening (increase in mean grain size) without densification (decrease in porosity). In extreme cases, this may lead to open-pore structures and lacking in structural integrity [2]. See figure (1.10).

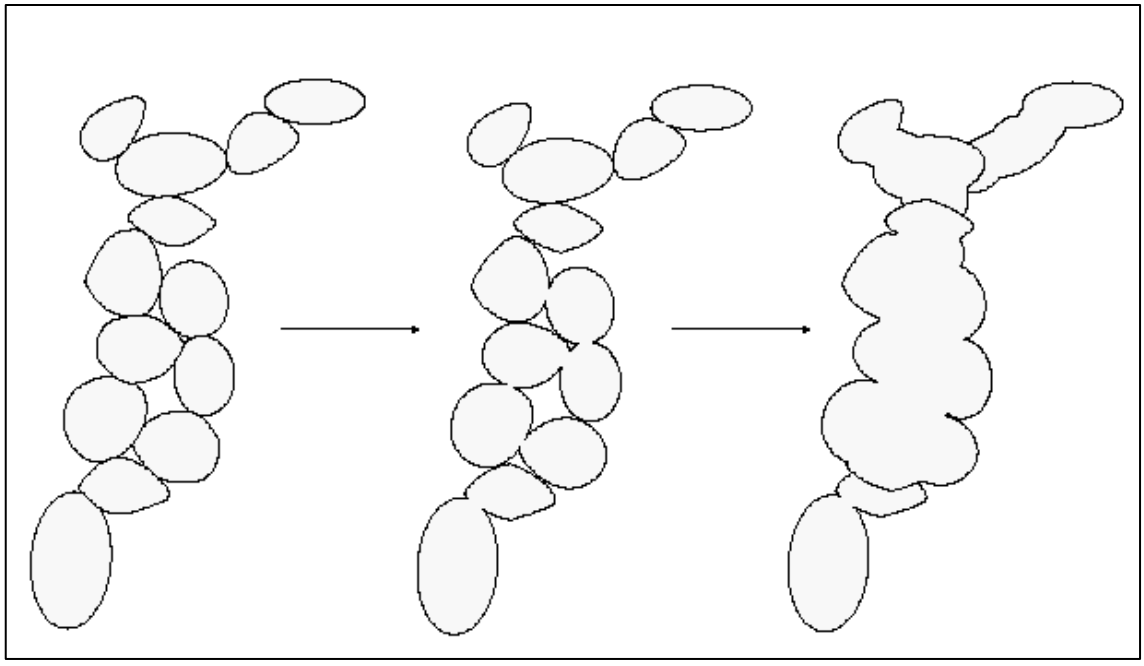

Figure (1.10) Coarsening resulting from low coordination number at intermediate stage of sintering [2].

During intermediate stage sintering, grains begin to form from the individual particles, and the material's final grain structure begins to

develop. Pore networks form along the grain boundaries. At the beginning of the intermediate stage, the pores form a network of interconnected cylindrical pores broken up by necks. By the end, the pores are smoother and begin to pinch off and become isolated from each other. Bulk transport mechanisms, such as grain boundary diffusion and volume diffusion, dominate the sintering process during this stage. As stated previously, these bulk transport mechanisms cause material to migrate from inside the particles to the surface, resulting in contact flattening and densification [2].

3. Final Stage: Begins when the pore phase is eventually pinched off and is characterized by the absence of continuous pore channels. Individual pores are either of lenticular shape, if they reside on the grain boundary, or rounded, if they reside within a grain [1]. Final stage sintering is much slower than the initial and intermediate stages. As grain size increases, the pores tend to break away from the grain boundaries and become spherical [2]. An important characteristic of this stage is the increase in pore and grain boundary mobilities, which have to be controlled if the theoretical density is to be achieved [1]. In some cases, pore growth during final stage sintering can lead to a decrease in density, as gas pressure in the larger pores tends to inhibit further densification. This can be mitigated by having the final stage sintering occur in a partial vacuum [2].

1.6 Models of Heterogeneous Systems:

Two models have been taken to apply them on the sintering process in heterogeneous systems, these models are, the composite sphere model, and the self-consistent model.

1.6.1 The Composite Sphere (CS) Model

The composite spheres model was introduced by Hashin [16]. This model is of interest principally as a model for a continuous matrix containing spherical inclusions [17]. The composite sphere (CS) model has also been used to model the densification rate of a composite consisting of a sintering powder (the matrix) containing rigid inclusions [18, 19, 20]. This is analogous to the analysis of thermal stress, with the strain rate of densification taking the place of the thermal strain. The rule of mixtures gives the contraction rate of the composite as a weighted average of the contraction rates of the matrix and the inclusions. The composite is predicted to sinter more slowly than the matrix alone, because the densification rate of the inclusions is zero. The CS model recognizes that the contraction rate of the matrix, represented by the cladding of the sphere, is retarded by stresses generated by inclusions, represented by the core of the sphere. Therefore, the densification rate is slower than predicted by the rule of mixtures [20]. The model is composed of a gradation of sizes of spherical particles embedded in a continuous matrix phase. The size distribution, however, is not random, but rather has a very particular characteristic. The composite spheres model is shown in figure (1.11). The broken curves shown in this figure are taken to define a region of the matrix phase associated with each particular particle. The ratio of radii a_{co}/b is taken to be a constant for each composite sphere, independent of its absolute size, where (a_{co}) is the radius of the core; (b) is the radius of the spherical particle.

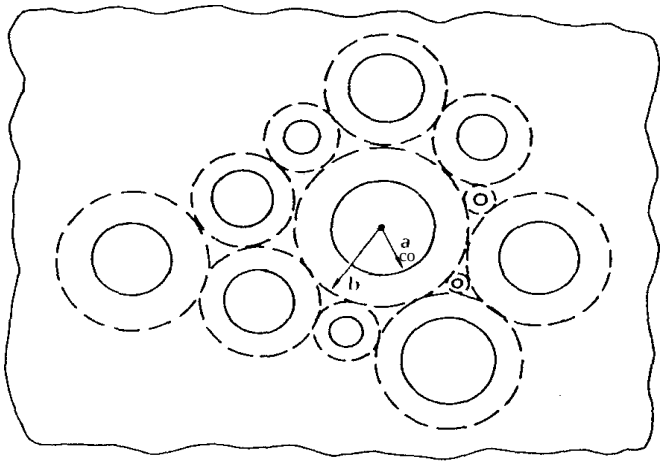

Figure (1.11) Composite sphere model [21].

Thus there must be a specific gradation of sizes of particles such that each composite sphere has (a_{co}/ b) = constant, while still having a volume filling configuration. Obviously, this distribution requires particle sizes down to infinitesimal sizes. This model would be expected to provide reasonable results for actual systems that do have a rather fine gradation of sizes. Quite obviously, this model would not be expected to provide reasonable results for systems containing single size particles, at high concentrations [21]. In the next chapter, the effect of the inclusions on the sintering rate of the matrix will be calculated by using the CS model [20].

1.6.2 The Self-Consistent(S-C) Model:

The method of the self-consistent scheme was first derived by Hershey [22] and Kroner [23] to model the behavior of polycrystalline materials. Such materials are just one phase media, but because of the random or partially random orientation of the crystals, discontinuities in properties exist across crystal interfaces. Thus, the properties vary with position, and this is certainly a particular type of heterogeneous media. When applying the method to polycrystalline aggregates, a single anisotropic crystal is viewed as a spherical

or ellipsoidal inclusion embedded in an infinite medium of the unknown isotropic properties of the aggregate. Then the system is subjected to uniform stress or strain conditions at large distances from the inclusion. Next, the average orientation of the stress or strain in the inclusion is set equal to the corresponding applied value of stress or strain. There results a condition from which the isotropic effective properties can be solved [21]. The extension of the self-consistent scheme to multiphase media was given by Hill [24] and Budiansky [25]. As discussed by Budiansky the method has a very simple geometric interpretation. Specifically, each phase of the composite is alternatively viewed as being lumped as a single ellipsoidal inclusion in an infinite matrix of the unknown effective properties of the problem. Applying uniform stress or strain conditions at infinity allows the determination of the average conditions in the inclusion. After this operation is performed for all phases, the average conditions are known in all phases, in terms of the individual phase properties and the effective properties. Hence, average conditions in the entire composite are known and the effective moduli can be calculated from the averages. Coupled equations are obtained to be solved for the effective shear and bulk modulus in terms of the properties of the individual phases and their volume fractions. Although the method for multiphase media seems straightforward, there are some problems with it. An indication of the difficulty can be observed in the cases of rigid inclusions and cavities. As noted in Budiansky [25] in the case of cavities, the predicted effective shear modulus G is given by

$$G = \frac{3(1-2V_{iv})G_m}{1-V_{iv}} \tag{1.5}$$

where V_{iv} is the volume fraction of the voids, and G_m is the shear modulus of the matrix. Whereas for rigid inclusions in an incompressible matrix phase

$$G = \frac{G_m}{1 - \frac{5}{2} V_{ir}} \qquad \text{for} \qquad 0 \le V_{ir} < \frac{2}{5} \qquad (1.6a)$$

and

$$G = \infty \qquad \text{for} \qquad V_{ir} = \frac{2}{5} \qquad (1.6b)$$

where in the last case $V_{ír}$ is the volume fraction of the rigid inclusions. Thus *(G)* becomes zero at a volume fraction of V_{iv}=0.5 in the case of voids, and (it becomes infinite at a volume fraction of $V_{ír}$ = (2/5) in the case of rigid inclusions. Clearly, there is a very strange behavior associated with the application of the self-consistent scheme to multiphase media. As Christensen [21] noted this is due to the liberties that the method takes with geometry of the material.

1.7 Historical Review

The starting of the theory of viscous sintering began in 1945 when Frenkel [9] assumed that the energy dissipated in viscous flow is equal to the energy gained by the decrease in surface area during densification. Using this assumption, he obtained expressions for the rate of growth of a neck between glass spheres and for the rate of linear shrinkage of a compact of glass spheres. Experimental studies by Kuczynski in 1949 [26] and by Kingery and Berg in 1951 [27] have supported the predictions of Frenkel's analysis.

Cutler and Henrichsen in 1968 [28] have shown that compacts of nonspherical particles depart markedly from the behavior predicted for spheres.

Mackenzie and Shuttleworth in 1949 [5] calculated the rate of densification of a viscous body containing closed spherical pores. They developed a model for the shrinkage of spherical bubbles in a viscous

matrix. The simplicity of the geometry enabled them to write exact expressions for the energy dissipation and change in surface area during sintering. This model can apply to bodies with a large volume fraction of pores, as long as the flow fields surrounding neighboring pores do not interact significantly. However, it most naturally applies to the last stages of densification, when the relative density is larger than 90% and the body contains only isolated closed pores.

Coble in 1961 [29] presented a model for the bulk diffusion transport with the grain boundaries as vacancy sinks when the pore phase is continuous and coincident with three grain edges, and also when the pore phase is discontinuous and located at four grain corners. These models predict that the rate of density change is constant when the diffusion coefficient and grain size are constant. He also divided the sintering process into three stages, and defined the stage as ‘it's an interval of time during which the pore remains constant in shape while decreasing in size’.

Beere in 1975 [30] presented a unifying theory for the stability of penetrating liquid phases and sintering pores, by presenting a model of grain edge porosity which is equally applicable to liquid precipitates, to fission gas swelling in nuclear fuels and to powder compacts. He showed that the morphology of the pores depends on the ratio of their surface to grain boundary energies and their volumes. And he showed that the stability of the porosity decreases with increasing the dihedral angle. And he predicted that liquid phases possess large driving forces for penetration and powder compacts have large driving forces for sintering.

Scherer in 1977 [6] proposed a model which describes the rate at which a cubic array of cylinders densifies by viscous flow driven by surface energy reduction, the surface area change can be expressed exactly, but the assumed flow pattern was approximated. The model was expected to provide a

reasonable representation of a flame oxidation preform; phase separated and leached glass or a silica gel.

At the same year Scherer [31] extended his previous model by considering a Gaussian distribution of pore sizes in the body of the compact, and he studied the effect of breadth of the distribution of pore sizes on the densification kinetics. He found that the effect is small except for very broad distribution, and his model manipulated sintering process at constant sintering temperature.

Rag and Bordia in 1984 [18] studied and analyzed the time dependent sintering of a bimodal powder compact, consisting of two regions which sintered at different rates. They assumed explicit spring–dashpot elements to represent the constitutive properties of a porous material. Their results were obtained in terms of a non-dimensional parameter, which equal to the ratio of the shear relaxation rate per densification rate. The small value of this parameter give negative values of Poisson's ratio, so they are unacceptable as references [32, 33] postulated.

Hsueh et al. in 1986 [34] developed a method for calculating viscoelastic stresses that develop around heterogeneities during sintering. The method had used constitutive laws derived from experimental data; and obtained on porous partially sintered body, however, the model predicted that Poisson's ratio is negative ($v_p \approx -1$) until the body is almost fully dense.

Scherer in 1987 [20] used two models of heterogeneous systems to approximate the viscous sintering in a material contains rigid inclusions. These models are the composite sphere model and the self consistent model. In the composite sphere model the compact is represented by a composite sphere with the core representing the solid inclusion. In the self-consistent model, the sintering material is regarded as being surrounded by a composite matrix with slower densification rate. The result differs only in that the shear

modulus of the matrix is replaced by the shear modulus of the composite in the self-consistent calculation.

Kellet and Lange in 1989 [35] put a model that describes the densification process in linear array and in closed array of particles, and they showed that the grain boundary motion in a sintering array of particles can be limited by the geometry of the sintered particle net work.

Scherer in 1991 [36] studied the effect of the cell shape that supposed in his model of viscous sintering, by assuming the shape of the cell as octahedral, tetrahedral, inverse tetrahedral and cubic, and he studied the effect of the cell shape on the densification process and he found that the effect is small.

Olevsky and Bert in 1997 [37] considered viscous sintering of a porous ball with various initial distributions of porosity versus radius. They elaborated the numerical algorithms based on the differential quadrature method (DQM) and an arbitrary Eulerian-Lagrangian version of the finite element method (FEM).

Olevsky et al. in 2002 [38] modeled Sintering shrinkage anisotropy using a coupled meso-macro-scale analysis. They simulated Microstructural evolution during sintering of 2D compacts of elongated particles incorporating ellipsoidal oriented pores at grain junctions using both a kinetic, Monte Carlo algorithm and a micro-mechanical continuum model.

Tikare et al. in 2003 [39] developed a model that can simulate sintering at the mesoscale. The mesoscale model is a kinetic, Monte Carlo model that simulates the microstructural evolution processes of curvature-driven grain growth, pore migration, and pore shape equilibration by surface diffusion and vacancy formation, in addition to diffusion, and annihilation in a powder compact.

1.8 The Aim of the Thesis

The general purpose of this thesis is to construct a mathematical model that serves in specifying the effect of various parameters on the densification during the sintering process of heterogeneous compacts consists from mixtures of several types of clays that prepared in reference [40]. Well known geometrical model for Scherer [6], which consider the viscous sintering with only a negligible ratio of solid inclusions in the compact, is developed to make it takes the effect of solid inclusions on the densification during sintering into consideration. This model is used to study the effect of the following parameters:

1. Effective viscosity of the compact on the densification during sintering.
2. The ratio of the solid inclusions on the densification during sintering.
3. The magnitude of firing temperature on the final density of the compact after sintering process.
4. Time of firing on the densification during sintering.
5. Pore size distribution on the densification process.

Another two models, the composite sphere model and the self-consistent model, that also take the effect of solid inclusion into consideration during the viscous sintering process are applied and compared with our modified model.

Chapter Two
Theoretical Analysis

2.1 Introduction

There are two entirely distinct phenomena occurring in clays heated at high temperatures, these are:

(a) Crystal formation due to the recombination and recrystallization reactions, and (b) liquid formation. This latter material may crystallize on cooling, but siliceous melts are prone to supercool and often 'freeze' to a homogeneous glass or a partially crystallized system. The relative rates of crystal formation and of liquid development in particular clay cannot be predicted because of the complexity and number of factors involved. The composition, grain-size and distribution of minerals, firing rate and maximum temperature all contribute to both types of reaction and, in addition, the two phases may mutually interact after they have been produced. Thus the liquid which develops during firing may dissolve some of the crystals formed by solid reaction processes and, conversely, some liquid may crystallize on contact with the solid by reason of the change in composition produced, or by the 'seeding' of a supercooled phase. The factors that influence glass formation on cooling are:

(a) The rate of cooling.

(b) The viscosity of the liquid in the temperature region of incipient crystallization.

(c) The composition of the liquid [12].

The theory of viscous sintering is based on an assumption proposed by Frenkel [9], that 'the energy dissipated in viscous flow is equal to the energy gained by the decrease in surface area during densification'. Using Frenkel's energy balance concept, Mackenzie and Shuttleworth [5] calculated the rate of densification of a viscous body containing closed

spherical pores. Scherer [6] and depending on the Frenkel's concept put a model to calculate the rate of densification of a viscous body containing open pores. In this chapter firstly, the last model will be modified to make it applicable to viscous sintering that contains rigid inclusions, and apply these modifications on the model of Scherer [31], which study the effect of pore size distribution on the densification process. Then in the second part of the chapter, two models of heterogeneous systems, which are the composite sphere model and the self-consistent model will be taken. Scherer [20] used these models in presenting models that describe the stresses and densification processes during viscous sintering of compacts contain rigid inclusions. The theoretical equations concerned with densification process of these two models will be summarized, to apply it on the sintering process in heterogeneous systems, for comparison with the results from the present modified model.

2.2 Development of the Scherer Model of Viscous Sintering:

2.2.1. Development of the Model of Viscous Sintering to be applied on Materials Contain Rigid Inclusions:

2.2.1.1. The Model

Scherer [6] put a model to describe the rate at which a cubic array of cylinders densifies by viscous flow; he chose a simple geometric form, which retains the essential features of the real material. He applied his model on Silica preform and silica gel. The model chosen (shown in figure (2.1a)) consists of a cubic array formed by intersecting cylinders. Each three cylinders intersect at a node. The cylinders represented the strings of oxide particles; the cylinder radius corresponded to the average particle radius in the Silica preform. A "unit cell" of the assumed

structure is presented in figure (2.1b); when those cells are stacked, the structure shown in figure (2.1a) is obtained. The choice of a cubic cell is quite arbitrary, but it has several factors in its favor. First, in general, the choice of any other polyhedron would be equally arbitrary, and the cube has the advantage of having a very simple geometry. Second, the cell shape is likely to have a small effect on the results and that point had

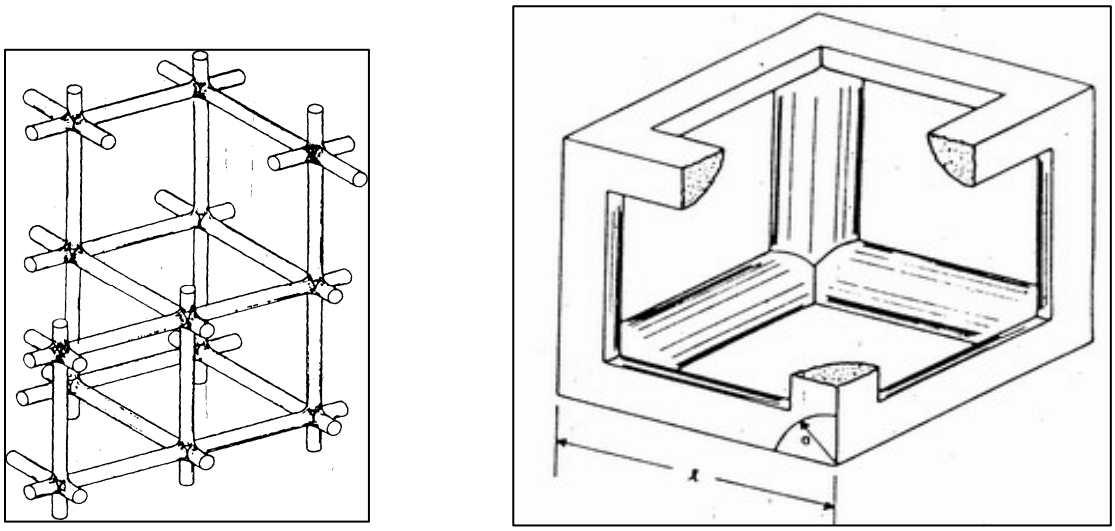

a b

Figure (2.1) Geometry of the Scherer model a) cylindrical array, b) Unit cell of the Scherer model, which is equivalent to the unit cell of the matrix structure in the present model [6].

been proved by Scherer [36].

The volume of the solid phase, V_S, in the cubic cell was determined by the equation [6]:

$$V_S = 3\pi a^2 l - 8\sqrt{2}\,a^3 \qquad (2.1)$$

where (a) is the cylinder radius and (l) is the side length of the unit cell. The last equation didn't consider the foundation of any solid inclusions, so in the case of the mixture of clays which consist from materials that will be discussed in chapter four, which contain relatively high ratio of

rigid inclusions (that have the effect of retarding densification[21, 20]) the previous equation must be changed or modified. In this case, to take the effect of solid inclusions, their effect on the densification process during viscous sintering will be simulated. The densification process in the composite will be simulated by manipulating the densification process in the matrix of the composite. In the case of clays, the matrix is usually represented by a viscous phase formed during sintering [12]. We will assume that the solid inclusions are represented in the unit cell by a ratio equal their ratio in the compact, so if we suppose (λ) represents the ratio of the solid inclusions side length to the viscous phase side length in the compact, then (λ) can be defined as

$$\lambda = \frac{l_{in}}{l_{vis}} = \left(\frac{V_{in}}{V_{vis}} \right)^{1/3} \qquad (2.2)$$

where (V_{in} and l_{in}) are the theoretical volume and side length of solid inclusions in the compact, (V_{vis} and l_{vis}) are the theoretical volume and side length of viscous phase in the compact. Here the compact is assumed to have a cubic shape and the length of each constituent in the compact is assumed to equal the cubic root of its corresponding volume. The solid inclusions are assumed to be arranged in the unit cell in away, which reduces the side length of the unit cell (and as a result reduces the cylinder length) that the viscous phase can propagate through to achieve the densification. If the length of the unit cell that the viscous phase can propagate through is (l*), which will be called as the effective side length of the composite unit cell that equal the side length of the matrix, and if the side length of the composite unit cell is (l), which will be called as the compacted length, then at the end of the sintering process for the full densification the ratio of (l*) to (l) will equal the ratio of the viscous

phase length (l_{vis}) to the summation of the solid inclusions length and the viscous phase length as in the equation

$$\frac{l^*}{l} = \frac{l_{vis}}{l_{vis} + l_{in}} \tag{2.3}$$

Substituting Eq. (2.2) after rearranging in the right side of the last equation gives

$$\frac{l^*}{l} = \frac{1}{1+\lambda} \tag{2.4}$$

or by rearranging

$$l^* = \frac{l}{1+\lambda} \tag{2.5}$$

The considered assumption will be as follows; the solid inclusions retard densification by decreasing the length of the cylinder, which the viscous phase can propagate through it. Therefore, the viscous phase is propagated through (l^*) not through (l), because the solid inclusions prevent the propagation of the viscous phase in the places where the solid inclusions are found. So each (l) in Scherer model will be replaced by (l^*), so Eq. (2.1) will be as:

$$V_S = 3\pi a^2 l^* - 8\sqrt{2}a^3 \tag{2.6}$$

When there is no inclusions in the compact (i.e. λ=0) Eq. (2.6) will equal Eq. (2.1). As in figure (2.1b) the density, ρ, of the matrix cell is given by:

$$\rho = \frac{\rho_S V_S}{l^{*3}} \tag{2.7}$$

where ρ_s is the theoretical density of the solid phase. Combining Equations (2.6) and (2.7), we find that the relative density, ρ/ρ_s, is a function only of (a/l) and (λ), as the following equations declares:

$$\frac{\rho}{\rho_s} = 3\pi\left(\frac{a^2}{l^{*2}} - \frac{ca^3}{l^{*3}}\right) = 3\pi\frac{a^2}{l^{*2}}\left(1 - \frac{ca}{l^*}\right) \tag{2.8a}$$

$$\frac{\rho}{\rho_s} = \frac{3\pi a^2(1+\lambda)^2}{l^2}(1 - \frac{ca(1+\lambda)}{l}) = 3\pi x^2(1+\lambda)^2(1 - cx(1+\lambda)) \tag{2.8b}$$

where $c = 8\sqrt{2}/3\pi$, $x=a/l$.

For (λ) equal zero the relation is plotted in figure (2.2).

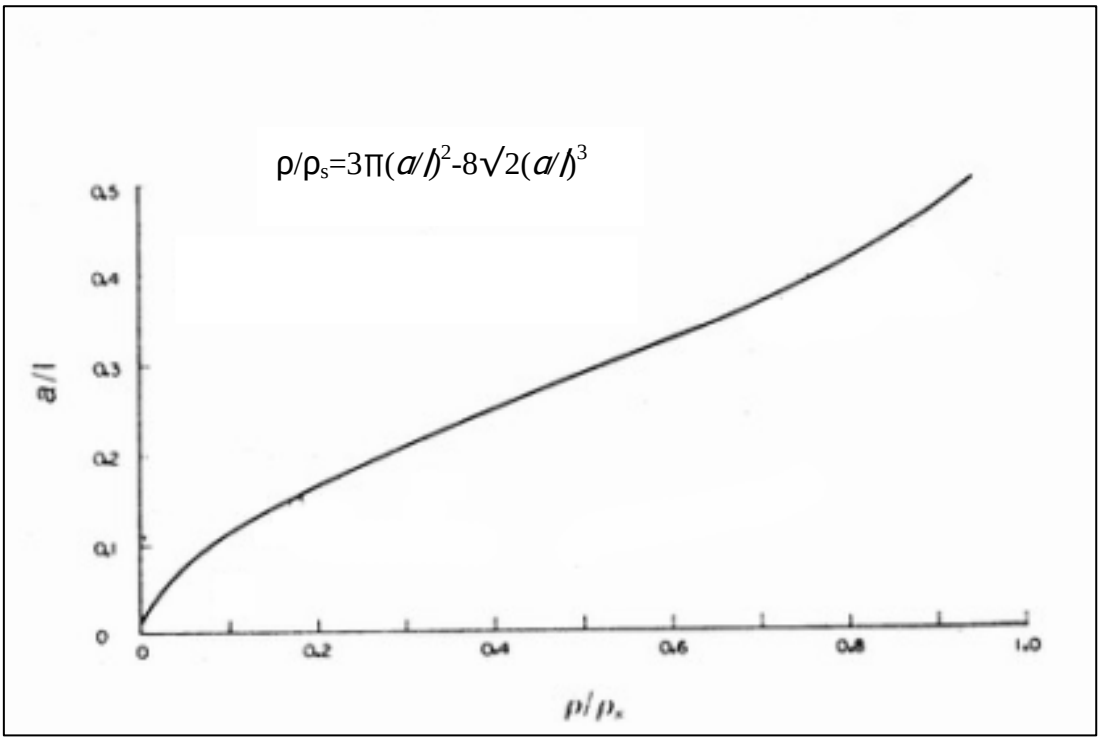

Figure (2.2) plot of *a/l* vs. ρ/ρ_s for λ=0 [6].

so for λ=0, *x* can be given as a function to the relative density by the relation [6]:

$$x = \left(\frac{\pi\sqrt{2}}{8}\right)\cos\left(\theta + \frac{4\pi}{3}\right) + \frac{\pi}{8\sqrt{2}} \tag{2.9a}$$

where

$$\theta = \frac{1}{3}\cos^{-1}\left(1 - \rho_{rd}\left(\frac{4}{\pi}\right)^3\right) \tag{2.9b}$$

where ρ_{rd} is the relative density.

Scherer [6] related the pore diameter (*d*), which may be obtained from Hg penetration porosimetry, to (l) by equating the cross-sectional area of the pore with the area of the opening in the side of the cell. Replacing (*l)* with (l^*) this approach leads to:

$$\pi d^2/4 \approx (l^* - 2a)^2 = \left(\frac{l}{(1+\lambda)} - 2a\right)^2 \qquad (2.10)$$

Scherer with these assumptions calculated the values of (a/l) for several preforms for which both particle size and porosimetry data were available. He suggested that Even if the particle size measurements are not available, the value for (l) can be obtained from an Hg penetration curve, as follows: From figure (2.2) he obtained, for a given density, the value of (a/l), This value can be used with equation similar to Eq. (2.10) to obtain l as a function of *d.* In the present case, this method can be applied for a given (λ) to find (*a*), but it will be more accurate if the Stereological ways is used with an image of scanning electron microscope to find (*a*) as we will see later. Scherer [6] assumed that a cell consisting of twelve-quarter cylinders (or three full cylinders); replacing (*l*) by (l^*), then the surface area of a single full cylinder in a compact unit cell, S_c, is given by:

$$S_c = 2\pi a l^* - 8\sqrt{2}a^2 \qquad (2.11)$$

When the volume of the solid phase is apportioned among the three cylinders in the unit cell,

$$V_S = 3V_C \qquad (2.12)$$

where V_C is the effective volume of one cylinder, and is given by

$$V_C = \pi a^2 \left[l^* - (8\sqrt{2}/3\pi)a\right] \qquad (2.13)$$

The quantity in brackets in Eq. (2.13) is the effective length of the cylinder. As the length of the cylinder decreases, the surface area of the cell decreases, as a result providing the driving force for the densification.

The reason for dividing the volume of the cell artificially among three cylinders is explained by Scherer [6] as follows; the sintering rate can be calculated only when the amount of energy dissipated in viscous flow has been determined. Since the flow pattern in the corner sections of the cell would be quite awkward to describe, so the choice was to make this a convenient approximation.

2.2.1.2. The Rate of Densification

To calculate the rate of densification during sintering of the model structure, we will follow Frenkel [9]: the energy dissipated in viscous flow will be set equal to the energy change resulting from the reduction in surface area. In the model, the rate of energy dissipation in viscous flow, E_f' , as a cylinder decreases in height is given by:

$$E_f' = \left(\frac{3\pi\eta r^2}{h}\right)\left(\frac{dh}{dt}\right)^2 \tag{2.14}$$

where (r) and (h) are the radius and height of the matrix unit cell cylinder respectively and η is the viscosity of the viscous phase. For a cell, $r=a, h=l^*-(8\sqrt{2}/3\pi)a$.

the energy supplied by the reduction in surface area, E_s' , is given by:

$$E_s' = \gamma\left(\frac{dS_c}{dt}\right) \tag{2.15}$$

where γ is the surface energy.

assuming E_f' equal ($-E_s'$) and by following the same procedure in reference [6], this gives:

$$\frac{dx}{dt} = \frac{\gamma}{2\eta}\frac{1}{l} \tag{2.16a}$$

where $x=a/l$ (2.16b)

recognizing that (V_s) is constant which means that the mass of solid matter is constant within the unit cell at any time so:

$$l_{\circ}^{*}\rho_{\circ}^{1/3} = l^{*}\rho^{1/3} \tag{2.17a}$$

multiplying Eq. (2.17a) by (1+λ) yields:

$$\frac{1}{l} = \frac{1}{l_o}\left(\frac{\rho}{\rho_o}\right)^{1/3} \tag{2.17b}$$

where l_o, ρ_o are the initial values of (l) and (ρ) respectively. substituting ρ from Eq. (2.8b) into Eq. (2.17b), we can have:

$$\frac{1}{l(t)} = \frac{1}{l_{\circ}}\left(\frac{(3\pi x^2(1+\lambda)^2 - 8\sqrt{2}x^3(1+\lambda)^3)\rho_s}{\rho_{\circ}}\right)^{1/3} \tag{2.18}$$

by rearranging, we get:

$$l(t) = \frac{l_{\circ}(\rho_{\circ}/\rho_s)^{1/3}}{(1+\lambda)\left(\frac{3\pi x^2}{(1+\lambda)} - 8\sqrt{2}x^3\right)^{1/3}} \tag{2.19}$$

substituting Eq. (2.19) into Eq. (2.16a) gives:

$$dx = \frac{\gamma}{2\eta}\frac{\left(\frac{3\pi x^2}{(1+\lambda)} - 8\sqrt{2}x^3\right)^{1/3}(1+\lambda)}{l_{\circ}(\rho_{\circ}/\rho_s)^{1/3}}dt \tag{2.20}$$

rearranging the last equation in away that each side becomes a function of one variable and integrating on (t) in the interval from (t_o) to (t) on the (t) side of the equation, which corresponding to the interval from (x_o=0) to (x) on the (x), side of the equation gives:

$$\frac{\gamma}{\eta l_{\circ}}\left(\frac{\rho_s}{\rho_{\circ}}\right)^{1/3}\int_{t=t_{\circ}}^{t} dt = \int_0^x \frac{2dx}{(1+\lambda)\left(\frac{3\pi}{(1+\lambda)x} - 8\sqrt{2}\right)^{1/3}x} \tag{2.21}$$

$$K(t-t_\circ)=\int_0^x \frac{2dx}{(1+\lambda)\left(\frac{3\pi}{(1+\lambda)x}-8\sqrt{2}\right)^{1/3}x} \tag{2.22}$$

where (K) is the proportionality constant between the reduced time (Kt) and the practical time (t_p)is given by:

$$K = \frac{\gamma}{\eta\, l_\circ}\left(\frac{\rho_s}{\rho_\circ}\right)^{1/3} \tag{2.23}$$

here t_o is the fictitious time at which (x=0). Eq. (2.22) determines (x) as a function of time; since for a certain value of (λ), ρ/ρ_s is a function only of x (t), so the density of the cell is determined as a function of time. The indefinite integral is readily evaluated as in Appendix (A) with the substitution

$$y_x{}^3 = \frac{3\pi}{(1+\lambda)x}-8\sqrt{2} \tag{2.24}$$

to give

$$K(t-t_\circ)=-\frac{2}{\alpha}(1+\lambda)^{-1}\left(\frac{1}{2}\ln\frac{\alpha^2-\alpha y_x+y_x{}^2}{(\alpha+y_x)^2}+\sqrt{3}\tan^{-1}\frac{2y_x-\alpha}{\alpha\sqrt{3}}\right)+K_o \tag{2.25a}$$

where $\alpha=(8\sqrt{2})^{1/3}$, (K_o) is a constant that corresponds to the value of (Kt) at $t=t_o$. From Eq. (2.23) and Eq. (2.25a), it is obvious that the viscosity is directly proportional with the factor (1+λ); in other word, the viscosity is increasing with increasing the solid inclusions.

Scherer equation corresponding to Eq. (2.25a) was from reference [6] as

$$K(t-t_\circ)=-\frac{2}{\alpha}\left(\frac{1}{2}\ln\frac{\alpha^2-\alpha y_x+y_x{}^2}{(\alpha+y_x)^2}+\sqrt{3}\tan^{-1}\frac{2y_x-\alpha}{\alpha\sqrt{3}}\right)+K_o \tag{2.25b}$$

and K_o has the same definition. According to the last equation, the relative density, ρ/ρ_s, is plotted in figure (2.3) versus (Kt). The experimental data can be fitted to the theoretical curve by plotting the

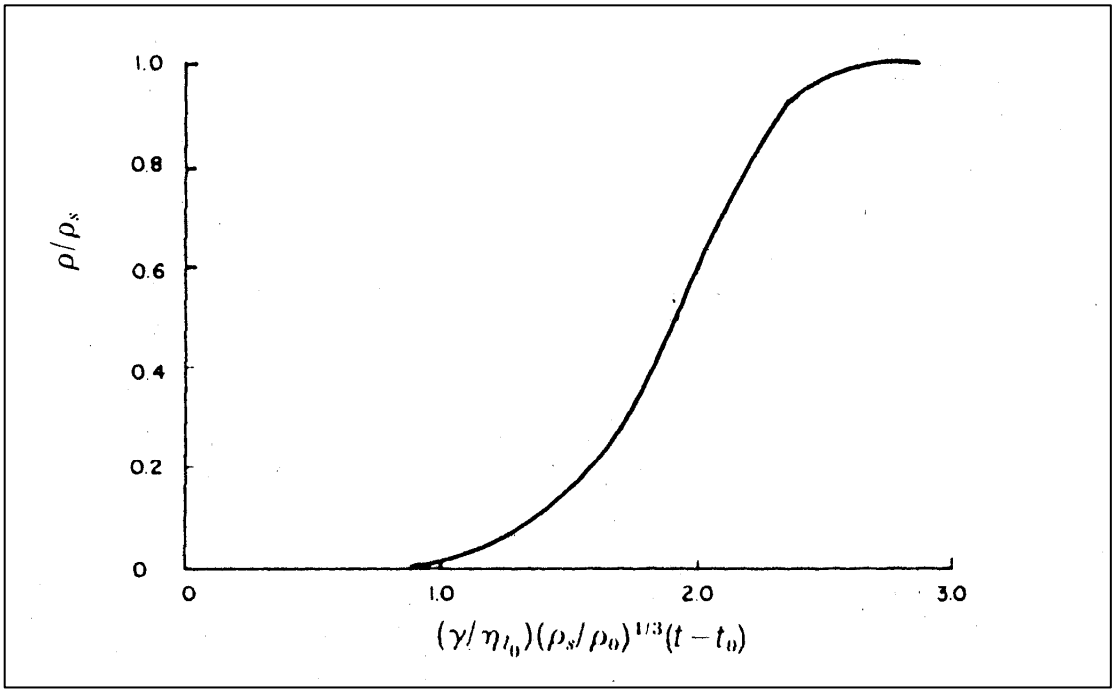

Figure (2.3) plot of ρ/ρ_s vs. K $(t-t_o)$, for $\lambda=0$ [6].

reduced times versus the experimentally determined times. The reduced times can be found from figure (2.3) if $\lambda=0$, or in other case from solving Eq. (2.25a) and Eq. (2.8b) for *x*, and for known values of the relative density and λ. The slope of the straight line formed by plotting *Kt* as a function of experimental times of sintering equals (*K*). When Eq. (2.25) is applied to the experimental results for the sintering of mixtures of clays, after determining the value of (*K*) for each sample, it has been found that it is inapplicable. This is due to the assumption that at the beginning of the sintering process the value of (*x*) (which is given by the ratio (a/l)) is equal zero. This assumption may be applicable on the case of silica gel (as an example) or other materials stated in reference [41], but it is inapplicable on the materials of our present work, due to the solid inclusions and the anisotropy in the structure that found in the body of the compact. Therefore, the interval of the integration on (*x*) will be assumed to start at (x_o) following reference [36] with a difference, that (x_o) $\neq 0$.

applying this to the integration of Eq. (2.22) by starting the integration from (x_o) to (x), yield the following equation:

$$K(t-t_o) = -\frac{2}{\alpha}(1+\lambda)^{-1}\left[\left(\frac{1}{2}\ln\frac{\alpha^2-\alpha y_x+{y_x}^2}{(\alpha+y_x)^2}+\sqrt{3}\tan^{-1}\frac{2y_x-\alpha}{\alpha\sqrt{3}}\right)\right.$$

$$\left.-\left(\frac{1}{2}\ln\frac{\alpha^2-\alpha y_{xo}+{y_{xo}}^2}{(\alpha+y_{xo})^2}+\sqrt{3}\tan^{-1}\frac{2y_{xo}-\alpha}{\alpha\sqrt{3}}\right)\right] \qquad (2.26a)$$

and the integration of Eq. (2.25b) will be:

$$K(t-t_o) = -\frac{2}{\alpha}\left[\left(\frac{1}{2}\ln\frac{\alpha^2-\alpha y_x+{y_x}^2}{(\alpha+y_x)^2}+\sqrt{3}\tan^{-1}\frac{2y_x-\alpha}{\alpha\sqrt{3}}\right)\right.$$

$$\left.-\left(\frac{1}{2}\ln\frac{\alpha^2-\alpha y_{xo}+{y_{xo}}^2}{(\alpha+y_{xo})^2}+\sqrt{3}\tan^{-1}\frac{2y_{xo}-\alpha}{\alpha\sqrt{3}}\right)\right] \qquad (2.26b)$$

where

$${y_{xo}}^3 = (3\pi/x_o) - 8\sqrt{2} \qquad (2.27)$$

and $x_o = a_o/l_o$,which is found from the initial relative density by numerically solving equation (2.8b) for x, and the same procedure is applicable for any relative density at any time of the sintering process. Eq. (2.26) is more applicable and gives a good approximation to the density values, as will be seen later.

Scherer noted that the window in the side of the cubic cell closes when

$$a = l^*/2 = l/(2(1+\lambda)) \qquad (2.28a)$$

where the side of the cell in Scherer model was equal (l), but in the present assumptions it is equal (l^*). So when (a/l^*) =0.5, the neighboring cylinders touch and the cell contains a closed pore; the relative density at that instant according to Scherer and to the present model according to Eq. (2.8b) is:

$$\frac{\rho}{\rho_s} = \left(\frac{3\pi}{4}\right) - \sqrt{2} = 0.942 \qquad (2.28b)$$

Scherer model and the present model are no longer applied for relative densities larger than that given by Eq. (2.28b) because the structure cannot be described as an array of cylinders in these ranges of relative densities [6]. To limit the maximum value of (x) (x_{max}) corresponding to the relative density given by Eq. (2.28b) for the modified Scherer model, Eq. (2.28a) and Eq. (2.16b) gives the following equation:

$$\frac{a}{l^*} = \frac{a(1+\lambda)}{l} = x(1+\lambda) \tag{2.29a}$$

So when (a/l^*) $=0.5$, then the maximum value of x (x_{max}) will be given by the following equation:

$$x_{\max} = \frac{0.5}{(1+\lambda)} \tag{2.29b}$$

In the present materials (λ) usually has a value around (0.7), so from Eq. (2.29b), the highest value of (x) at which this model is still applicable is about 0.294 when ($\lambda=0.7$). For relative densities greater than 0.942, Scherer suggested using the analysis of Mackenzie and Shuttleworth [5] for viscous sintering of a body containing closed pores. For relative densities greater than that given in Eq. (2.28b), the results of the Mackenzie-Shuttleworth (M-S) analysis were used to construct figure (2.3) at (λ=0). Mackenzie and Shuttleworth plotted ρ/ρ_s versus the reduced time in the form

$$\frac{\gamma n^{1/3}}{\eta}(t - t_o) = \frac{2}{3}\left(\frac{3}{4\pi}\right)^{1/3} \int_0^{\rho} \frac{d\rho_{rd}}{(1-\rho_{rd})^{2/3}\,\rho_{rd}^{1/3}} \tag{2.30a}$$

where (n) is the number of closed pores per unit volume of solid phase. ρ_{rd} is the relative density. Scherer supposed when x=0.5, the body consists of closed pores with $n=1/V_S$,

or

$$n^{1/3} = \frac{1}{l_\circ}\left(\frac{\rho_s}{\rho_\circ}\right)^{1/3} \tag{2.30b}$$

Using the same arguments used in finding Eq. (2.26) it will be assumed that the integration in Eq. (2.30a) begins from initial value ρ_{rdo} and following reference [5] the assumption will be as:

$$z^3 = (1-\rho_{rd})/\rho_{rd} \tag{2.30c}$$

by integration, the following formula will be given:

$$\frac{\gamma n^{1/3}}{\eta}(t - t_o) = \left[\frac{1}{2}\ln\frac{1 + z^3}{(1 + z)^3}\right] - \left[\sqrt{3}\tan^{-1}\frac{2z - 1}{\sqrt{3}}\right]$$

$$-\left[\frac{1}{2}\ln\frac{1+z_o^3}{(1+z_o)^3}\right]+\left[\sqrt{3}\tan^{-1}\frac{2z_o-1}{\sqrt{3}}\right] \tag{2.31a}$$

where $z_o^3 = (1-\rho_{rdo})/\rho_{rdo}$

For the present model from Eq. (2.7) by comparison with Eq. (2.30b), the following equation will be concluded:

$$n^{1/3} = \frac{1}{l_\circ^*}\left(\frac{\rho_s}{\rho_\circ}\right)^{1/3} \tag{2.31b}$$

Substituting Eq. (2.31b) into Eq. (2.31a), the left hand side becomes

$$\left(\frac{\gamma}{\eta l_\circ^*}\right)\left(\frac{\rho_s}{\rho_\circ}\right)^{1/3}(t - t_\circ) \tag{2.31c}$$

Eq. (2.31c) differs from that in Scherer model by a factor $(1+\lambda)$ in the numerator. Thus to give the same time scale used in Eq. (2.26a), the equation of Mackenzie-Shuttleworth must be divided by a factor equal $(1+\lambda)$, or the final modified Mackenzie-Shuttleworth equation will be:

$$\frac{\gamma}{\eta l_{\circ}}\left(\frac{\rho_s}{\rho_{\circ}}\right)^{1/3}(t-t_o)=(1+\lambda)^{-1}\left[\left[\frac{1}{2}\ln\frac{1+z^3}{(1+z)^3}\right]-\left[\sqrt{3}\tan^{-1}\frac{2z-1}{\sqrt{3}}\right]\right.$$

$$\left.-\left[\frac{1}{2}\ln\frac{1+z_o^{\,3}}{(1+z_o)^3}\right]+\left[\sqrt{3}\tan^{-1}\frac{2z_o-1}{\sqrt{3}}\right]\right] \qquad (2.32)$$

Once (K) has been determined by fitting the experimental results to the theoretical curve, then the measured values of ρ_o and l_o can be used to obtain the quantity (γ/η). An Hg penetration porosimetry curve is presented in figure (2.4), showing the cumulative pore size distribution in a flame hydrolysis preform of SiO_2. Typically, greater than or equal to (2/3) of the pores have diameters within 15% of the average value. The average pore diameter is found from figure (2.4) by choosing the pore size corresponding to half the maximum pore volume, i.e. half the pore volume consists of pores with diameters smaller than the average. Average values for (a) and (l) can be derived from the average pore diameter [6].

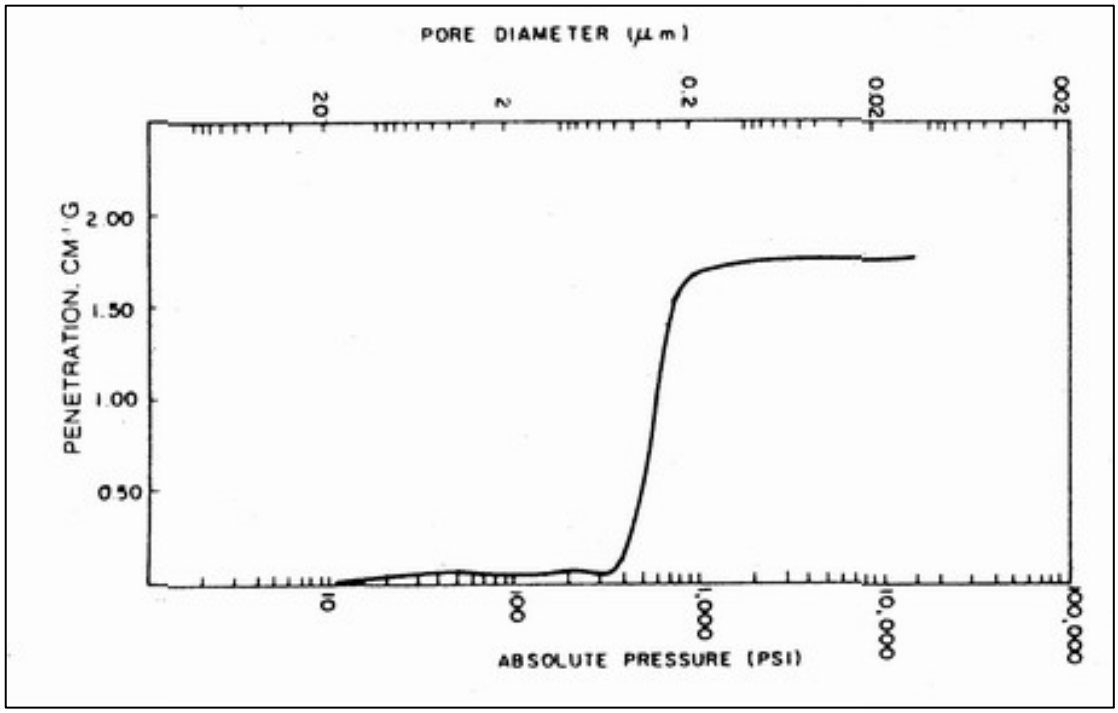

Figure (2.4) Hg porosimetry curve [6].

As noted earlier, the reduced-time expression used in the M-S analysis is equivalent to that of the Scherer analysis when the unit cell contains a single pore. On this basis, the two curves had been plotted together in figure (2.5) and shifted so that they coincide for relative densities larger than 94%. The close agreement over most of the density range suggests the remarkable result that the shape of unit cell chosen does not have a strong effect on the predicted sintering kinetics. The principle reason for using the present analysis rather than the M-S theory is that the model structure bears a rational relation to the actual structure. Moreover, to find a value for (*n*) to use it in the M-S theory, it is necessary to adopt some sort of realistic structural model.

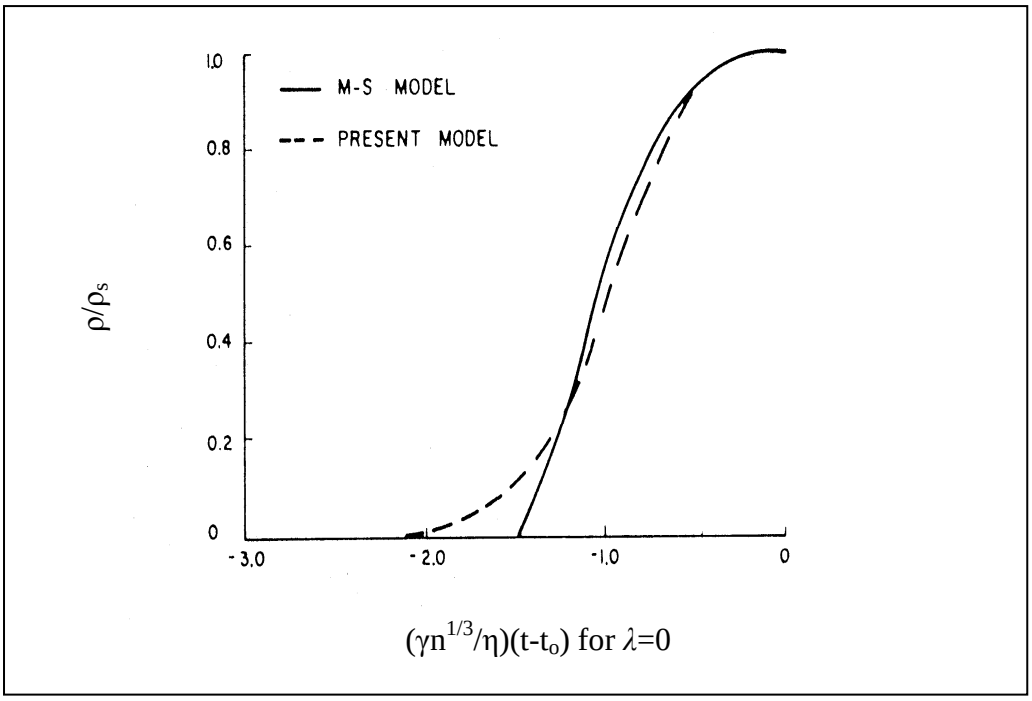

Figure (2.5) Comparison of M-S and Scherer model for ρ/ρ_s vs. Kt at λ=0 [6].

2.2.2 Development of the Model of the Effect of the Distribution of Pore Sizes on Densification:

2.2.2.1. Introduction

Scherer [31] extended the sintering model presented previously by considering a Gaussian distribution of pore sizes in the body. He studied the effect of the breadth of the distribution of pore sizes on the densification kinetics in a typical pure Silica preform made by flame hydrolysis of $SiCl_4$. Here the model is developed and then used to study the effect of the breadth of the distribution of pore sizes on the densification kinetics during sintering process of some of the Iraqi clays. The pore size distribution can be obtained by Hg penetration porosimetry. An example of the data obtained by this technique is given in figure (2.4) for a typical pure SiO_2 preform made by flame hydrolysis of $SiCl_4$. A curve similar to that in figure (2.4) was obtained for Iraqi clays mixtures. The fraction of the total pore volume having a particular diameter is determined by finding the slope of the cumulative distribution at that diameter. Scherer took this approach, using figure (2.4) and the result is shown in figure (2.6). A Gaussian distribution of the following form can approximate the solid line in figure (2.6):

$$n'(d) = \overline{n'} \exp\left[-\frac{\left(d - \overline{d}\right)^2}{2\sigma_d^{\,2}} \right] V_p(d) \qquad \textbf{(2.33)}$$

where $\overline{d}$ is the mean pore diameter, σ_d is the standard deviation of the distribution, d is the pore diameter, $n'(d)$ is the number of pores with diameter d, $\overline{n'}$ is the number of pores with diameter $\overline{d}$, and $V_p(d)$ is the volume of pores with diameter d. In figure (2.6) $\overline{d}$ =2800 Å and σ_d =700Å**.** The scatter in the points is a result of the difficulty in measuring the slope of the cumulative distribution and of a lack of smoothness in that

experimental curve. The uncertainty of measurement of the slope is greatest where the slope is least, accounting for the long tails on the distribution in figure (2.6). When these factors are taken into account, the actual distribution seems to be adequately described as Gaussian.

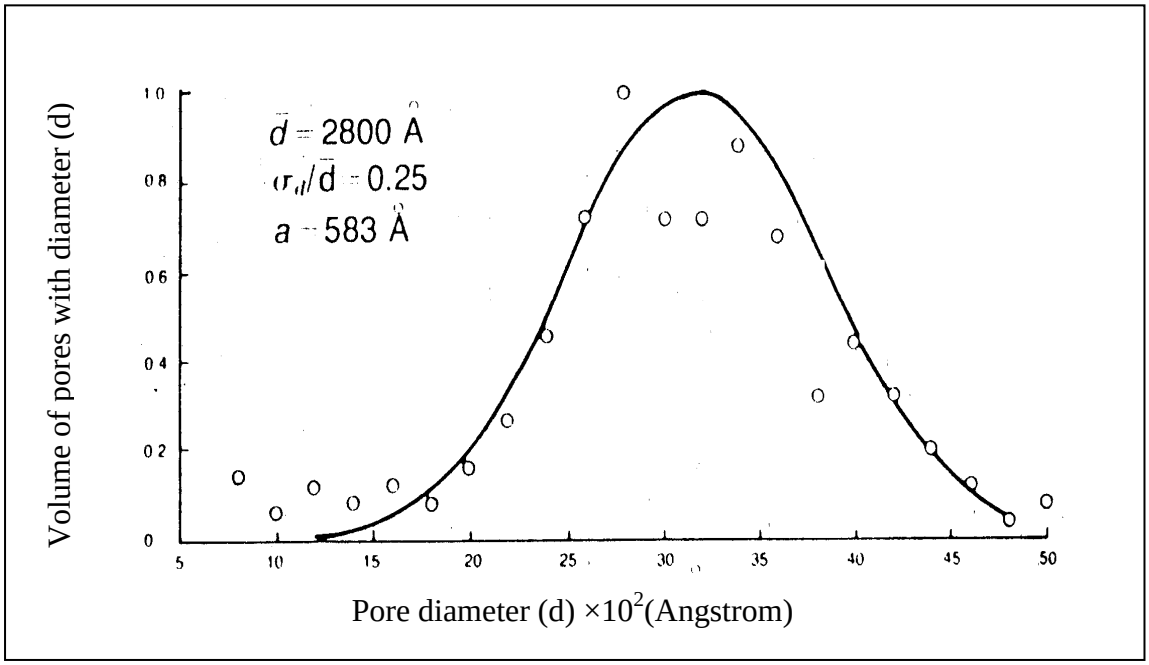

Figure (2.6) Distribution of pore sizes obtained from
Hg penetration porosimetry curve [31].

In this part, we want to develop Scherer model for the effect of pore size distribution on sintering to become applicable on the sintering process of clays mixtures. Scherer model studied the sintering process of samples consisting from homogeneous materials like silica gel as an example. Hence, the goal is to study the sintering process for heterogeneous systems for some of the clay types. The samples are prepared by Rasen [40]. The studied samples are consisted from mixing different types of Iraqi clays, which are listed in chapter four. The present work is concerned with the sintering process. These samples are fired at different temperatures between (1100 to 1400) ^{o}C, each sample was fired

at constant temperature. Before the firing temperature is reached, the temperature of the sample is raised gradually by a rate of 100 ^{o}C/hr until the firing temperature, each sample put under the measurement of Hg porosimetry after the sintering process so the standard deviation of the pore size distribution can be found only after sintering, but not before the firing process. A model that describes the effect of the standard deviation of pore size distribution on the densification during sintering process in heterogeneous systems represented by mixtures of clays have been suggested. In all these manipulations, the standard deviation of pore size distribution will be assumed constant during sintering following Scherer assumption.

2.2.2.2. The Analysis of the Model

The two parameters of the model structure are the cylinder radius (a) and the distance between the axes of neighboring parallel cylinders (l^*). (d) is related to (a) and (l^*) by Eq. (2.10), and x is related to the relative density through Eq. (2.8b). Thus two equations are available to determine (a) and (l), if the values of (d) and the bulk density and (λ) are given. The cylinder radius (a) corresponds to the particle size of the body of the compact will be assumed constant throughout the body and during the sintering process for the present analysis. Scherer [31] expected that the cylinder radius (a) represents the average particle size in the silica preform. In present case, the particle size is measured from the grain (or particle size) (dp), which is found using the stereological ways with the aid of a scanning electron microscope image in figure (2.7) , then the following formula will be applied to find (a):

$$a = \frac{dp}{2} \tag{2.34}$$

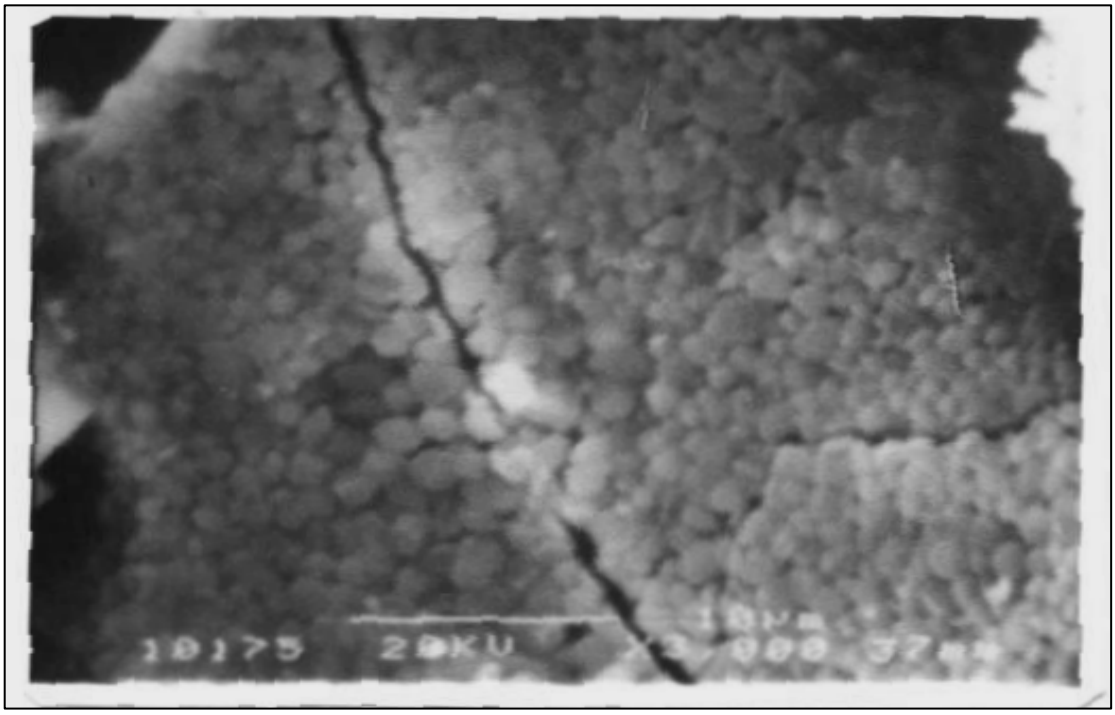

Figure (2.7) SEM; Microstructure for fractured sample of group M22 sintered at 1400^{o}C for 2 hr (rating 100^{o}C/hr) [40]

The Gaussian distribution will be assumed as Scherer did. This assumption came from the figure (2.8), which was found by following the

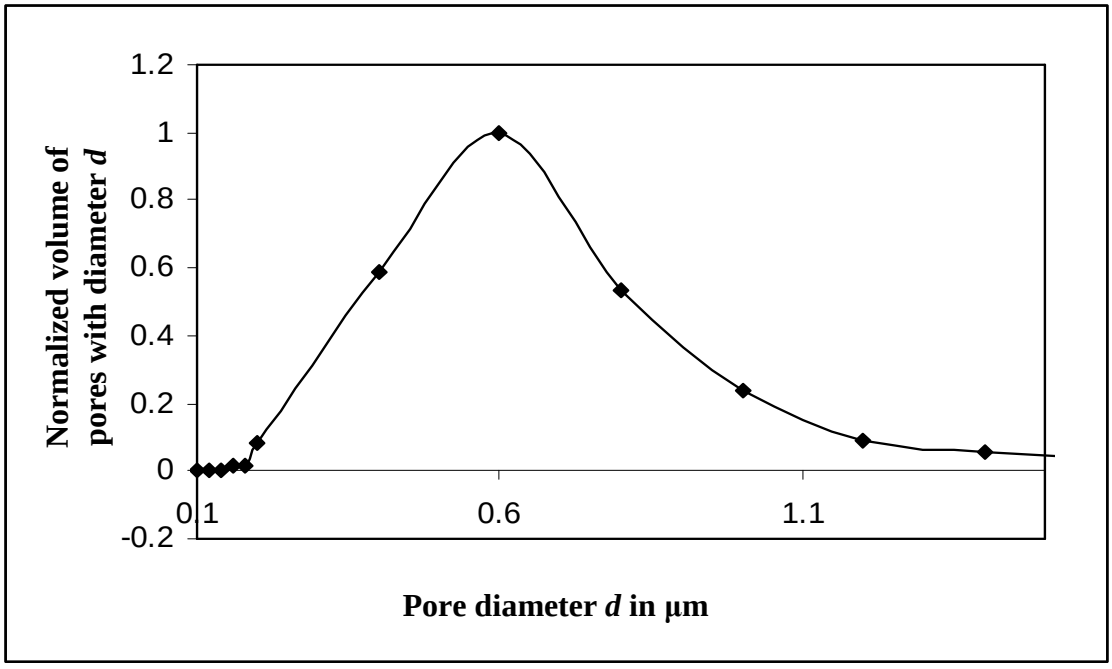

Figure (2.8) Distribution of pore sizes obtained from Hg penetration porosimetry curve for sample of group M21.

same steps done by Scherer in finding figure (2.6). The figure represent the graph between normalized volume of pores, measured by Hg porosimetry for the sample composed from (60% kaolin, 30% ninivite rock, 10% Al_2O_3) and the pore diameter (d), the similarity between the figure and the Gauss distribution can be observed. In figure (2.8) the values of $\bar{d}$ and σ_d are 6000 Å and 1900 Å respectively.

The number of cells with side length between (l^*) and ($l^* + dl^*$) is dN (l), here dN will be assumed as a function of (l), because (λ) is constant for a given sample.

where

$$dN(l) = \frac{n(l)dl}{(1+\lambda)} \tag{2.35}$$

for a Gaussian distribution,

$$\begin{aligned} n(l) &= \bar{n} \exp\left(\frac{-(l^* - \bar{l}^*)^2}{2(\sigma_l^*)^2} \right) \\ &= \bar{n} \exp\left(\frac{-(l - \bar{l})^2}{2(\sigma_l^*)^2 (1+\lambda)^2} \right) \end{aligned} \tag{2.36}$$

and from Eq. (2.10)

$$l^* = \frac{l}{(1+\lambda)} = (d\left(\frac{\sqrt{\pi}}{2} \right) + 2a) \tag{2.37}$$

therefore,

$$n(l) = n\left((\frac{d\sqrt{\pi}}{2} + 2a) \right) = \bar{n} \exp\left(\frac{-(d - \bar{d})^2}{2(\sigma_d^*)^2} \right) \tag{2.38a}$$

where $\bar{d} = 2\left(\frac{\bar{l}}{(1+\lambda)} - 2a \right)$ (2.38b)

and $$\sigma_d^* = \frac{2\sigma_l^*}{\sqrt{\pi}} \tag{2.39}$$

where the σ_d^*,σ_l^* are the standard deviation of pore size distribution and cell size distribution in the compact respectively. $\bar{n}$ is the number of cells with pore diameter $\bar{d}$ or side length $\bar{l}$.

With Equations (2.38) and (2.39), the mean ($\bar{l}$) and the standard deviation (σ_l^*) of the (l^*) distribution are simply obtained from the corresponding parameters of the pore size distribution. The density (ρ) of the model structure during sintering is a function of the reduced time (Kt). A cell, which has a dimension ($l_\circ$) will at time (Kt) have a dimension $l(l_\circ, Kt)$. The distribution of the cell sizes at any time is uniquely determined by the initial distribution [31]. When the cells are assumed to shrink independently, the average relative density at time $\overline{Kt}$, where $\overline{K} \equiv K(\bar{l}_o)$, is

$$\frac{\bar{\rho}(\overline{Kt})}{\rho_s} = \frac{\int_{2a}^{\infty} n(l_o) V_s \, dl_o}{\int_{2a}^{\infty} n(l_o)(l^*(l_o^*, \overline{Kt}))^3 \, dl_o} \tag{2.40}$$

where V_s is given in Eq. (2.6).

(a_o) and ($l_\circ$) are the initial values of (a) and (l) respectively.

To evaluate the integral in the last equation let us assume that

$$y = \frac{(l^* - \bar{l}^*)}{\sigma_l^* \sqrt{2}} = \frac{(l - \bar{l})}{\sigma_l^* \sqrt{2}(1 + \lambda)} \tag{2.41}$$

The initial value of (y) is (y_o), which associated with ($l_\circ$). Alternatively, by rearranging this gives:

$$l_o^* = \frac{l_o}{(1+\lambda)} = \frac{y_o \sigma_l^{\,*} \sqrt{2}(1+\lambda) + \bar{l}}{(1+\lambda)} \tag{2.42}$$

By differentiating Eq. (2.42) yields:

$$dl_o = \sqrt{2}\sigma_l^{\,*} dy_o (1+\lambda) \tag{2.43a}$$

where $\sigma_l^{\,*} = \dfrac{\sqrt{\pi}\sigma_d^{\,*}}{2}$ (2.43b)

Substituting Eq. (2.42) in Eq. (2.6) and Eq. (2.41) in Eq. (2.36) yields:

$$V_s = \frac{3\pi a^2 (y_o \sigma_l^{\,*} \sqrt{2}(1+\lambda) + \bar{l})}{(1+\lambda)} - 8\sqrt{2}a^3 \tag{2.44}$$

$$n(l_o) = \bar{n} \exp(-y_o^2) \tag{2.45}$$

Then substituting equations (2.44), (2.45) & (2.43a) in Eq. (2.40) yields after canceling the similar constants in the numerator and denominator:

$$\frac{\overline{\rho}(\overline{K}t)}{\rho_s} = \frac{\displaystyle\int_{\frac{-(\bar{l}^* - 2a)}{2\sigma_l^*}}^{\infty} \exp\left(-y_o^2\right)\left(\frac{3\pi a^2 (y_o \sigma_l^{\,*} \sqrt{2}(1+\lambda) + \bar{l})}{(1+\lambda)} - 8\sqrt{2}a^3\right) dy_o}{\displaystyle\int_{\frac{-(\bar{l}^* - 2a)}{2\sigma_l^*}}^{\infty} \exp\left(-y_o^2\right)(l^*(l_o, \overline{K}t))^3 dy_o} \tag{2.46}$$

From the fact that (V_s) is time independent, this means:

$$V_s(a_o, l_o) = V_s(a, l) \tag{2.47}$$

From Eq. (2.7) $\quad V_s = \dfrac{l^{*3}\rho}{\rho_s}$

So $\dfrac{(l^*(l_\circ, Kt))^3 \rho}{\rho_s} = \dfrac{(l_o^{\,*})^3 \rho_o}{\rho_s}$ (2.48)

Taking the third root of the previous equation, and then substituting Eq. (2.8b) in it, solving for $l(l_\circ, Kt)$, yields

$$l^*(l_o, Kt) = l_o^{\,*}\left[\left(\frac{x_o}{x}\right)^2 \left(\frac{(1+\lambda)^{-1} - cx_o}{(1+\lambda)^{-1} - cx}\right)\right]^{1/3} \tag{2.49}$$

Substituting Eq. (2.42) in Eq. (2.49) gives:

$$l^*(l_o, Kt) = \frac{\left(y_o \sigma_l^* \sqrt{2}(1+\lambda) + \bar{l}\right)}{(1+\lambda)} \left[\left(\frac{x_o}{x} \right)^2 \left(\frac{(1+\lambda)^{-1} - cx_o}{(1+\lambda)^{-1} - cx} \right) \right]^{1/3} \tag{2.50}$$

If $(l^* - 2a) >> \sigma_l \sqrt{2}$, the area under the distribution curve, for values of (y_o) smaller than the lower limit shown in Eq. (2.46), will be small. In that case, the lower limit may be changed to (-∞) without appreciable error, and the integrals in Eq. (2.46) are readily evaluated. Applying this change to integration intervals and substituting Eq. (2.50) in (2.46) yields:

$$\frac{\rho(\bar{K}t)}{\rho_s} = \frac{\int_{-\infty}^{\infty} \exp(-y_o^2) \left(3\pi a^2 \frac{(y_o \sigma_l^* \sqrt{2}(1+\lambda) + \bar{l})}{(1+\lambda)} - 8\sqrt{2}a^3 \right) dy_o}{\int_{-\infty}^{\infty} \exp(-y_o^2) \left(\frac{(y_o \sigma_l^* \sqrt{2}(1+\lambda) + \bar{l})}{(1+\lambda)} \right)^3 \left[\left(\frac{x_o}{x} \right)^2 \left(\frac{(1+\lambda)^{-1} - cx_o}{(1+\lambda)^{-1} - cx} \right) \right] dy_o} \tag{2.51}$$

Putting the constants outside the integration and multiplying the numerator and the denominator by (1+λ) the last equation will be

$$\frac{\rho(\bar{K}t)}{\rho_s} = \frac{3\pi a^2 (1+\lambda)^2 \int_{-\infty}^{\infty} \exp(-y_o^2) \left((y_o \sigma_l^* \sqrt{2}(1+\lambda) + \bar{l}) - ca(1+\lambda) \right) dy_o}{\left[\left(\frac{x_o}{x} \right)^2 \left(\frac{(1+\lambda)^{-1} - cx_o}{(1+\lambda)^{-1} - cx} \right) \right] \int_{-\infty}^{\infty} \exp(-y_o^2) \left(y_o \sigma_l \sqrt{2}(1+\lambda) + \bar{l} \right)^3 dy_o} \tag{2.52}$$

where $c = 8\sqrt{2}/3\pi$ .The integral is in a form, which it can be solved numerically using Gauss-Hermite quadrature [42]. This technique offers, the approximation:

$$\int_{-\infty}^{\infty} \exp(-y^2) f(y) dy = \sum_{i=1}^{N} A_i f(y_i) \tag{2.53}$$

where the coefficients A_i and the abscissas y_i are tabulated, *f(y)*: is a mathematical function of a variable *y*. By comparison between the last equation and the integration terms in the numerator and the denominator, and after replacing y_o by y_i it is concluded that For the numerator integration term ($f(y_i)$) is given by:

$$f(y_i)_{numerator} = 3\pi a^2(1+\lambda)^2\left((y_i\sigma_l^{*}\sqrt{2}(1+\lambda)+\bar{l}) - ca(1+\lambda)\right) \quad (2.54)$$

And For the denominator integration term ($f(y_i)$) is given by

$$f(y_i)_{denominator} = \left[\left(\frac{x_o}{x}\right)^2\left(\frac{(1+\lambda)^{-1} - cx_o}{(1+\lambda)^{-1} - cx}\right)\right]\left(y_i\sigma_l\sqrt{2}(1+\lambda)+\bar{l}\right)^3 \quad (2.55)$$

The steps for applying the model can be summarized as the following:

1. First step is the fitting process, which will be discussed, in the following chapter.

2. The second step is substituting all the parameters in Eq. (2.52) and solving the integral numerically using Eq. (2.53).

2.3. Studying the Applicability of Heterogeneous Models on Sintering Process of Clays Mixtures:

2.3.1. Introduction:

In this part, two models that describe the behavior of heterogeneous media will be used to study the densification process. These models assume that, there are solid inclusions embedded in the homogeneous matrix. These models are the composite sphere model and the self-consistent model. Scherer [20] used these models in connection with his previous model in reference [43], to put the equations that describe the densification process during sintering in materials that contain solid inclusions surrounded by the matrix phase. In this work, the applicability of these equations on the densification in sintering process in clays mixtures will be studied. A list of the important equations that related to densification process will be given below.

2.3.2. The Constitutive Equations:

The constitutive equation for an elastic material is [44]:

$$\varepsilon_x = \varepsilon_f + E^{-1}\left[\sigma_x - \nu_m(\sigma_y + \sigma_z)\right] \quad (2.56)$$

where ε_x is the strain in the x direction, ε_f is the free strain, E is Young's modulus, ν_m is Poisson's ratio, and σ_x, σ_y, and σ_z; are the stresses in the x, y, and z directions, respectively. The observed strain ε_x is a linear combination of the free strain ε_f and the strain caused by stresses. The analogous result for a viscous material is

$$\varepsilon'_x = \varepsilon'_f + (3\eta)^{-1}\left[\sigma_x - (1/2)(\sigma_y + \sigma_z)\right] \quad (2.57)$$

where ε'_x and ε'_f are the strain rate in x direction and the free strain rate respectively; η is the viscosity and ν = ½, indicating that the material is incompressible. The sintering matrix is compressible, because it contains pores, so Eq. (2.57) becomes [43]

$$\varepsilon'_x = \varepsilon'_f + (E_m)^{-1}\left[\sigma_x - \nu_m(\sigma_y + \sigma_z)\right] \quad (2.58)$$

where E_m, is the apparent Young's modulus and ν_m, is Poisson's ratio. Scherer [20] supposed E_m not a modulus, but a viscosity, he defined it as the viscous response of the porous material to a uniaxial stress, so it will be called the uniaxial viscosity of the porous matrix. As the porosity goes to zero, $E_m \rightarrow 3\eta$ and $\nu_m \rightarrow 1/2$, so Eq. (2.58) reduces to Eq. (2.57).The functional dependence of E_m and ν_m, on porosity depends on the microstructure. The observed contraction rate of a sintering body is attributed to an effective pressure resulting from interfacial energy. The strain rate depends on the magnitude of that pressure and the bulk modulus of the body. The relationship between these quantities can be established as follows:

If the applied stress is hydrostatic, $\sigma_x = \sigma_y = \sigma_z = P$, then Eq. (2.58) becomes

$$\varepsilon'_x = \varepsilon'_f + \frac{P(1-2\nu_m)}{E_m} = \varepsilon'_f + P/(3K_m) \tag{2.59}$$

where K_m is the apparent bulk modulus, which defined by

$$K_m = E_m/[3(1-2\nu_m)] \tag{2.60}$$

by analogy to the elastic bulk modulus. As E_m, K_m is not a true modulus: it represents the viscous response of the porous body to a hydrostatic stress, so it will be called the bulk viscosity of the porous matrix. K_m becomes infinite (i.e., the matrix becomes incompressible) when the porosity vanishes ($\nu_m = 1/2$). If P is equal and opposite to the sintering pressure, P_o, then densification stops ($\varepsilon'_x = 0$); according to Eq. (2.59) this occurs when

$$P = -3K_m\varepsilon'_f$$

Therefore

$$P_o = 3K_m\varepsilon'_f \tag{2.61}$$

The pressure is regarded as negative when it is compressive; i.e. the same sign convention is used for pressure and for stress.

The viscous or elastic response of an isotropic material to stress or strain can be described by two independent functions. The constitutive equation can be written in terms of E_m, and ν_m, as in Eq. (2.58), or equivalent expressions can be obtained in terms of K_m and the apparent shear modulus, G_m that is given by the following equation [44]:

$$G_m = \frac{E_m}{[2(1+\nu_m)]} \tag{2.62}$$

Again, G_m is not a true modulus: it represents the viscous response of the porous material to a shear stress, so it will be called the shear viscosity of the porous matrix. The uniaxial and shear viscosities are finite when the porosity is zero ($E_m = 3\eta$ and $G_m = \eta$), while the bulk viscosity diverges. No microscopic model is implied by the constitutive equation. The

fundamental assumption is that the strain rate produced by the applied stress is linearly additive with the free strain rate. This may apply to crystalline materials undergoing creep such that the strain rate is linearly proportional to the stress (as discussed in References 18 and 19), and is expected to apply to viscous materials. However, the assumption may be violated if the applied stress causes a change in densification mechanism or a significant change in pore shape. The properties of ε'_f, E_m, and ν_m are assumed isotropic. This may cease to be valid after significant densification occurs, because the inclusions will inhibit shrinkage in the circumferential, but not in the radial direction. This may cause the sintering particles to develop necks of different sizes along these directions, resulting in anisotropic properties for the matrix. The predictions of the present analysis are consistent with experimental results for composites with noncrystalline matrices, but not with polycrystalline matrices. As discussed in References 33 and 34 it seems likely that the discrepancy results from the development of anisotropy in polycrystalline matrices.

2.3.3. The Composite Sphere Model:

We are interested in the sintering behavior of a composite sphere in which the core (radius a_{co}) is a nonsintering inclusion and the cladding (radius b) is sintering powder. Quantities related to the core (inclusion) are denoted by the subscript (i), those related to the powder (matrix) by subscript (m), and those related by the composite (matrix plus inclusions) by subscript (c). The stresses in the sphere consist of one radial component (σ_r) and two equal circumferential components (σ_θ). In spherical coordinates, the elastic constitutive equations are given by [44]:

$$\varepsilon_r = \varepsilon_f + E^{-1}\left(\sigma_r - 2\nu\sigma_\theta\right) \tag{2.63}$$

$$\varepsilon_\theta = \varepsilon_f + E^{-1}\left[\sigma_\theta - \nu\left(\sigma_r + \sigma_\theta\right)\right] \tag{2.64}$$

The free strain of the inclusion is zero (ε_{fi}, = 0). The inclusion was regarded as incompressible (i.e. the bulk modulus $K_i \rightarrow \infty$) under these conditions. The elastic solution was given in reference [20] as:

$$\sigma_{ri} = \sigma_{\theta i} \equiv \sigma_i = (1 - V_i) K_{cs}^E \varepsilon_{fm} \tag{2.65}$$

$$\sigma_{rm} = \left[\left(\frac{a_{co}}{r} \right)^3 - V_i \right] K_{cs}^E \varepsilon_{fm} \tag{2.66}$$

$$\sigma_{\theta m} = -\left[\frac{1}{2} \left(\frac{a_{co}}{r} \right)^3 + V_i \right] K_{cs}^E \varepsilon_{fm} \tag{2.67}$$

$$K_{cs}^E = \left[\frac{1}{4G_m^E} + \frac{V_i}{3K_m^E} \right]^{-1} \tag{2.68}$$

where G_m^E, and K_{cs}^E, are the elastic shear and bulk moduli, respectively, of the matrix. The volume fraction (V_i) is the current value, which increases as the matrix densifies. The radial displacement (u) at the surface of the composite sphere is also given by [20] as:

$$\frac{u_m(b)}{b} = \frac{(1 - V_i) K_{cs}^E \varepsilon_{fm}}{4G_m^E} \tag{2.69}$$

and the constitutive equations of the sintering matrix in spherical coordinates are given as:

$$\varepsilon_r' = \varepsilon_f' + E_m^{-1} (\sigma_r - 2\nu_m \sigma_\theta) \tag{2.70}$$

$$\varepsilon_\theta' = \varepsilon_f' + E_m^{-1} [\sigma_\theta - \nu_m (\sigma_r + \sigma_\theta)] \tag{2.71}$$

The solution for the sintering problem was obtained from the thermal stress problem by replacing G_m^E and K_{cs}^E with G_{m} and K_{m}, (defined by Eqs. (2.60) and (2.62)) and replacing the strains with the respective strain rates. Thus, the stresses in the sintering composite sphere are given by

$$\sigma_i = (1 - V_i) K_{cs} \varepsilon_{fm}' \tag{2.72}$$

$$\sigma_{rm} = \left[\left(\frac{a_{co}}{r}\right)^3 - V_i\right] K_{cs}\varepsilon'_{fm} \tag{2.73}$$

$$\sigma_{\theta m} = -\left[\frac{1}{2}\left(\frac{a_{co}}{r}\right)^3 + V_i\right] K_{cs}\varepsilon'_{fm} \tag{2.74}$$

$$K_{cs} = \left[\frac{1}{4G_m} + \frac{V_i}{3K_m}\right]^{-1} \tag{2.75}$$

the circumferential stress in the matrix is tensile (since $\varepsilon'_{fm} < 0$), so cracks tend to propagate radially from rigid inclusions [18, 19]. The linear strain rate of the composite is derived from Eq. (2.69):

$$\varepsilon'_c = \frac{u'_m(b)}{b} = \frac{(1-V_i)K_{cs}\varepsilon'_{fm}}{4G_m} \tag{2.76a}$$

substituting Eq. (2.75) in last equation gives:

$$\varepsilon'_c = \frac{(1 - V_i)\,\varepsilon'_{fm}}{\left(1 + V_i * (\frac{4G_m}{3K_m})\right)} \tag{2.76b}$$

Let ρ be the relative density (i.e. bulk density divided by theoretical density). The densification rate of the composite is

$$\frac{\rho'_c}{\rho_c} = -3\varepsilon'_c \tag{2.77}$$

rearranging gives

$$\frac{1}{dt}\frac{d\rho_c}{\rho_c} = -3\varepsilon'_c \tag{2.78}$$

multiplying the last equation by (dt) and integrating both sides gives

$$\ln\left(\frac{\rho_c(t)}{\rho_{co}}\right) = -3\varepsilon'_c t \tag{2.78b}$$

Taking the exponential and multiplying by (ρ_{co}) gives

$$\rho_c(t) = \rho_{co}\exp(-3\varepsilon'_c t) \tag{2.79}$$

where (ρ_{co}) and (ρ_c) are the densities of the composite at time equal (0) and (t) respectively. Given expressions for the free strain rate and moduli of the matrix, Eq. (2.79) can be used to describe the densification process in the composite. The densification rate of the matrix is

$$\frac{\rho'_m}{\rho_m} = -\left(\varepsilon'_{rm} + 2\varepsilon'_{\theta m}\right) \tag{2.80}$$

using Equations (2.70) and (2.71) leads to

$$\frac{\rho'_{m`}}{\rho_m} = -\left[\varepsilon'_{fm} + E_m^{-1}\left(\sigma_{rm} - 2\nu_m\sigma_{\theta m}\right)\right] + 2\varepsilon'_{fm} + 2E_m^{-1}\left[\sigma_{\theta m} - \nu_m\left(\sigma_{rm} + \sigma_{\theta m}\right)\right]$$

$$= -\left[3\varepsilon'_{fm} + \frac{3(1-2\nu_m)}{E_m}\left(\sigma_{rm} + \sigma_{\theta m}\right)\right] \tag{2.81}$$

substituting Eq. (2.60) in the last equation, gives

$$\frac{\rho'_m}{\rho_m} = -\left[3\varepsilon'_{fm} + \frac{\left(\sigma_{rm} + 2\sigma_{\theta m}\right)}{3K_m}\right]$$

$$\frac{\rho'_m}{\rho_m} = -\left[3\varepsilon'_{fm} + \frac{\sigma_m}{3K_m}\right] \tag{2.82}$$

with similar rearranging and integrating, as done in Eq. (2.77) we get

$$\rho_m(t) = \rho_{mo}\exp\left(-\left(3\varepsilon'_{fm} + \frac{\sigma_m}{3K_m}\right)t\right) \tag{2.83}$$

where (ρ_{mo}) and (ρ_m) are the densities of the matrix at time equal zero and (t) respectively. σ_m is the hydrostatic stress in the matrix, is given by [20] as:

$$\sigma_m = \frac{\sigma_{rm} + 2\sigma_{\theta m}}{3} \tag{2.84}$$

Thus, the sintering rate is affected by the hydrostatic component of the stress in the matrix, which is independent of radial position. Substituting equations (2.73) and (2.74) in Eq. (2.84) gives

$$\sigma_m = \frac{\left[\left(\frac{a_{co}}{r}\right)^3 - V_i - \left(\frac{a_{co}}{r}\right)^3 - 2V_i\right] K_{cs}\varepsilon'_{fm}}{3} = -V_i K_{cs}\varepsilon'_{fm} \qquad (2.85)$$

2.3.4. Self-Consistent Model:

The matrix region can be regarded as an island of sintering material in a continuum (the composite) that is contracting at a slower rate (see figure (2.9)). The mismatch in free strain rates of the island and the continuum causes stresses that affect the densification rates of each [20]. The hydrostatic tensile stress in the island of matrix can be calculated from Selsing solution [45] for the stress in an isolated inclusion. Using that stress in the constitutive equation of the matrix, one can calculate the sintering rate of the matrix, which controls the sintering rate of the composite. The hydrostatic stress in the island, which represents any region of matrix, is found by applying the viscous analogy to Selsing's solution: strains are replaced by strain rates and the respective moduli of the island and continuum are replaced by (K_m) and (G_c). Thus

$$\sigma_m = \left(\varepsilon'_c - \varepsilon'_{fm}\right)\left[\frac{1}{3K_m} + \frac{1}{4G_c}\right]^{-1} \qquad (2.86)$$

where G_c is the shear viscosity of the continuum (i.e., the composite) ;
for spherical inclusions, the Hashin-Shtrikman equation [46] for G_c is appropriate. Eq. (2.86) indicates that the stress in the (island of) matrix is proportional to the difference between its free strain rate and the strain rate of the surrounding composite. The linear contraction rate of the composite, ε'_c, is related to the densification rate of the matrix by [20] as:

$$\varepsilon'_c = -\frac{(1-V_i)\rho'_m}{3\rho_m} = (1-V_i)\left[\varepsilon'_{fm} + \frac{\sigma_m}{3K_m}\right] \qquad (2.87)$$

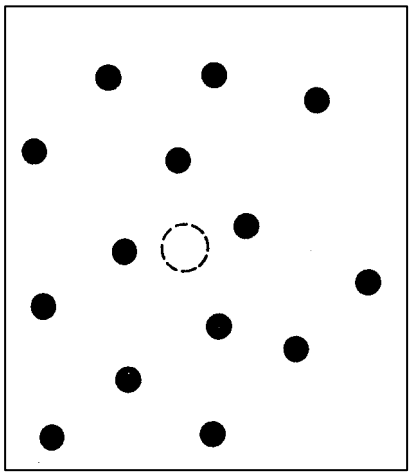

Figure (2.9) in the self-consistent calculation, the region of matrix within the dashed circle is regarded as an isolated island surrounded by an infinite continuum (the composite) with a slower densification rate. Similarly, any of the inclusions (solid circles) can be treated as being isolated in the continuum [20].

where the second equality follows from Eq. (2.82). Substituting Eq. (2.87) into Eq. (2.86) gives

$$\sigma_m = \left[-V_i \varepsilon'_{fm} + \frac{(1-V_i)\sigma_m}{3K_m} \right] \left[\frac{1}{\frac{1}{3K_m} + \frac{1}{4G_c}} \right] \tag{2.88}$$

Solving the previous equation for σ_m gives

$$\sigma_m = \frac{-V_i \varepsilon'_{fm}}{\left[\frac{1}{4G_c} + \frac{V_i}{3K_m} \right]} \tag{2.89}$$

$$\sigma_m = -V_i \varepsilon'_{fm} K_{s-c} \tag{2.90}$$

where

$$K_{s-c} = \left[\frac{1}{4G_c} + \frac{V_i}{3K_m} \right]^{-1} \tag{2.91}$$

substituting Eq. (2.90) in Eq. (2.87), gives

$$\varepsilon_c' = (1-V_i)\left[\varepsilon_{fm}' - \frac{V_i \varepsilon_{fm}' K_{s-c}}{3K_m}\right]$$

$$\varepsilon_c' = (1-V_i)\varepsilon_{fm}' K_{s-c}\left[\frac{1}{K_{s-c}} - \frac{V_i}{3K_m}\right] \tag{2.92}$$

$$\varepsilon_c' = \frac{(1-V_i)\varepsilon_{fm}' K_{s-c}}{4G_c} \tag{2.93}$$

2.4 Applying the Previous Models on Viscous Sintering:

In this section, the stress and strain rates are evaluated for the case of viscous sintering. The microstructure of the matrix is assumed to consist of a network of cylinders with radius (a) that intersect at right angles, and the distance between neighboring parallel cylinders is (l). For such a structure, the free strain (i.e. linear contraction) rate is given by reference [43] as:

$$\varepsilon'_{fm} = -\left(\frac{\gamma}{\eta\, l_o\, \rho_o^{\,1/3}}\right)\left(\frac{(3\pi)^{1/3}}{6}\right)\left[\frac{2-3cx}{x^{1/3}(1-cx)^{2/3}}\right] \tag{2.94}$$

where (x) is a geometric parameter, $x \equiv a/l$, (γ) is the interfacial energy; (η) is the viscosity, (l_o) and (ρ_{mo}) are the initial values of (l) and (ρ_m), respectively, and the constant $c = 8\sqrt{2}/3\pi$. From the same reference Poisson's ratio is given by

$$\nu_m = 2\sqrt{2}x/\pi \approx \frac{1}{2}\left[\frac{\rho_m}{(3-2\rho_m)}\right]^{1/2} \tag{2.95}$$

where (ρ_{m}), is the relative density of the structure, which is given by [6] as

$$\rho_m = 3\pi x^2 (1 - cx) \tag{2.96}$$

The "apparent Young's modulus" (uniaxial viscosity) is [43]:

$$E_m = 3\eta\pi x^2 \approx \frac{3\eta\rho_m}{(3 - 2\rho_m)} \tag{2.97}$$

K_m is given from the substitution of equations (2.96) and (2.95) in Eq. (2.60) as follows

$$K_m = \frac{2\eta\pi x^2}{(2 - 3cx)} \tag{2.98}$$

For this microstructure the load-bearing function of the cross-sectional area, φ, is (πx^2), so Eq. (2.95) and Eq. (2.97) imply $E_m = 3\eta\varphi$ and $\nu_m = \sqrt{\varphi}/2$. The expressions for σ_i, σ_m and ε'_c involve the ratio of the shear to the bulk viscosity. According to equations (2.60) and (2.62) we get:

$$\frac{4G_m}{3K_m} = \frac{2(1 - 2\nu_m)}{(1 + \nu_m)} \tag{2.99}$$

Equations (2.95) and (2.99) are used to evaluate the results for the CS model. The Hashin-Strikman equation [46] for (G_c) leads to

$$\frac{4G_c}{3K_m} = \frac{4G_m}{3K_m}\left[1 + \frac{15}{2}\left(\frac{V_i}{1 - V_i}\right)\left(\frac{1 - \nu_m}{4 - 5\nu_m}\right)\right] \tag{2.100}$$

Equations (2.95), (2.99) and (2.100) are used to evaluate the results for S-C model. The current volume fraction of inclusions, (V_i), is related to the final volume fraction in the fully sintered body, (V_i^f) by [20]:

$$V_i = \rho_m \left[\rho_m + \left(\frac{1 - V_i^{\,f}}{V_i^{\,f}} \right) \right]^{-1} \tag{2.101}$$

The difference between the CS and S-C models becomes significant only at high concentrations of inclusions.

Figure (2.10) shows a similar comparison between the prediction of the S-C model and the CS model. The results are indistinguishable for (V_i) less than 0.2.

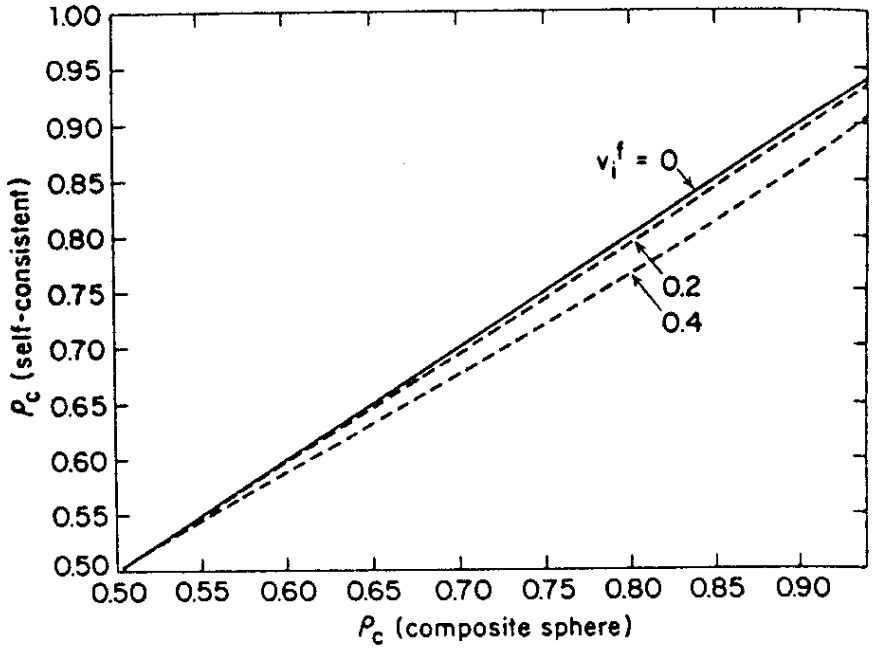

Figure (2.10) Relative density of composite, ρ_c, from self-consistent model (by integration of Eq. (2.93)) versus, ρ_c, from composite sphere model (by integration of Eq. (2.76a)) [20].

These analyses do not allow for the fact that the inclusions will come into contact and stop densification at some critical volume fraction, V_i*. For inclusions of uniform size, percolation theory indicates that the inclusions will form a contiguous network when V_i* equal approximately 0.16. If this network is stiff enough to resist the sintering stress, then V_i* equal 0.16 in this case; for inclusions with a wide distribution of sizes, the

critical volume fraction could be smaller. The extent of the contiguous network of particles, increases abruptly as V_i approaches V_i*, so the present analyses should fail only near V_i* [20].

Chapter Three
Fitting Data and Programs Design

3.1 Introduction

In this chapter, the following points are discussed, explaining the fitting process and the way to determine the relationship between the constant (K) ,which is the proportionality constant between the reduced time (Kt) and the practical time, in Eq. (2.23) and the temperature of sintering. Then shortly describe the simulated samples and their raw materials, then listing the input data in each program and the way to get each parameter from the practical measurements. Then a flow chart diagram is drawn which contains the basic relations used and the origin of their equations for each program. Basically; there are three programs:

The first concerned with the modified Scherer model. It simulates the sintering process in the clay mixtures, and manipulates the effect of sintering temperature and time on the densification process.

The second simulates the effect of pore size distribution on the densification process in the mixtures of the used clays using the modified Scherer model.

The third program uses the composite sphere model and the self-consistent model to simulate the sintering process in the clays mixtures, and manipulates the effect of sintering temperature and time on the density after firing.

3.2. Fitting Process

3.2.1 Fitting procedure:

The goal of this operation is to find a relation between the values of the constant (K) in (hr^{-1}) from Eq. (2.26a) versus the temperature of the sintering (T) in (^oC) using the practical data. From

Eq. (2.23) it is obvious that the basic parameter that is affected by temperature is the viscosity coefficient (η), so it is the basic factor that makes (K) changed with temperature. The fitting process is divided into the following steps:

A. The value of (K) is found for each sample at each temperature by finding the slope of the line formed from plotting the data between the reduced time (Kt) versus the practical time (t). The $K\,(t\text{-}t_0)$ values are calculated using Eq. (2.26a) for the modified Scherer program and Eq. (2.26b) for the composite sphere and the self consistent program by substituting the values of x and x_o. the values of x_o and x before and after sintering respectively can be found by knowing the values of (λ) from Eq. (2.2) (which will be discussed later) and by knowing the relative densities for each sample before and after sintering from the practical data, then solving numerically Eq. (2.8b) to get the value of (x) corresponding to a given (ρ) value. The (K) value is given by the equation:

$$slope = K = \frac{K(t - t_o)}{t_p} \qquad (3.1)$$

where (t_p) is the time of sintering, for the present it equals two for all samples. The rest parameters have their same previous definitions.

B. The graph of the data between (K) and the corresponding firing temperature is drawn. Then, fitting is accomplished to find a formula describing the change of (K) with temperature. If a relation between K and temperature is determined then (K) values are substituted in equation (2.23) in addition to the rest parameters to find the relation

between the factor (γ/η) and sintering temperature by fitting the resulting curve.

3.2.2 Viscosity:

The most important physical factor that can be found from fitting process is the viscosity of the viscous liquid that formed during the sintering process. Viscosity is the internal friction of flowing substance [47]. In ceramic materials, the viscosity (shear viscosity) of the matrix depends in a complex way on the microstructure. It represents the major difference between the sintering of a glass and a ceramic. In glass it depends merely on the self diffusion coefficient. In ceramic it depends on the grain size in addition to the diffusion coefficient, since matter must be transported across a distance of the grain size to achieve shear deformation [48]. The dependence on grain size may be the same as in Coble creep [49] where the viscosity of polycrystal varies with grain size, dp, according to the relation $\eta \alpha dp^3$. So it may be concluded that the viscosity of glass will always be lower than the viscosity of polycrystalline ceramic, provided that the ceramic is deformed by Coble creep mechanism. In viscous sintering the densification process depends basically on viscous flow [12, 13] so the value of viscosity during the process plays a major role in limiting the density after firing. In this work Scherer concepts [6] in finding the values of viscosity are followed, first the values of (K) are calculated from the fitting process as discussed previously, where (K) is the proportionality constant between the reduced time (Kt) calculated from Eq. (2.26b) and the practical time. Then Eq. (2.23) is used after rearranging the parameters to find the viscosity coefficient (η) at different temperatures, and a relationship between the viscosity coefficient and the sintering temperatures can be found by fitting process.

3.3 The Groups Undergoing the Simulation:

The samples used for applying the simulation are prepared by Rasen [40]. Two groups were selected as an experimental results data that was applied to examine the models. The materials of samples regarded as heterogeneous ceramic systems. Since the present work is not concerned here with the details of preparation, but only with the parameters related to the sintering process, like the composition of these materials, and the ratio of the solid inclusions, then the raw materials of their groups will be defined to follow the results come from the process parameters. The raw materials applied for the groups are:

1. Kaolin Dukhla: the composition of kaolin is in the table (3.1).

2. Ninivite Rock: It is a white, light silica brick, porous and low bulk density rock (less than 0.3gm/cm^3 in the pure rock). Quartz is the main mineral constituent; gypsum is the main pollutant of the rock. Since this rock differs in origin and is not recorded in geological dictionaries, it is suggested to name it as "NINIVITE" for this form of porcelainite which is produced by sulphure leaching of clay stones. The chemical analysis of a semi- pure ninivite rock and that is used in the present work are given in table (3-1).

There are two groups used in applying the simulation the groups are defined as Group M21 and Group M22. Group M21 is a mixture of compositional weight percentage of 60% kaolin duekhla raw material powder, 30% of ninivite raw material with particle size range 'D' ($22\mu m$<D<$32\mu m$), and 10% weight of α-Al_2O_3, particle size range (D≤$32\mu m$). These components were dried, mixed and milled.

Group M22 is a mixture of compositional weight percentage of 70% kaolin duekhla raw material mixed with 30% of ninivite raw

material with particle size range 'D' is given by ($D< 50\mu m$) . Then it was dried, mixed and later milled for 10 hours.

Table (3.1) the chemical composition of the raw materials of the used groups [40].

Chemical composition data for Kaolinite			Chemical composition data of Ninivite rock		
Material	Percentage before firing	Percentage after firing	Material	Percentage Before firing	Percentage After firing
SiO_2	52.35	58.82	SiO_2	93.76	96.233
Al_2O_3	34.02	38.225	Al_2O_3	0.28	0.28739
Fe_2O_3	1.31	1.472	Fe_2O_3	0.16	0.1642
TiO_2	0.21	0.236	Na_2O	0.09	0.0924
CaO	1.20	0.1348	CaO	0.82	0.8416
MgO	1.11	1.2472	MgO	0.031	0.0318
SO_3	0.45	1.472	SO_3	0.26	_
L.O.I	12.54	_	P_2O_5	0.06	0.06158
			K_2O	0.06	0.06158
			Cl	0.13	_
			L.O.I	2.57	_

3.4. The Modified Scherer Model Program (Effect of Sintering Temperature and Time of Sintering):

This program simulates the sintering process and manipulates the effect of sintering temperature and time on the final density and densification. It is written in the FORTRAN 90 language. Here we will concentrate on the temperature effect, and by a same manner the time effect on densification can be found.

3.4.1 Input Data

The input data to this program are the

1. Initial densities.

2. Theoretical density of the samples used.

3. The sintering temperature and the ratio λ, and they are found as follows:

3.4.1.1 The Theoretical Densities and the True Volumes

The theoretical density for each compact is calculated by summing the multiples of the theoretical density of each component in the compact by its weight percent from the compact after subtracting the loss on ignition from the weight of the compact, because at the end of firing process this volume will be lost from the compact.

The true volume is given by the following relation [50]

$$\text{True volume} = \text{Weight} / \text{True density} \qquad (3.2)$$

The weight of each material in the compact is given by the multiple of its weight percent in the compact taken from table (3.1) by the mass of the compact.

3.4.1.2 The Temperature:

In this program as being mentioned previously the basic objective is finding the effect of sintering temperature on the final density of the compact, so the temperature must be a variable here. The temperature will be substituted in the equation of (K) results from the fitting process. The values of the temperatures will be between (1100 to 1500) ^{o}C.

3.4.1.3 The Ratio λ:

The ratio λ, From Eq. (2.2) is determined by determining the volume of solid inclusions V_{in} and the volume of viscous phase V_{vis} in compact. This is done by: first, deciding which materials have the solid inclusions manner and which have the viscous phase manner. In the present case the materials in the table (3.2) is assumed to have the viscous phase effect and other oxides specially alumina have the solid inclusions effect.

Table (3.2) Fusion temperatures of fluxes associated with alumina and silica [12]

Oxide	Lowest eutectic temperature in ^{o}C
Na_2O	732
K_2O	695
CaO	1170
MgO	1345
Fe_2O_3	1073

Second, determining the weight of the solid inclusions in the compact from the weight percent of the solid inclusions materials by multiplying the weight percent of the solid inclusions by the mass of the

sintered compact, then dividing the weight of solid inclusions materials by the theoretical density of the solid inclusions materials to determine the true volume of the solid inclusions. By the same manner the true volume of the viscous phase is found for each compact, then λ is found from Eq. (2.2).

3.4.2 Program Design:

A computer program in FORTRAN 90 language is designed and applied to calculate the final relative density of the compacts after sintering process. This program needs the following input data:

Input: the data file for the model consists from the following information: 1. Initial density for each sample (ρ_o). 2. Theoretical density for the used sample ρ_s and the ratio λ defined by Eq. (2.2) for the simulated sample. 3. Temperature of sintering of each sample. Let N : the number of the sintered samples, t: is a counter, f(t): is a function that represent the relation between *K* and the sintering temperature, Kt :is the value of *Kt* , acc: the accuracy, ρ_o: is the initial density, ρ_s: is the theoretical density, ρ_r: is the relative density, x=a/*l*, where (a) is the particle size, *l*: is the length of the compacted unit cell, which is the cell contains the viscous phase, the porosity and the solid inclusion phases, x_o: the initial value of (*x*), xr: is a real function that solves Eq. (2.8) numerically for x for known values of the relative density (ρ/ρ_s) and (λ), λ: is a parameter given by Eq. (2.2), l_o: is the effective length of the cell, pi: is the constant ratio ≈ 3.14, rρρs : is the final relative density. t: is a counter. Root: is a subroutine that determines the value of x corresponds to a given *Kt* value by solving Eq. (2.26a) numerically; here we used Newton-Raphson method. The program design is explained in the following flow chart.

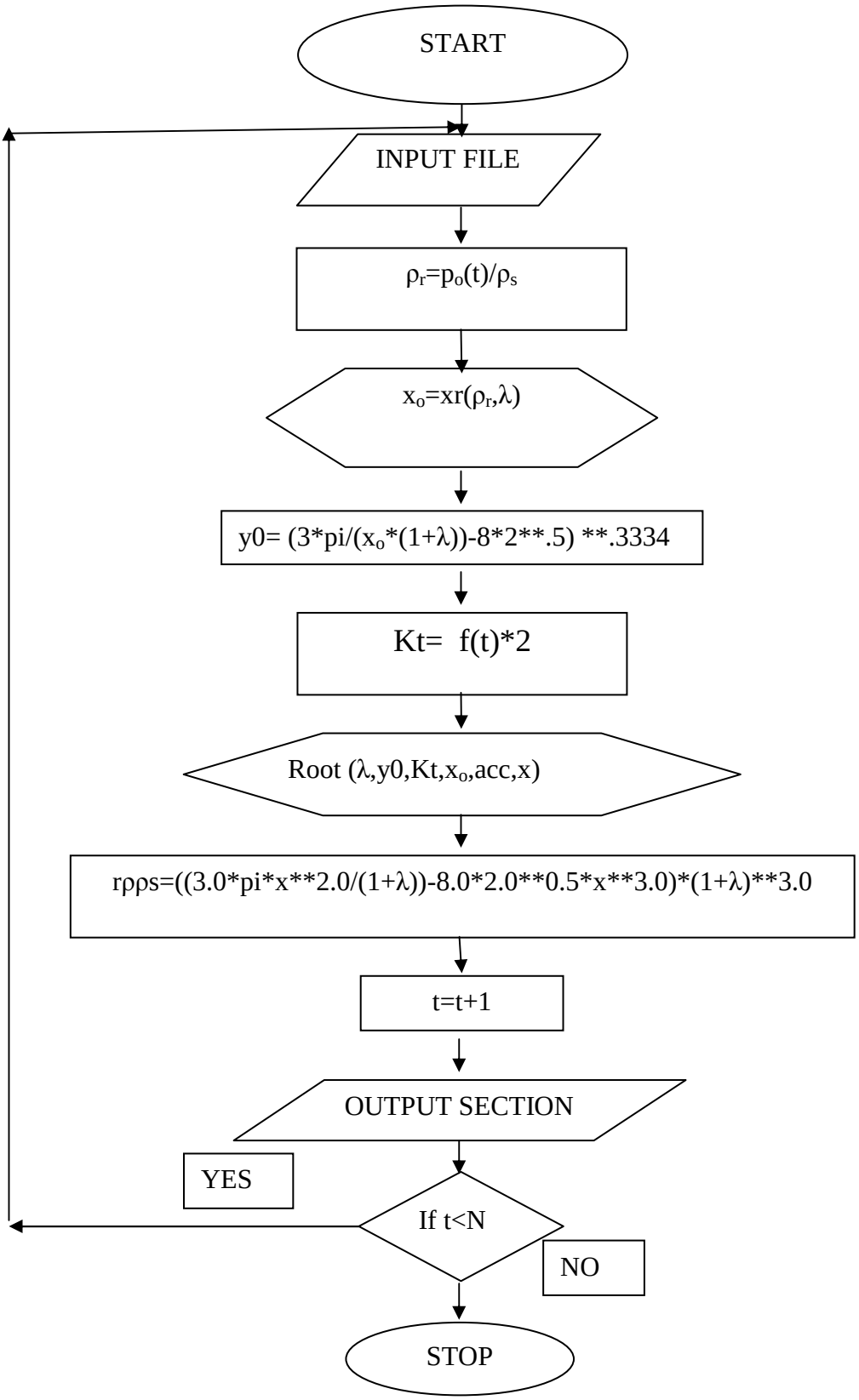

Figure (3.1) Flow chart of the modified Scherer model (temperature effect) program

3.5. The Modified Scherer Model Program (Effect of Pore Size Distribution):

This program simulates the effect of pore size distribution on the densification process. A program EFFECT OF PORE SIZE is written in FORTRAN 90 language to simulate the effect of pore size distribution.

3.5.1 Input Data

To perform the calculations of this program the input data must be provided. These data includes the compact particle size, the initial relative density of the compact, the standard deviation of the pore size distribution, the temperature of sintering of the simulated sample, λ which is the ratio of the true solid inclusions volume to the true viscous phase volume in the compact and the necessary information for the numerical methods used in the program. We will discus the foundation of the parameters that didn't discussed previously.

3.5.1.1 The Standard Deviation (σ_d):

The standard deviation σ_d of the pore diameters is found from mercury porosimetry data, by drawing a curve between the intruded volume versus the diameter of pores like that in figure (2.8). Then we get (σ_d) by following reference [51] the integral of the probability function (p_r) of a normally distributed variable (x) about its mean, say, x=0 in the interval -X< 0< X is given by

$$p_r = \frac{2}{\sqrt{\pi}} \int_0^{X/\sigma\sqrt{2}} \exp(-t^2)dt \qquad (3.3)$$

Where $t=x/\sigma\sqrt{2}$

The integral of equation (3.3) can be evaluated using the error function by the substitution y=X/σ√2 the equation can be written as

$$erf(y) = \frac{2}{\sqrt{\pi}} \int_0^y \exp(-t^2) dt \qquad (3.4)$$

Comparing the last two equation gives

$$p_r = \text{erf}\ (X/\sigma\sqrt{2}) \qquad (3.5)$$

(p_r) is the probability that a value of x lies within the range |x| <X. the values of erf (y) are tabulated in reference [51]. For the case

$$\text{erf}\ (X/\sigma\sqrt{2}) = 0.99 \qquad (3.6)$$

Yielding

$$\frac{X}{\sqrt{2}\sigma} = 1.820 \qquad (3.7)$$

or $$\sigma = \frac{X}{2.58} \qquad (3.8)$$

Where (X) is the upper or lower limit of the pore size distribution. For a mean (m) not equal to zero Eq. (3.8) will be as

$$\sigma = \frac{|X - m|}{2.58} \qquad (3.9)$$

(m): is defined by the value of the diameter that corresponds to maximum intruded volume see Figure (2.8). if the difference (X-m) for the upper limit differs from the lower limit it's better to take the average.

3.5.1.2 The Particle Size

The particle size will be found using stereological methods. Stereology is a method of analyzing the structure of a three-dimensional solid from the information provided by a two-dimensional plane section taken through the solid [2]. In figure (2.7) there is an image of the sample M22, (which sintered at $1400^{o}C$) after the firing process, this image will be used to find the particle size using the stereological methods as followed. By computing the mean intercept size (dp) that is equivalent to grain size, where (dp) is the ratio of the fractional density (ρ/ρ_s) to the number of grain (or pore) intercepts per unit length of test line (N_L):

$$dp = \frac{\rho / \rho_s}{N_L} \tag{3.10}$$

This is illustrated in figure (3.2) [2].

If grain size distribution is important, the mean intercept size can be calculated for multiple slices at different orientations. Here the same value of the particle size for M22 is assumed during the sintering process and at all the firing temperatures following Scherer assumption [31], and also because of the unavailable practical measurement, so in other study it is suggested taking this factor in consideration. In addition, it is noticed that there is a similarity in composition between M22 sample and M21 so the same value of particle size is applied to M21 for the previous reason.

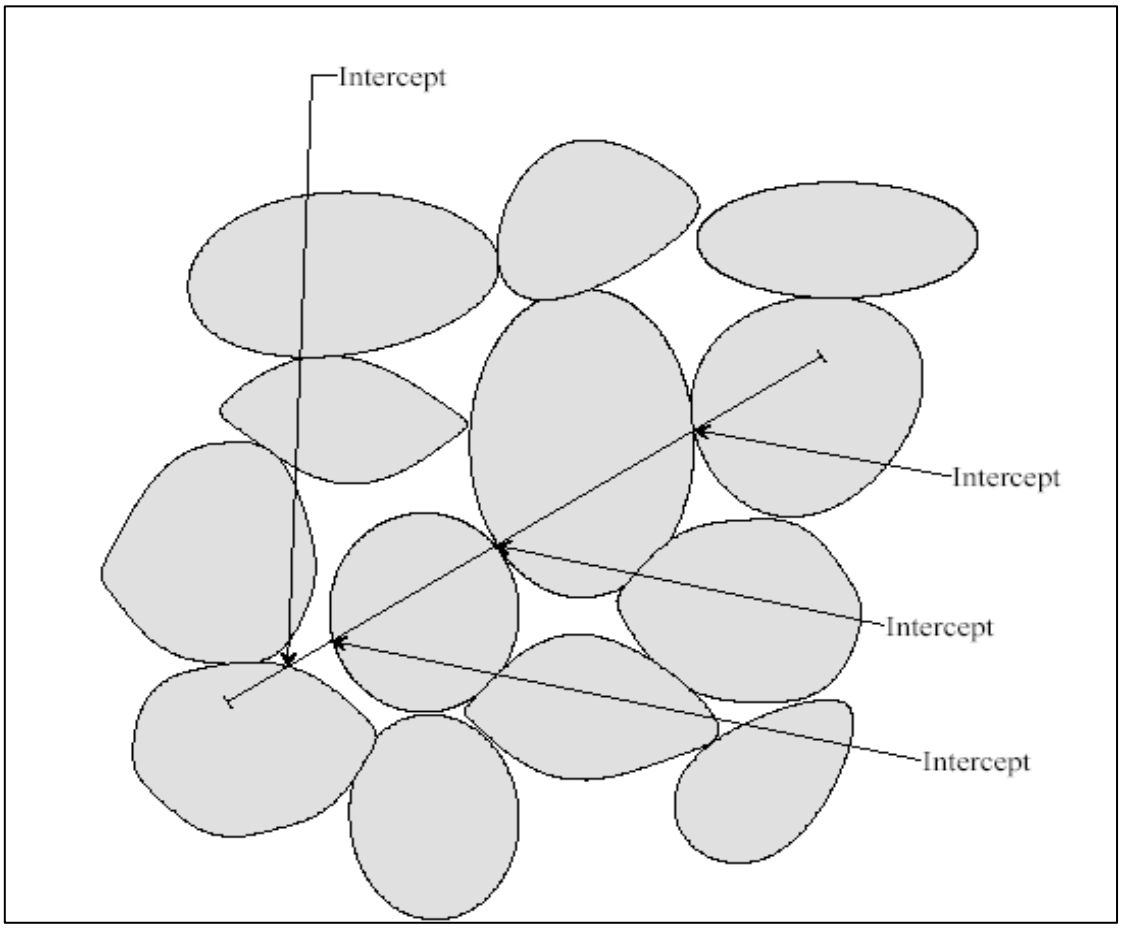

Figure (3.2) Calculating the Mean Intercept Size [2].

3.5.2 Program Design

A computer program PORE SIZE DISTRIBUTION EFFECT in FORTRAN 90 language is designed and applied to simulate the densification process. This program needs the following input data:

Input: the data file for the model consists from the following information:

a) particle size
b) theoretical density
c) standard deviation
d) accuracy
e) average pore diameter
f) Magnitude of sintering temperature.

The values of the input parameters are listed in table (3.3)

Table (3.3) Values of input data

Parameter	Symbol	Value	
		M22	M21
Compact particle size	dp (μm)	0.5777	0.5777
Theoretical density	ρ_s (gm/cm^3)	3.04362237	3.995213
Standard deviation of pore size (measured value)	σd (μm)	0.19	0.19
Mean pore diameter	d0a (μm)	0.6	0.6
Third root of solid inclusion to silica volume ratio	λ	0.669	o.723

Let σ_d, σ_l: be the standard deviation of pore size distribution and cell length side distribution respectively. d0a: the average pore diameter, acc: the accuracy, N: the number of the sintering temperatures, ttm: is the value of the sintering temperature, ρ_r: the relative density, x_o: the initial value of (x), xr: is a real function that solves Eq. (2.8) numerically for x

for known values of (ρ/ρ_s) and (λ), l_o: the effective length of the cell, pi: is the constant ratio ≈ 3.14, a0: the particle size. t: time in hour, f(t) a function yielded from the fitting process ,which describes the variation of (K) as a function of sintering temperature. Then the following Flow diagram can explain the logical steps of the program:

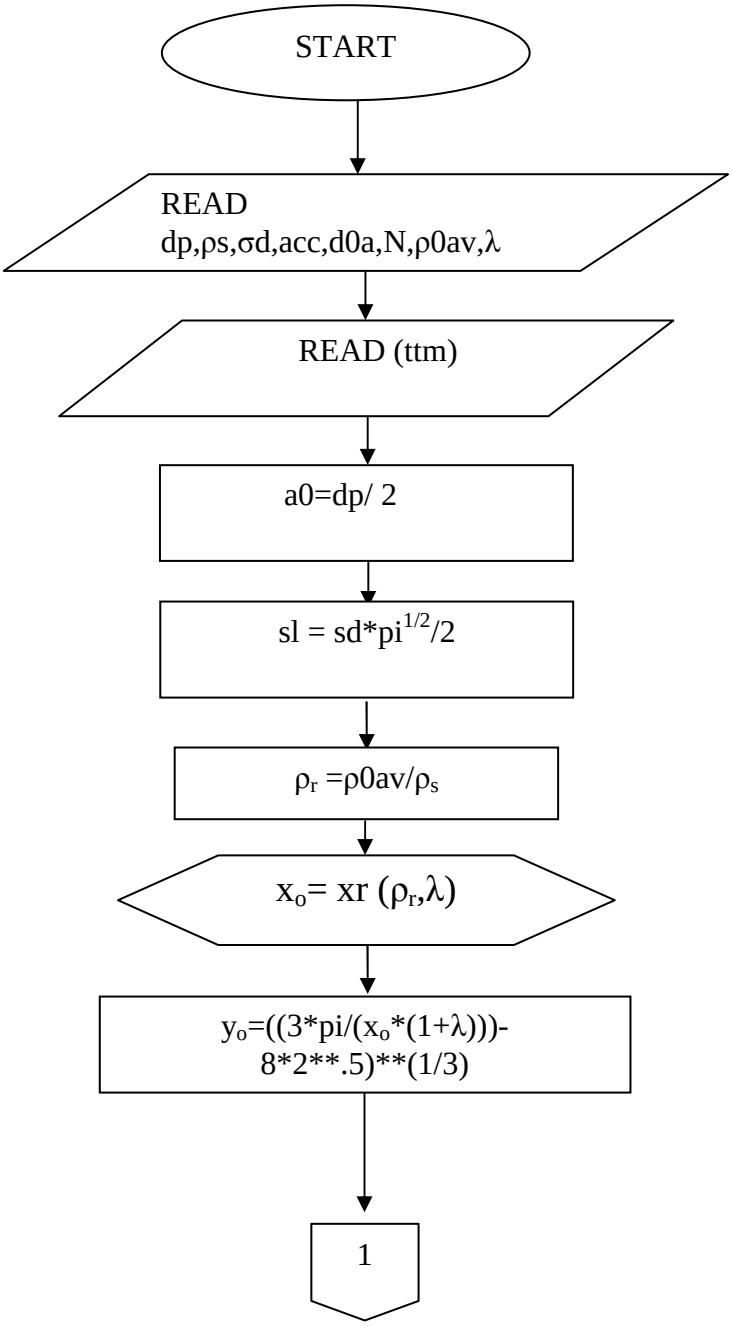

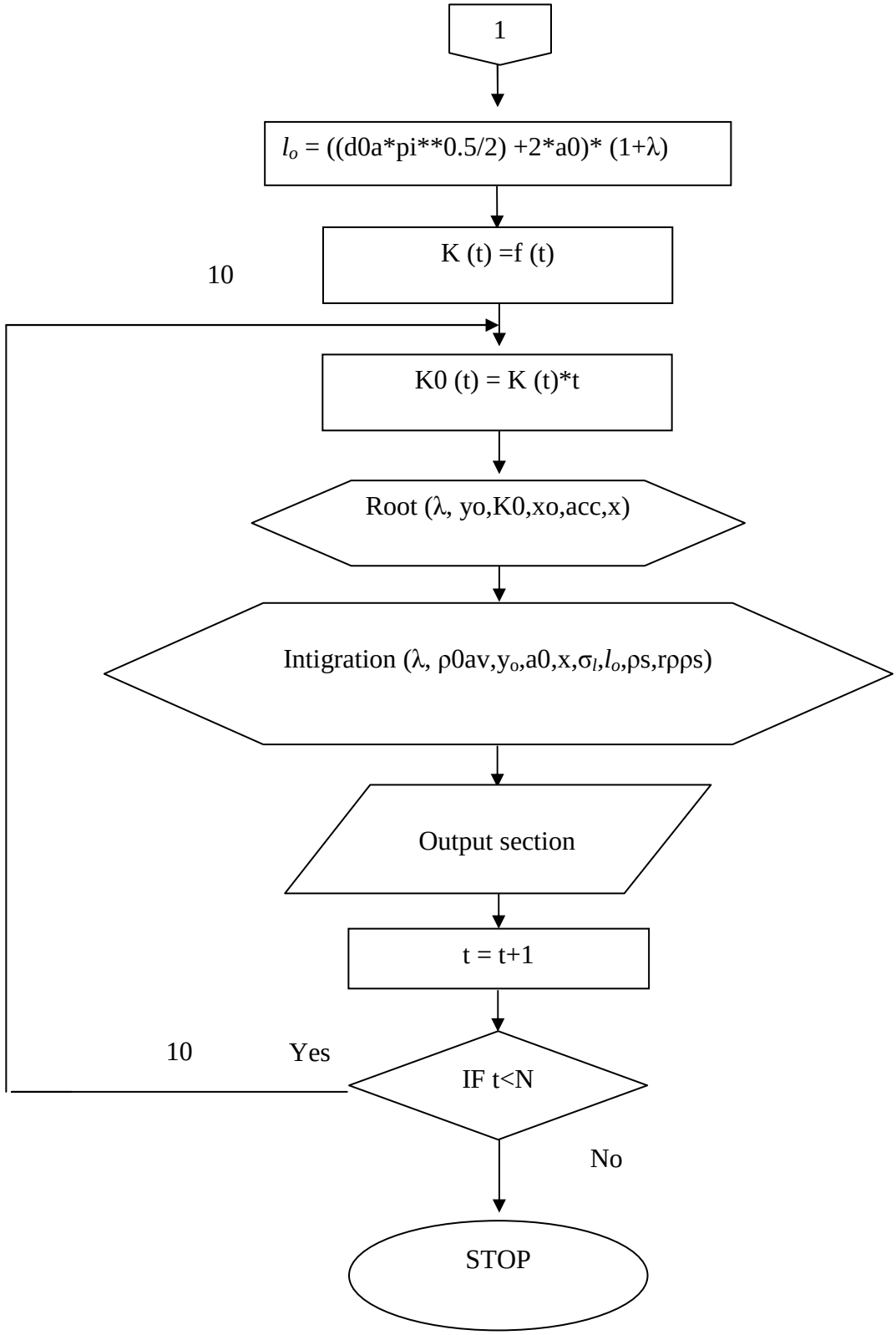

Figure (3.3) the Flow diagram of (the effect of pore size distribution on densification) program

By giving (σ_d) different values and from the graph between (ρ/ρ_s) versus reduced time we can see the effect of (σ_d) on the densification process.

3.6. The Program of Applying the Heterogeneous Models on Sintering Process:

This program applies two models of heterogeneous systems; named as the self consistent model and the composite sphere model to simulate the sintering process and manipulate the effect of sintering temperature on the final density, to compare the result with the result from the modified Scherer model.

3.6.1 Input Data

This program needs the following input data:

Input: is a data file for the model consists from the following information:

a) Particle size

b) Theoretical density

c) Average pore diameter

d) Number of temperature intervals

e) Magnitude of temperature at each interval

f) Final volume fraction of inclusions in each sample at each temperature interval.

g) Initial density for each sample.

All the parameters are evaluated as the way in the previous programs. The only new parameter is the final volume fraction of solid inclusions in the compact. To find this parameter the volume of the

compact will be divided as (done in finding λ) according to the type of the material into three parts, these parts are:

a) Volume of viscous phase.

b) Volume of solid inclusions.

c) Volume of pores.

The volume of viscous phase can be found as explained previously, it will be assumed equal to the true volume. The volume of pores is found from mercury porosimetry and it's equal to the cumulative porosity after firing. So the final volume fraction of the solid inclusions will be given by:

$$V_i^{\ f} = \frac{V_{compct} - \left(V_{pore} + V_{silca}\right)}{V_{compact}} \qquad (3.11)$$

where V_i^f: is the final volume fraction of the solid inclusion., $V_{compact}$: is the volume of the compact after sintering measured by Hg porosimetry. V_{pore}: is the volume of pores from Hg porosimetry. V_{silica}: is the true volume of viscous phase which is mostly formed from silica.

Applying Eq. (3.11) we get the final volume fraction of the solid inclusion in the compact as in the table (3.4).

Table (3.4) the final volume fraction of the solid inclusions (V_i^f) In the compacts.

temperature in(^{o}C) / sample	1200	1300	1400
M21	0.1909627	0.3248233	0.2215987

3.6.2 Program Design:

A computer program is written in FORTRAN 90 language to compute the density after firing process using the composite sphere model and the self consistent model. The Flow chart of this program is as in the figure (3.4).

All the previously defined parameters in the first program will have the same definition here. The new defined symbols are:

$\rho_o(i)$: is a matrix represent the initial density.

γ: is the interface energy.

xr (ρ): is a real function that uses Eq. (2.8b) to give the value of (x) that corresponds to a given value of (ρ/ρ_s) .

t_i: is the time of sintering (or firing process).

V_i^f: is the final volume fraction of the solid inclusions.

V_i: is the instantaneous volume fraction of the solid inclusions.

defm: is a subroutine that used to compute the rate of free strain energy ($d\varepsilon_{fm}$) as defined by Eq. (2.94).

etg(i) : is a matrix that computes the ratio (η/γ) which is the ratio of viscosity per interface energy.

η: represents the viscosity.

υ_m: is Poisson's ratio.

e_m: is The apparent Young's modulus as defined by Eq.(2.97).

G_m: is the apparent shear modulus as defined by Eq. (2.62).

K_m : is the bulk viscosity of the porous matrix as defined by Eq. (2.60).

G_mpK_m: represents the ratio ($4G_m/3K_m$) as defined by Eq. (2.99).

G_c: is the shear viscosity of the continuum (in the self consistent model).

G_cpK_m: is the ratio ($4G_c/3K_m$) as defined by Eq. (2.100).

K_{cs}: is the bulk modulus of the matrix as defined by Eq. (2.75).

$d\varepsilon_{cs}$: The linear strain rate of the composite according to composite sphere model as defined by Eq. (2.76b).

$d\varepsilon_{sc}$: The linear strain rate of the composite according to self consistent model as defined by Eq.(2.87).

$\rho_{ccs}(i)$: is a matrix represent the relative density of the composite after sintering as predicted by the composite sphere model.

σ_m: is the hydrostatic stress in the matrix as defined by Eq. (2.90).

$\rho_{mcs}(i)$: is a matrix represent the relative density of the matrix after sintering as predicted by the composite sphere model.

$\rho_{csc}(i)$: is a matrix represent the relative density of the composite after sintering as predicted by the self consistent model.

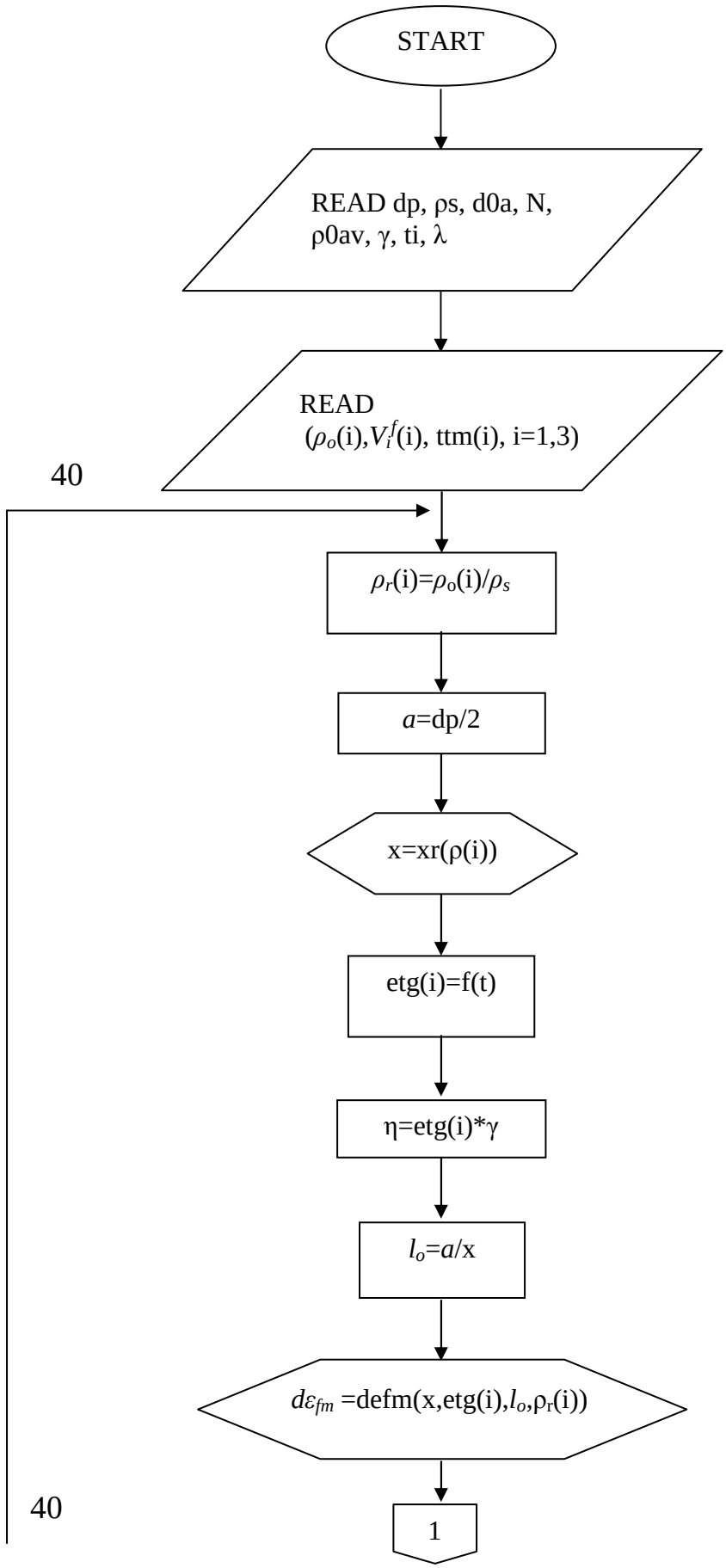
START
READ dp, ρs, d0a, N,
ρ0av, γ, ti, λ
READ
(ρ_o(i),V_i^f(i), ttm(i), i=1,3)
40
ρ_r(i)=ρ_o(i)/ρ_s
a=dp/2
x=xr(ρ(i))
etg(i)=f(t)
η=etg(i)*γ
l_o=a/x
$d\varepsilon_{fm}$ =defm(x,etg(i),l_o,ρ_r(i))
40
1

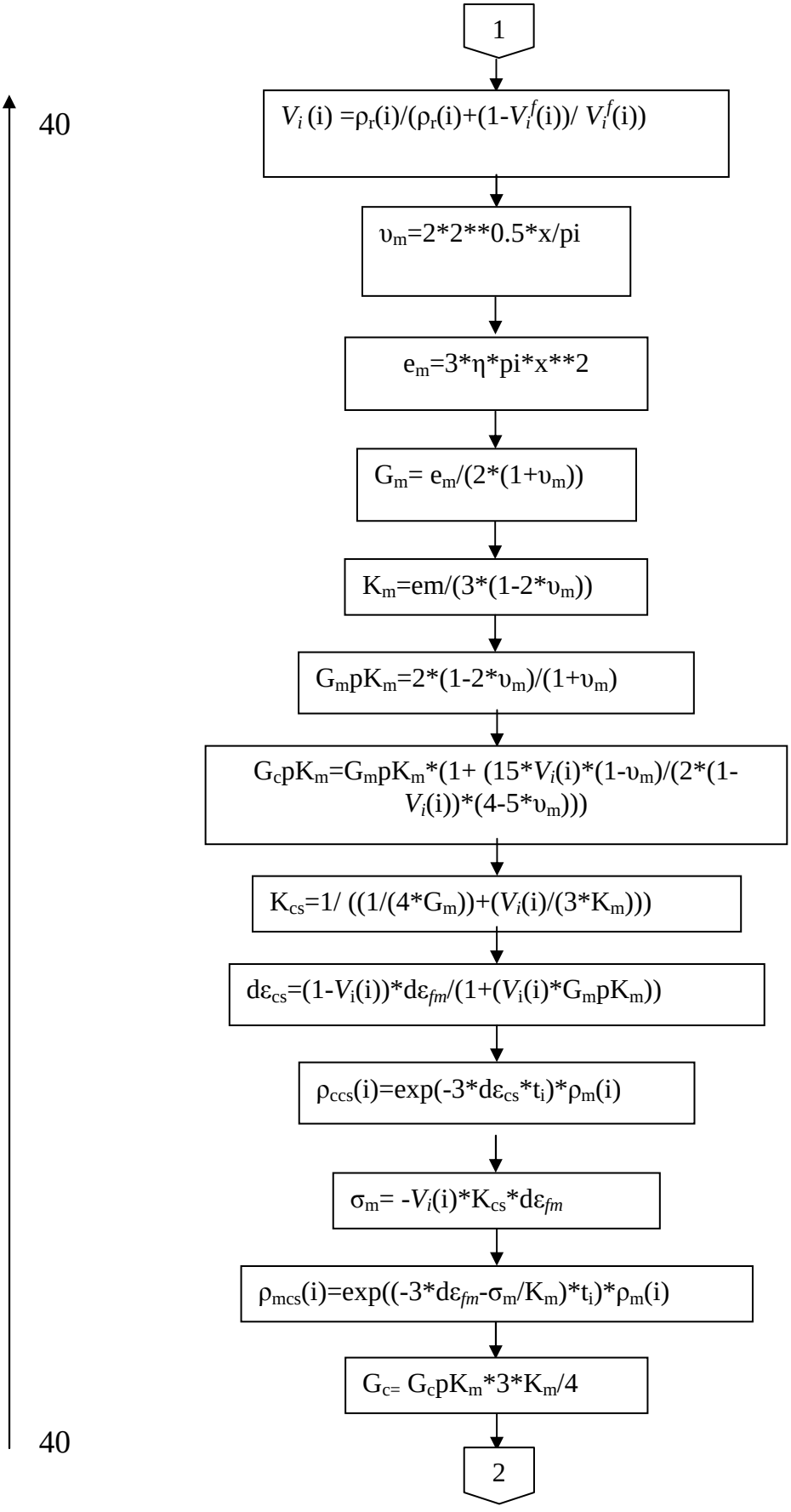
1
40
V_i (i) =ρ_r(i)/(ρ_r(i)+(1-V_i^f(i))/ V_i^f(i))
υ_m=2*2**0.5*x/pi
e_m=3*η*pi*x**2
G_m= e_m/(2*(1+υ_m))
K_m=em/(3*(1-2*υ_m))
G_mpK_m=2*(1-2*υ_m)/(1+υ_m)
G_cpK_m=G_mpK_m*(1+ (15*V_i(i)*(1-υ_m)/(2*(1-V_i(i))*(4-5*υ_m)))
K_{cs}=1/ ((1/(4*G_m))+(V_i(i)/(3*K_m)))
$d\varepsilon_{cs}$=(1-V_i(i))*$d\varepsilon_{fm}$/(1+(V_i(i)*G_mpK_m))
ρ_{ccs}(i)=exp(-3*$d\varepsilon_{cs}$*t_i)*ρ_m(i)
σ_m= -V_i(i)*K_{cs}*$d\varepsilon_{fm}$
ρ_{mcs}(i)=exp((-3*$d\varepsilon_{fm}$-σ_m/K_m)*t_i)*ρ_m(i)
$G_{c=}$ G_cpK_m*3*K_m/4
40
2

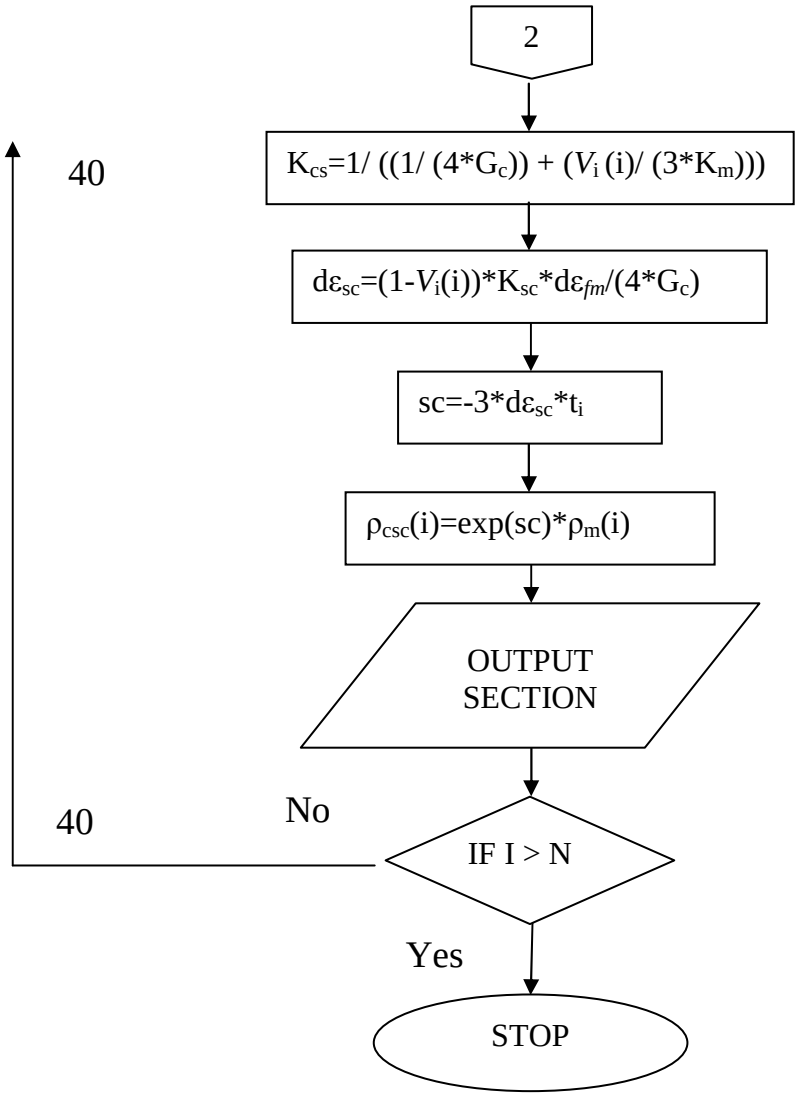

Figure (3.4) Flow chart of the program of the Composite Sphere and Self Consistent model.

Contents

Examination Committee Certificate

We certify that we have read the thesis entitled

"Mathematical Manipulation to Study the Changes of Porous Structure with the Formation Conditions of Porous Materials"

And as Examining Committee, examined the student

Sadeem Abbas Fadhil Al-Qassab

In its contents and what is related to it, and that in our opinion it is adequate as standard of thesis, with *Excellent* standing of

Degree of Master of Science

In *Physics*

Signature:
Name: **Dr. Fadhil A. Chiad**
Title: Chief Researcher (Chairman)
Address: Ministry of Science and Technology
Date: / /2005

Signature:
Name: **Dr. Emad Kh. Al-Shakarchi**
Title: Assist. Professor (Member)
Address: Al-Nahrain University
Date: / /2005

Signature:
Name: **Dr. Kadim J. Kadim**
Title: Assist. Professor (Member)
Address: Al-Mustansiria University
Date: / /2005

Signature:
Name: **Dr. Fadhil A. Rasen**
Title: Chief Researcher (Supervisor)
Address: Ministry of Science and Technology
Date: / /2005

Signature:
Name: **Dr. Ahmad K. Ahmad**
Title: Assist. Professor (Supervisor)
Address: Al-Nahrain University
Date: / /2005

Approved by the University Committee of Postgraduate Studies

Signature:
Name: **Dr. Laith A. Al-Ani**
(Dean of the college of science)
Date: / /2005

LIST OF FIGURES

جمهورية العراق
وزارة التعليم العالي و البحث العلمي
جامعة النهرين
كلية العلوم

معالجة رياضية لدراسة تغير التركيب المسامي مع ظروف التشكيل للمواد المسامية

رسالة

مقدمة إلى كلية العلوم في جامعة النهرين كجزء من متطلبات نيل شهادة الماجستير في الفيزياء

من قبل

سديم عباس فاضل القصاب
بكالوريوس ٢٠٠٢

ربيع الأول ١٤٢٦ نيسان ٢٠٠٥

Republic of Iraq
Minister of Higher Education &
Scientific Research
AL-Nahrain University
College of Science

Mathematical Manipulation to Study the Changes of Porous Structure with the Formation Conditions of Porous Materials

A Thesis
Submitted to the College of Science
Al-Nahrain University
in Partial Fulfillment of the Requirements for
the Degree of Master of Science in
Physics

BY

Sadeem Abbas Fadhil Al-Qassab

(B.Sc. 2002)

Rabia Al-Aowal 1426 H. **April 2005 A. D.**

Reference

1. M. W. Barsoum, Fundamentals of Ceramics, McGraw-Hill, New York, 1997.
2. A. C. De Bellis, Computer Modeling of Sintering in Ceramics, M. Sc. thesis in Mechanical Engineering, University of Pittsburgh, Russia, 2002.
3. C. Herring, J. Applied Physics, **21**, 301, 1950.
4. W. D. Kingery, H. K. Bowen and D. R. Uhlmann, Introduction to Ceramics, Wiley, Canada, 1976.
5. J.K.Mackenzie and R.Shuttleworth, Proc.Phys.Soc.London, **62,** 12-B, 833, 1949.
6. G. W. Scherer, J.Am.Ceram. Soc., **60,** 236, 1977.
7. B. J. Kellett and F. F. Lange, J.Am.Ceram. Soc., **72,** 735, 1989.
8. N. J. Shaw, Powder metallurgy international, **21,** 16, 1989.
9. J. Frenkel, J. Phys (USSR), **9,** 385, 1945.
10. W. D. Callister, Materials Science and Engineering, Wiley, New York, 2000.
11. W. L. Bragg, Atomic Structure of Minerals, Cornell Univ. Press, 1937.
12. R. W. Grimshaw, The Chemistry and Physics of Clays and Allied Ceramic Materials, Ernest Benn Limited, London, 1971.
13. R. Pampuch, Ceramic Materials: An Introduction to their Properties, Elsevier Scientific Publishing Company, Poland, 1976.
14. R. L. Coble, J. Appl. Phys., **36,** 2327, 1965.
15. M. F. Richard and A. P. Joseph, Ceramic Microstructures: Their Analysis, Significance, and Production, Wiley, New York, 1976.

16. Zvi Hashin, J. Appl. Mech., **29,** 143, 1962.
17. G. W. Scherer, Relaxation in glass and composite, Canada, 1986.
18. R. Raj and R. K. Bordia, Acta Metall., **32,** 1003, 1984.
19. C. H. Hsueh. A. G. Evans and R.M. Cannon, Acta Metall., **34**, 927, 1986.
20. G.W. Scherer, J. Am. Ceram. Soc., **70,**719, 1987.
21. R. M. Christensen, Mechanics of composite materials, Wiley, Canada (1979).
22. A. V. Hershey, J.Appl.Mech. , **21**, 236, 1954.
23. E. Kroner, Z. Phys., **151,** 504, 1958.
24. R. Hill, J.Mech.Phys.Solids, **13,** 213, 1965.
25. B. Budiansky, J. Mech. Phys. Solids, **13,** 223, 1965.
26. G. C. Kuczynski, J. Appl. Phys., **20,** 1160, 1949.
27. W.D. Kingery and M. Berg, ibid, **26,** 1205, 1951.
28. I. B. Culter and R. E. Henrichsen, J. Am. Ceram. Soc., **51,** 604, 1968.
29. R. L. Coble, J. Appl. Phys., **32,** 787, 1961.
30. W. Beere, Acta Metallurgica, **23,** 131, 1975.
31. G.W. Scherer, J. Am Ceram. Soc., **60**, 243, 1977.
32. R. K. Bordia and G. W. Scherer, Acta Metall., **36,** 2411, 1988.
33. R. K. Bordia and G. W. Scherer, Acta Metall., **36,** 2393, 1988.
34. C. H. Hsueh. A. G. Evans. and R.M. Cannon. , Acta Metall., **34,** 927, 1986.
35. F. F. Lange and B. J. Kellett, J. Am. Ceram. Soc., **72,** 735, 1989.
36. G.W. Scherer, J. Am. Ceram. Soc., **74**, 1523, 1991.
37. E. A. Olevsky and C. W. Bert, Communications in Numerical Methods in Engineering, **13,** 355, 1997.

38. E.A. Olevsky, B. Kushnarev, A.L. Maximenko; M. Braginsky, V. Tikare, "Multi-Scale Modeling of Sintering Shrinkage Anisotropy", 2002.
http://www.mri.psu.edu/conferences/sint03/pdf/Olevsky_2_Plenary.pdf.
39. V. Tikare, M.V. Braginsky, T. Garino, and J.G. Argüello; and E.A. Olevsky, "Numerical Simulation of Sintering at Multiple Length Scales", 2003.
http://www.mri.psu.edu/conferences/sint03/pdf/Tikare_2_4.pdf.
40. F. A. Rasen, The Use of Iraqi Siliceous Rocks as Electrical Insulators in Industry, Ph. D. thesis in physics, Al-Nahrain University, Iraq, 1998.
41. G. W. Scherer and D. L. Bachman, J. Am. Ceram. Soc., **60,** 239, 1977.
42. F. B. Hildebrand, Introduction to numerical analysis, Dover, Canada, 1987.
43. G. W. Scherer, J.Non-Cryst. Solids, **34,** 239, 1979.
44. S. P.Timoshenko and J. N. Goodier, Theory of Elasticity, McGraw-Hill, New York, 1970.
45. J. Selsing, J. Am. Ceram. Soc., **44**, 8, 419, 1961.
46. Z. Hashin and S. Shtrikman, J. Mech. Phys. Solids., **11**, 127, 1963.
47. F. H. Stross and P. E. Porter, Encyclopedia of Chemical Technology, Interscience, New York, **14,** 756, 1955.
48. R. K. Bordia and R. Raj., J. Am. Ceram. Soc., **69,** C55, 1986.
49. R. L. Coble, J. Appl. Phys., **34,** 1679, 1963.
50. R. Griffiths and C. Radford, Calculations in Ceramics, London, 1965.
51. J. Heading, Mathematical Methods in Science and Engineering, Edward Arnold, London, 1979.

52. F. H. Norton, Fine Ceramic: Technology and Applications, MaGraw-Hill, Florida, 1987.
53. P. C. Panda and W. M. Mobley and R. Raj, J. Am. Ceram. Soc., **72,** 2361, 1989.
54. M. N. Rahaman and L.C. De Jonghe, J. Am. Ceram. Soc., **70**, 12, C-348, 1987.

Supervisor's Certification

We certify that this thesis was prepared under our supervision at the 'AL-Nahrain University' as a partial requirement for the degree of Master of Science in Physics.

Signature:		Signature:	
Name:	*Dr. Ahmad K. Ahmad*	Name:	*Dr. Fadhil A. Rasen*
Title:	*Assist Professor*	Title:	*Chief Researcher Assist*
Address:	*Head of Physics Department College of Science AL-Nahrain University.*	Address:	*Ministry of Science and Technology.*
Date:	*/ 4 / 2005*	Date	*/ 4 / 2005*

In the view of the recommendation. I forward this thesis for debate by the examination committee.

Signature:	
Name:	*Dr. Ahmad K. Ahmad.*
Title:	*Assist Professor*
Address:	*Head of Physics Department College of Science AL-Nahrain University.*
Date:	*/ 4/ 2005*

LIST OF TABLES